The degree of freedom of nuclear triaxial deformation and K-isomeric decays

A Thesis presented
by
Naoki Tajima
to
the Division of Science
of
the Graduate School
for
the Degree of Doctor of Science

Institute of Physics, University of Tokyo

December, 1988

Contents

Chapter 1

Introduction

As for the description of the degree of freedom of axially asymmetric deformation in the nucleus (the γ degree of freedom), there are two extreme models having apparently different features. One is the γ-vibrational model of Bohr and Mottelson [1], in which a nucleus vibrates around an axially symmetric shape. The other is the triaxial rotor model given by Davydov and Filippov [2], in which a nucleus has a static axially asymmetric deformation and rotates around all three principal axes of the deformation. In the former model γ is considered as a dynamical variable, while in the latter model it is treated as a parameter to specify a nuclear shape. There have been a wide variety of arguments concerning the two models for thirty years. A brief review is presented in chapter 2.

The two models give roughly similar results for most of the observables (like some energy levels and collective transitions) despite the obvious distinction in their formulations [3]. It seems due to the fact that these observables are determined by some average value of γ and scarcely dependent on the size of the fluctuation in γ : The triaxial rotor model can be obtained by neglecting the fluctuation in γ and fixing γ at the average value.

It is interesting to find quantities which bring about the information not only on the average value of γ but also on the fluctuation in γ. An existing method to see the fluctuation in γ is a systematic determination of the quadrupole matrix elements in Coulomb excitation experiments [4] [5] . In this paper we present a new example of such quantity, i. e. the degree of violation of the K-selection rule in K-isomerism, which is found very sensitive to the size of the fluctuation in γ. As a result, we can distinguish the two extreme models of axial asymmetry very clearly. In this paper, we investigate

the effects of the fluctuation in γ by changing the shape of the potential energy for γ-deformation and show that the potential shape can be known to some extent from the half-lives of K-isomers.

In electromagnetic transitions between states having definite K-quantum numbers[1], not only the change in the total angular momentum but also the change in the K-quantum number cannot exceed the multipolarity of the radiation (the K-selection rule). The K-quantum number is conserved fairly well in well-deformed nuclei with axial symmetry. Hence states which have large expectation values of the K-quantum number are likely to become long-lived isomers when they can decay only into states with small expectation values of K. More detailed explanations are given in chapter 3.

Experimentally, very roughly speaking, the probabilities of K-forbidden transitions are hindered by a factor of 10^2 for each one increment of the K-quantum number [6] [7] [8]. An extreme example of K-isomer is a $K = 16$ state in ^{178}Hf, which has a half-life as long as 31 years [9] [10].

But recently some high-K isomers in neutron deficient Os isotopes are observed decaying with much shorter half-lives than those predicted by the above-mentioned empirical rule [11] [12] [13]. The most remarkable one is a $K^\pi = 25^+$ isomer in ^{182}Os, which decays (in part) directly into the I=24 member of the s-band [13] [14] quickly in spite of the difference of the K-quantum number of ~ 20 (see the footnote [2]). The configuration of the isomer is speculated to be of six-quasi particle state [13] [15].

In this thesis we study the $K^\pi = 10^+$ isomers in ^{182}W and ^{184}Os which have a very simple configuration, i. e. a two-quasi-particle ($\nu[624]9/2^+$, $\nu[615]11/2^+$) state involving only a unique-parity (intruder) orbital ($\nu i_{13/2}$,ν means neutrons). (Mixing ratio of other configuration ($\pi[514]9/2^-$, $\pi[505]11/2^-$) might be large in the case of ^{184}Os from the g-factor measurement [13] but we assume only the above-mentioned configuration for both nuclei in this paper.) Illustrating this simple configuration, we can concentrate our attention on the study of the γ-degree of freedom, since we need not worry about

[1]The K-quantum number is defined as the component of the total angular momentum along the third principal axis of nuclear shape. This axis is conventionally the symmetry axis in prolate shape.

[2]The expectation value of K is not ~ 0 in the s-band states, because K is rather widely spread for rotationally aligned orbitals.

ambiguities concerning the complicated microscopic structure.

The $K^\pi = 10^+$ isomer observed in ^{184}Os [13] decays into the $I = 8$ ($8^+_{\rm gr}$) and the $I = 10$ ($10^+_{\rm gr}$) members of the ground band with a partial half-life of 180 ns and 360 ns respectively [3]. The partial half-life with these two transitions is 120 ns [4]. In an isotone ^{182}W of N=108 having Z smaller by 2, the isomer which is considered to have the same configuration decays with a half-life of 1.4 μs into the $8^+_{\rm gr}$ state and the $10^+_{\rm gr}$ state [16]. The half-life is about 12 times as long as the partial half-life of the isomer in ^{184}Os with these two transitions, although the transition energies are very similar in both nuclei: In ^{182}W (^{184}Os) the energy of the γ-ray of the transition from the isomer to the $10^+_{\rm gr}$ state is 0.519 MeV (0.495 MeV) and that to the $8^+_{\rm gr}$ state is 1.087 MeV (1.092 MeV). It should be noted that even the isomer in ^{182}W has a much shorter half-life than the half-life predicted by the above-mentioned empirical rule. The decay properties of the two isomers are summarized in fig. 3.2.

Chowdhury and his co-workers suggested that the difference in the half-lives can be attributed to the difference of the softness with respect to γ-deformation (γ-softness), because γ-deformation mixes the K-quantum number and the K-selection rule breaks down. Nuclides like ^{182}W and ^{184}Os are classified into transitional nuclei, which are located between the well-deformed rotational nuclei and the spherical vibrational nuclei on the chart of the nuclides. They are less deformed and more γ-soft than typical rotational nuclei in the rare earth region. The degree of γ-softness can be estimated from the ratio of the excitation energy of the $I = 2$ state of the γ-band (γ-bandhead or 2^+_γ) to that of the $I = 2$ state of the ground band ($2^+_{\rm gr}$). The ratio is 12.2 in ^{182}W while it is 7.87 in ^{184}Os (fig. 3.1). Therefore it is quite natural to consider that the nucleus ^{184}Os is more γ-soft than the nucleus ^{182}W.

These clear violations of the K-selection rule seem so strange that they are expected to inform us new aspects of nuclei concerning the γ-degree of freedom. Some explanations for these fast K-isomeric decays are presented, in which the γ-degree of freedom plays

[3]The former partial half-life is explicitly given in ref. [13]. The latter one is estimated from the intensities of γ-rays given in ref. [13].

[4]The total half-life of the isomer is 20 ns. It decays with a large portion into an $I = 9$ state whose configuration is not identified.

the leading role. At first, in the papers [11] [12] reporting the observation of the $K^\pi = 25^+$ isomer in ^{182}Os, Pedersen and his collaborators suggested the coexistence of axially symmetric shape (for the ground-band states and the isomer) and triaxial shape (for the s-band states). They speculated that the polarizing effect of the rotation-aligned particles may triaxialize the nuclear shape if the nucleus is very γ-soft. If it is so, many triaxial-rotation levels having various expectation values of the K-quantum number are created just above the s-band. Passing through these states as stepping stones, the high-K isomer can be de-excited quickly by repeating transitions with small ΔK. The observed complicated decay pattern of the isomer is consistent with this picture: The isomer decays by the emission of as many as 100-150 γ-rays [17] and the s-band states are populated in a scattered manner. If such three-dimension rotational levels of a triaxial nucleus are really observed, a great impact will be made especially on the theories of nuclear collective motions [18]. But no such triaxial-rotation levels are found on the decay paths in the subsequent detailed experiment [13].

Onishi and the author studied the $K^\pi = 25^+$ isomer from a different point of view [14]. We assumed that the isomer had an angular-momentum-aligned configuration of two protons and two neutrons in the intruder orbitals [5] , with emphasis on the importance of the interaction between a proton and a neutron. Using a model in which $h_{11/2}$ protons and $i_{13/2}$ neutrons are coupled to a (γ-soft) rotor, we calculated the de-excitation paths of the isomer and found that these paths go through many excited two-particle-rotation-aligned bands before reaching the s-band states. This work pointed out the possibility of observing excited rotation-aligned bands by utilizing the delayed decay of isomers lying much higher than the yrast level, although the configuration did not turn out to be the assumed one [13] [15].

Chowdhury and his coworkers presented a new picture to explain the fast decays of the K-isomers in the next paper [13], in which the detailed decay paths of the $K^\pi = 25^+$ isomer in ^{182}Os and the finding of the $K^\pi = 10^+$ isomer in ^{184}Os are reported. If the nuclear shape is very soft toward γ-deformation, large quantum fluctuation in γ can mix

[5] When we published the work, the spin of the isomer was not assigned yet and was speculated to be $(20 \pm 2)\hbar$ in refs. [11] [12].

the K-isomeric state and the s-band (or the ground-band) state via barrier penetration through the oblate shape in spite of the large difference in their structures: The angular momentum is aligned with the symmetry axis in the K-isomer, while it is perpendicular to the symmetry axis in the s-band (or the ground-band) state, though equilibrium shapes of the two states are the same (γ=0°). Calculation of barrier heights and penetration factors (in the framework of the cranking model) are proposed for the future work in the paper. T. Bengtsson is attempting to make such calculations [15].

It is uncertain, however, whether the above simplified picture can be applied to real nuclei. As for the quantitative estimation of penetration factors, it is much more uncertain. Since the size of deformation is not large ($\beta \sim 0.2$) in transitional nuclei, the assumption of adiabaticity for the intrinsic motions does not seem to be a good approximation. The motions of particles may be disturbed considerably by the quantum fluctuation in the rotational motion and the shape deformation. In order to settle the problems of these ambiguous points in the semiclassical picture, three kinds of motions — the rotation, the shape deformation, and the intrinsic particle motions — should be treated on an equal footing in a quantum mechanical way. Only in that case, we can be sure that quantitative estimations are made.

In this paper we are going to make this fully quantum mechanical calculation in order to examine how the half-lives are altered by introducing the γ-degree of freedom, with other effects taken into account quantitatively as well. It is expected that we can obtain new information about the axial asymmetry — such as the size of the fluctuation in γ — from decays of K-isomers.

As for the framework of the calculation, we use the particle-rotor model rather than the cranking model. The former is a fully quantal model and conserves the angular momentum, while the latter is a semiclassical model in which states are not eigenvectors of angular momentum. The latter model is not suitable for our purpose because it suffers from spurious mixing of states having different angular momentum and also because it cannot take into account the effect of the fluctuation of the rotation axis. A unique point of our approach is that we describe the particle-rotor model in the laboratory frame using spherical bases for the particles, not in the intrinsic frame of the nuclear shape using the

Nilsson bases. This formulation of the particle-rotor model is quite suitable for treating the large-amplitude motion in the nuclear shape, i. e. for treating the oblate shape as well as the prolate shape in a single model space.

Now let us mention the contents of the following parts of this paper. In chapter 2 the similarity and the difference between the γ-vibrational model and the triaxial rotor model are reviewed and discussed. In chapter 3 the general empirical facts concerning K-isomers are reviewed. In chapter 4 the framework of our calculations are given. The formulation of the quantal liquid-drop model of Bohr [1] is reviewed. We employ the model so as to treat the collective motions. Next, the particle-rotor model is re-formulated in the laboratory frame in a somewhat original way. The relation of the model to the strong-coupling particle-rotor model is also discussed.

In chapter 5 the procedures of numerical calculations are explained in detail. We have to use accurate wave functions in order to calculate decay amplitudes of isomers, in which small components of wave functions can have large effects. Thus we take the utmost care in order to obtain the accurate wave functions of the eigenstates of our model hamiltonian. For example, full $(\nu i_{13/2})^n$ (n=0,2,4,$\cdots$,14) configurations are taken into account for the particle space. Moreover, special cares are taken for the truncation of the highly-excited γ-vibrational states. It is confirmed that this truncation has no influence on the quantities concerning the decay of the K-isomers.

In chapter 6 the results of numerical calculations are presented and are discussed. We summarize this paper in chapter 7.

Chapter 2

Treatment of the γ-degree of freedom

2.1 Similarity of the γ-vibrational model and the rigid triaxial rotor model

According to microscopic calculations, equilibrium shapes of well-deformed nuclei are axially symmetric and prolate (γ=0°). For instance, Baranger and Kumar applied the pairing-plus-quadrupole model to even-even nuclei with N=82-126, Z=50-82 and found that the equilibrium shapes are spherical or axially symmetric prolate except for Z=76-80 (Os, Pt, Hg) [19]. In the region of Z=76-80, where the deformation disappears gradually as Z and/or N increase, some nuclides are predicted to have axially asymmetric (in other word, triaxial) or oblate equilibrium shapes. The nuclei treated in this paper — ^{182}W and ^{184}Os — are predicted to have axially symmetric prolate equilibrium shapes.

A basic model was proposed by A. Bohr to treat the quadrupole surface-vibrations and rotations (the Bohr model) [1]. In this paper we treat collective motions of the nucleus only in the framework of the Bohr model for simplicity, though there is another successful model for nuclear collective motions, i. e. the interacting boson model of Arima and Iachello [20]. In the work [1], Bohr and Mottelson supposed that the γ-degree of freedom, which expresses the deviation from the axially symmetric shape, manifests itself as the vibration of nuclear shape around axially symmetric shape. It is widely accepted that this γ-vibration is associated with the γ-band, i. e. the rather low-lying $K^\pi = 2^+$ band which occurs in most deformed even-even nuclei and which has large E2 matrix elements for its excitation.

Several years later, however, Davydov and Filippov introduced an alternative model

which also includes a motion associated with the γ-degree of freedom [2]. It was the triaxial rotor model, in which the nucleus is assumed to have a rigid [1] axially asymmetric shape. The triaxial nucleus can rotate around the 3-axis (the third principal axis of the nuclear quadrupole deformation), while the axially symmetric nucleus can not rotate around the axis because it is symmetric around the axis. The γ-band is associated with the excitation of rotation around the 3-axis in this model. Many experimental data like energy levels and transition amplitudes in the ground and the γ-band of even-even nuclei are explained rather well in the framework of this model. The model was extended in order to take into account the β-vibration (the nucleus is still stiff in the direction of γ) and the β-band was reproduced successfully [21].

Considering the shallowness of microscopically calculated energy surfaces for γ-deformation, it seems that the nucleus can not have such stable rigid triaxial shape. According to Bohr's model, the amplitude of zero-point motion in the variable γ is as large as the size of static γ-deformation assumed in Davydov's calculation. Bohr expressed sharp criticism to the triaxial rotor model: The rigid triaxial deformation does not hold in the real nucleus since the concept of deformation can be applied only if the average value is greater than the fluctuation [22]. Moreover it was pointed out by many authors that many features reproduced by the triaxial rotor model are also accounted for equivalently by the conventional γ-vibrational model [23] [24] [25].

At first sight, it is rather strange that the predictions of the two models are so similar in spite of the difference in their pictures. In the γ-vibrational model, the variable γ fluctuates around γ=0°, while in the triaxial rotor model, γ is fixed at a constant value γ_0 where $\gamma_0 > 0°$.

We can demonstrate the origin of this similarity through the examination of the matrix elements of functions of γ in the subspace of low excitations as for the γ-degree of freedom. This point of view was mentioned by Preston in the Kingston Conference [22], and an explicit explanation was given by Yamazaki [26]. When $|\gamma| \ll 1$ in the γ-vibrational model with a harmonic potential, we can restrict the motion in γ to the ground state with K=0

[1] The word "rigid" means that the shape of the surface is stiff against deformations, not that the nucleus is regarded as a rigid body.

($|K{=}0_1\rangle$ [2]) and the first excited state with $K{=}2$ ($|K{=}2_1\rangle$) to a good approximation. For $|\gamma| \ll 1$, γ can be regarded as the radial variable for a two-dimensional motion of a particle, where the azimuthal angle is expressed by $2\theta_3$, where θ_3 is one of the Euler angles representing the rotation around the 3-axis [1]. When we consider terms up to $\mathcal{O}(\gamma^2)$, there are only three non-vanishing matrix elements on account of this interplay between γ and the rotation around the 3-axis,

$$\langle K = 0_1 |\, \gamma \,| K = 2_1 \rangle = \gamma_{00}, \tag{2.1}$$

$$\langle K = 0_1 | \gamma^2 | K = 0_1 \rangle = \gamma_{00}^2, \tag{2.2}$$

$$\langle K = 2_1 | \gamma^2 | K = 2_1 \rangle = 2\gamma_{00}^2, \tag{2.3}$$

where γ_{00} is the amplitude of zero-point motion in the variable γ in the ground state. Therefore we can replace the dynamical variable γ by a static parameter γ_{00} to an accuracy of $\mathcal{O}(\gamma)$. Through this replacement, the γ-vibrational model is reduced into the triaxial rotor model with $\gamma_0{=}\gamma_{00}$. Although the excitation energy of γ-vibration is twice as large as the energy of rotation around the 3-axis in rigid triaxial rotor model with $\gamma_0{=}\gamma_{00}$, it can be said that gross features of the similarity are accounted for by this argument. Hence we do not have to conclude the rigidity of triaxial shape even if the triaxial rotor model can reproduce many features of the states with zero or one γ-vibrational phonon.

The rigid triaxiality is revived by Meyer-ter-Vehn [27]. He applied the triaxial-rotor-plus-particle model to some transitional odd-A nuclei (A=135,190). As a result, he found that the experimental energy spectrum of the odd-A nuclei are reproduced fairy well by this model. To his surprise, the value of static γ-deformation (γ_0) can be determined within $\pm 2^\circ$ to reproduce the energy spectra of an odd-A nucleus and the adjacent even nuclei. Considering the strong γ-driving effects of the last odd particle, the core seems to have much deeper potential well around γ_0 than the soft potentials predicted by microscopic calculations [19]. He suggested the existence of rigid triaxial shape for these transitional nuclei. Toki and Faessler drew the same conclusion using an improved model with a variable moment of inertia [28].

Against Meyer-ter-Vehn's suggestion, Yamazaki and his collaborators argued that the

[2]The subscript 1 means that the state is the lowest one having the quantum number $K{=}0$.

coupling of the particle motion to the γ-degree of freedom is also equivalent between the two models as far as $|\gamma|$ is small [29]. The coupling is expressed by a quadrupole-quadrupole interaction and the quadrupole matrix elements are already shown to be equivalent. Now it is commonly believed that the odd particle is not a probe sensitive enough to identify triaxial deformation [30] [31], at least for weakly deformed nuclei.

As for the microscopic calculation of the potential energy surface for deformation, Hayashi and his collaborators discussed the effects of three-dimensional angular momentum projection on the Hartree-Fock-Bogoliubov ground states [32]. Angular momentum projection has large effects in the case of weak symmetry violation like in the case of γ-deformation of transitional nuclei. They calculated the microscopic potentials and obtained the wave functions in the β-γ plane for such potentials. They found for ^{188}Os that ,while the unprojected wave function is γ-unstable, the projected wave function rather localizes in the region $20^\circ < \gamma < 40^\circ$. But the value of the wave function at $\gamma = 0^\circ$ is still half as large as the value at the peak ($\gamma \sim 30^\circ$). Hence we cannot say that the triaxial deformation is realized in ^{188}Os.

In the real nucleus, which is composed of finite number of nucleons, the concept of the shape of the surface is more or less ambiguous. Recently Otsuka and Sugita pointed out in terms of the interacting boson model (IBM) that the extreme limits of the two models — the γ-unstable model (i. e. the O(6) limit of IBM) and the rigid triaxial model with γ=30°(a coherent state of γ=30° deformed boson with angular momentum projection) — have equivalent low-lying states when the number of bosons is small enough [33]. This result is interpreted that when the number of degrees of freedom is small enough, they are exhausted in order to define the principal-axis frame of the shape and more specific determination of the shape — like determination of the value of γ — is impossible on account of the lack of available degrees of freedom.

2.2 Difference of the two models in energy levels

As we have just seen in the last section, the similarity of the two models originates in the fact that we look at only γ_{00} (the root mean square value of γ in the ground-band states). Therefore if we have a quantity that can distinguish the two models, we can obtain more

information on the motion in γ than γ_{00}.

Although the two descriptions of the triaxiality resemble each other at low-lying states, higher excited states can be utilized to distinguish the two models. For example, the energy splitting of the doublet of the double-γ-vibrational states (K=0_2 and K=4_1) can be used to investigate the shape of the potential for γ-deformation [34] [35]. If the potential is harmonic around γ=0°, the two double-γ-vibrational states are degenerate. As the potential minimum is shifted from zero to positive values of γ, the K=4_1 level goes downward while the K=0_2 level goes upward. In the limit of rigid triaxial rotor, the K=0_2 level disappears completely. The K=0_2 double-γ-vibrational state has not been found yet.

From a different viewpoint, the situation can be expressed that the energy ratio of the K=4_1 state to the K=2_1 state is 2 in the case of harmonic potential, but it is 4 in the case of the rigid triaxial rotor. For example, Yamazaki and his coworkers pointed out that the energy of the K=j+4 band in Ir isotopes, in which the odd particle with spin j (=Ω=11/2) is confirmed to be coupled to the K=4_1 double γ-vibrational state, is too low to be consistent with the prediction of the triaxial-rotor-plus-particle model [29].

The spectrum of the (K=2_1) γ-band can be also utilized in order to distinguish the two models, though the physical meaning of the phenomena is less transparent than in the case of the double-γ-vibrational states. In the γ-vibrational model, the spectrum show a (3^+,4^+), (5^+,6^+), $\cdots$ bunching pattern, which is opposite to the (4^+,5^+), (6^+,7^+), $\cdots$ clustering pattern predicted in the triaxial rotor model [36] [37]. In the transitional nuclei, the spectrum clearly shows the former bunching pattern and these nuclei seem rather γ-vibrational than rigid triaxial.

It is, however, worth while noting that energy levels of these highly excited states can be shifted easily because the states tend to couple with quasi-particle excitations. Hence more direct investigation of the wave functions are desirable in order to distinguish between the γ-vibration and the rotation of rigid triaxial nucleus.

2.3 Direct investigation of wave functions

Now let us consider how we can investigate the shape of the wave function for γ in more direct manners. Though there are many detailed investigations of the transition matrix elements, we do not describe them here. In stead, we give more intuitive considerations. In the part **(a)** of figure 2.1 we show the schematic shape of wave functions for γ-vibration around γ=0° and for stiff triaxial deformation. Two regions of γ are missing in the latter wave function, i. e. the region **A** ($\gamma < \gamma_0$) and the region **B** ($\gamma > \gamma_0$). The crucial point to decide if the deformation is triaxial or not is whether the wave function is vanishing or not in the region **A**.

The information on the wave function for γ is not included in M1 transition amplitudes, because M1 operator is only the total angular momentum operator multiplied by a constant factor and does not concern to the intrinsic shape.

By E2 transitions, we can only obtain some mean deviation in γ from γ=0° and can not investigate the more detailed shape of wave functions, because the E2 operator depends on γ only through $\cos\gamma$ and $\sin\gamma$,

$$\mathcal{M}(\mathrm{E2},\mu) = \frac{3ZeR_0^2}{4\pi}\,\alpha_{2\mu} \tag{2.4}$$

$$= \frac{3ZeR_0^2}{4\pi}\,\beta\left\{\cos\gamma\; D^2_{\mu 0} \;+\; \sin\gamma\;\frac{D^2_{\mu 2}+D^2_{\mu -2}}{\sqrt{2}}\right\}. \tag{2.5}$$

Details of the above equations are explained in chapter 4 . As is illustrated in the part **(b)** of figure 2.1, the E2 operator changes much slowly compared to the wave functions for γ.

Therefore, to learn the shape of wave functions in detail, we must use operators whose variation in the interval $0 \le \gamma \le \gamma_0$ is very large. Cline and his collaborators developed a computer code to analyze complicated data of Coulomb excitation experiment [4] [5]. Using this code, they can derive the matrix elements of not only $\cos\gamma$ and $\sin\gamma$ but also more complicated functions of γ like $\cos 3\gamma$ and $\cos^2 3\gamma$ from experiments . These functions are sketched in the part **(c)** of figure 2.1. Thus the shape of wave functions for γ can be known to some extent by this method. It is, however, worth while noting that when we make inner products of these wave functions, we have to include the volume element

$|\sin 3\gamma|$ (sketched in the part **(d)** of figure 2.1), which diminishes the contribution from the regions near γ=0° and γ=60°. Hence it is rather difficult to examine the shape of the wave function in the region **A**.

For another example, some particle transfer reactions may be employed to investigate the shape of wave functions [38]. Cross sections of particle transfer are sensitive to single particle levels near the Fermi level, while these single particle levels are changed largely by the nuclear shape. Reactions which depend on γ very sensitively can teach us the distribution in γ if deformation β is so large that particles are very adiabatically coupled to the nuclear shape.

In this paper we show that K-isomeric decays can be used as very sensitive probes in order to obtain information about the wave functions in the region **B** ($\gamma > \gamma_0$), and we investigate the mechanism associating the fluctuation in γ into $\gamma > \gamma_0$ with the K-isomeric decays. In the next chapter, we discuss about the K-isomerism and the recent experiments in which flagrant violations of the K-selection rule are observed.

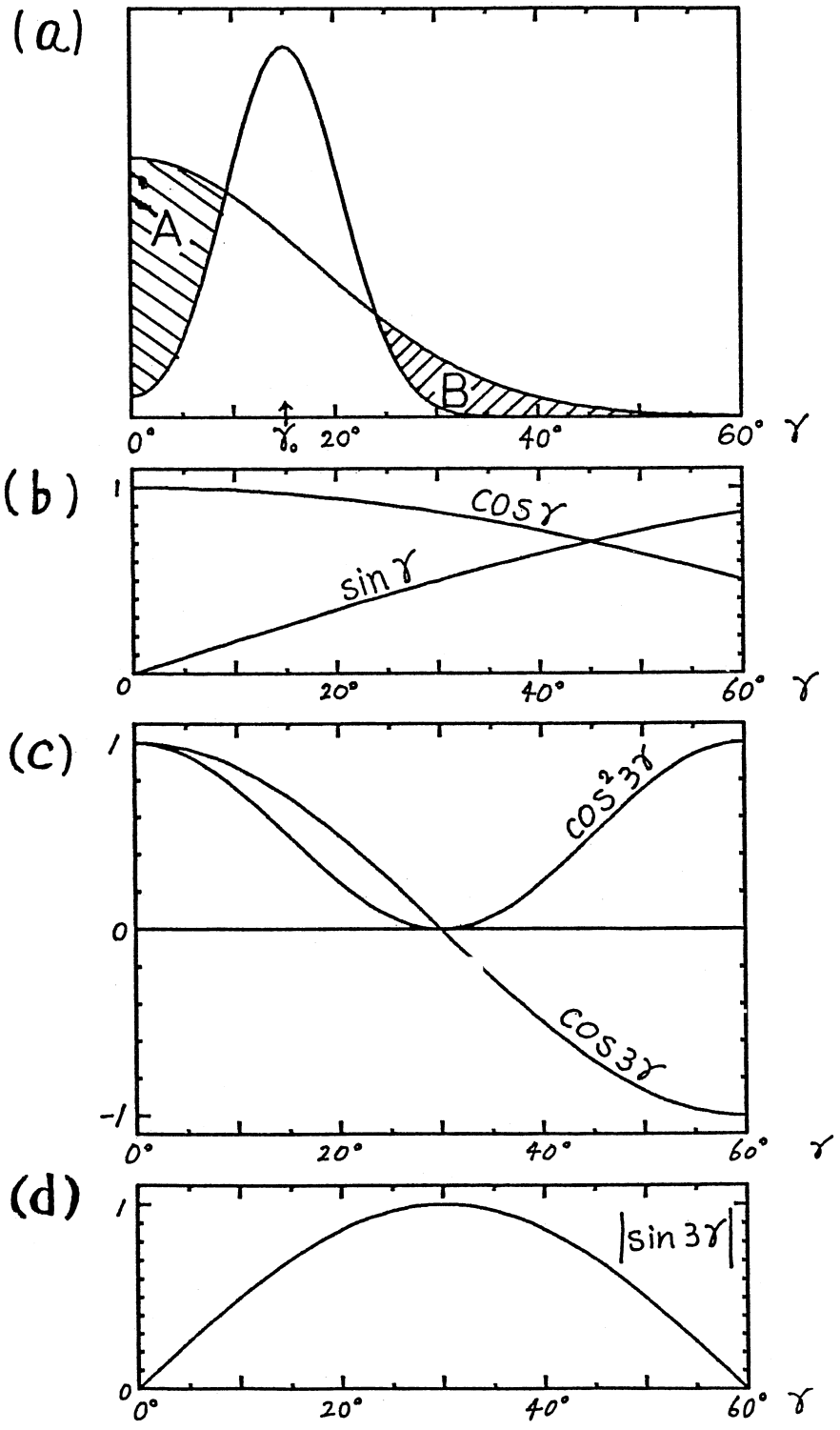

Figure 2.1: Schematic pictures of the wave functions for γ in the γ-vibrational model and the triaxial rotor model. Some functions of γ are also shown.

Chapter 3

The K-selection rule and K-isomers

3.1 The K-selection rule and its violation

In axially symmetrically well-deformed nuclei the component of the total angular momentum along the symmetry axis (K) is conserved fairly well. Therefore, in such nuclei, a state can be separated to a good approximation into the rotational part for the orientation angles (Ω) and other intrinsic-motion part

$$|IMK\alpha\rangle = |IMK(\Omega)\rangle \otimes |K\alpha\rangle \ , \tag{3.1}$$

where I, M, and K are the quantum numbers for rotation, while other necessary quantum numbers are expressed by α. If the nuclear shape is invariant with respect to π-rotation around an axis perpendicular to the symmetry axis, the state should be a linear combination of two states having K and $-K$ in order to fulfill the single-valuedness of the wave function with respect to nuclear deformation seen in the laboratory frame. Even if this is applied to eq. (3.1), the following discussion about the K-selection rule is not altered.

The moments associated with electromagnetic multipole quanta can be expressed using the moments referring to the intrinsic frame of the nucleus,

$$\mathcal{M}(\lambda\mu) = \sum_{\nu=-\lambda}^{\lambda} \mathcal{M}^{\rm intr}(\lambda\nu) D^{\lambda}_{\mu\nu}(\Omega) \ , \tag{3.2}$$

where $D^{\lambda}_{\mu\nu}(\Omega)$ is the rotation-matrix in the notation of ref. [8]. Matrix elements of $\mathcal{M}(\lambda\mu)$ are given as follows.

$$\langle I_2 M_2 K_2 \alpha_2 | \mathcal{M}(\lambda\mu) | I_1 M_1 K_1 \alpha_1 \rangle$$

$$= \sum_{\nu=-\lambda}^{\lambda} \langle K_2\alpha_2|\mathcal{M}^{\rm intr}(\lambda\nu)|K_1\alpha_1\rangle\langle I_2M_2K_2(\Omega)|D^{\lambda}_{\mu\nu}(\Omega)|I_1M_1K_1(\Omega)\rangle$$

$$= \sum_{\nu=-\lambda}^{\lambda} \langle K_2\alpha_2|\mathcal{M}^{\rm intr}(\lambda\nu)|K_1\alpha_1\rangle\sqrt{\frac{2I_1+1}{2I_2+1}}\langle I_1M_1\lambda\mu|I_2M_2\rangle\langle I_1K_1\lambda\nu|I_2K_2\rangle \ . \quad (3.3)$$

In the last line of the above equations, the first Clebsch-Gordan coefficient demands $|\Delta I|$ $\equiv |I_2 - I_1| \leq \lambda$ and $|\Delta M| \equiv |M_2 - M_1| \leq \lambda$, while the second one requires further

$$|\Delta K| \ \equiv \ |K_2 - K_1| \ \leq \ \lambda. \quad (3.4)$$

This restriction (eq. 3.4) is called *the K-selection rule*: The change in the K-quantum number can not exceed the multipolarity of the radiation in transitions between states having definite K-quantum numbers.

The K-selection rule is violated to some extent on account of the mixing of states having different K-quantum numbers (K-mixing) in real nuclei. The hindrance factor $F_{\rm W}$ for K-forbidden transitions is defined usually on the basis of the Weisskopf unit [1] for transition probabilities,

$$F_{\rm W} \ = \ \frac{\rm B_{Weisskopf\ unit}(E\ or\ M,\ \lambda)}{\rm B_{experimental}(E\ or\ M,\ \lambda)} \ . \quad (3.5)$$

Empirically, $F_{\rm W}$ is known to obey an exponent-rule,

$$F_{\rm W} = (f_{\rm W})^n \quad , \quad n = |\Delta K| - \lambda \ , \quad (3.6)$$

where n is the K-forbiddenness and $f_{\rm W}$ is the hindrance factor per n. Rusinov [6] proposed that

$$f_{\rm W} \ \sim \ 100 \ , \quad (3.7)$$

which implies that the amplitude for band-mixing with $|\Delta K|$=1 is $\sim 10^{-1}$ [8]. Löbner compiled many experimental data and confirmed that the reduced transition probabilities decrease approximately by a factor of 100 per n. He found, however, that the usage of the Weisskopf unit for basis is not always meaningfull since absolute values of $F_{\rm W}$ are likely to be shifted to higher values in comparison with eqs. (3.5 - 3.7) [7]. This is not a serious problem for largely K-forbidden cases because of the exponent-dependence of $F_{\rm W}$ on n.

[1] The Weisskopf unit [39] [8] is calculated using a nuclear radius parameter r_0=1.2 fm in this paper.

It is worth while noting that eq. (3.7) gives only a rough estimation and the values of $f_{\rm W}$ for various nuclei scatter in the interval

$$1 \lesssim \log_{10} f_{\rm W} \lesssim 2, \tag{3.8}$$

which is found e. g. in ref. [16].

The main origin for the mixing of the K-quantum number is the Coriolis interaction, i. e. excitation of intrinsic motions due to collective rotation. The expression for the Coriolis interaction is obtained naturally in the strong-coupling-scheme particle-rotor model [8], which includes the collective rotational motion of the entire nucleus in addition to single-particle motions in deformed nuclear potential,

$$\begin{aligned} H_{\rm PR}^{\rm strong} &= H_{\rm intr} + \sum_{\kappa=1}^{2} \frac{\hbar^2}{2\mathcal{J}}(I_\kappa - J_\kappa)^2 \quad , \qquad (I_3 = J_3) \\ &= H_{\rm intr} + \frac{\hbar^2}{2\mathcal{J}}(\vec{I}^2 - I_3^2) - \frac{\hbar^2}{2\mathcal{J}}(J_+ I_- + J_- I_+) + \frac{\hbar^2}{2\mathcal{J}}(\vec{J}^2 - J_3^2) \ , \end{aligned} \tag{3.9}$$

where $\vec{I}$ and $\vec{J}$ are the total and the non-collective angular momenta respectively. The four terms in the last line of eqs. (3.9) are the intrinsic, rotation, Coriolis, and the recoil terms, respectively, in which only the Coriolis term can mix states having different I_3 ($=K$). The Coriolis interaction has no effects only when I=0 (and hence K=0). What should be noted is that K-mixing occurs even in bandhead states — like K-isomers — when the band has non-zero K.

It is not certain whether we can apply the empirical rule (eqs. (3.5 - 3.8)), which is obtained mainly for well-deformed nuclei, to the K^π=10^+ isomers in ^{182}W and ^{184}Os treated in this paper. The first reason is that these nuclei are transitional nuclei having relatively small deformation ($\beta \sim 0.2$). Since the strength of the Coriolis interaction is proportional to the reciprocal of the moment of inertia $1/\mathcal{J}$ (eq. (3.9)), its effect is enhanced in these less deformed nuclei. The second reason is that these isomers have a configuration involving only an intruder orbital $\nu i_{13/2}$. The intruder orbital is affected strongly by the Coriolis interaction on account of the largeness and the purity of its angular momentum. Hence the Coriolis interaction should be treated carefully in order to study the structure of these K-isomers.

Another possible origin for K-mixing is the triaxial deformation of the nucleus, which mixes K even in single-particle orbitals. The γ-vibration can also mix K as well as the static triaxiality, as is described in the last chapter. It is probable that K-isomeric decays are sensibly affected by the triaxiality besides the Coriolis interaction.

3.2 K-isomers in Hf-W-Os region

Many high-K isomers are found at or near the yrast levels in Hf isotopes and in the neighboring nuclei. This situation is caused by a strong shell effect: There are many Nilsson orbitals having large Ω [2] near the Fermi level for Hf, W and Os nuclei. By exciting quasi-particles in these orbitals, high-spin states can be formed at excitation energies as low as the energy of collective rotation [40].

The K-isomers observed in Hf isotopes have the typical characters of K-isomer like long half-lives and K-selective decay patterns. The neighboring even-even nuclides — W and Os — are also expected to have similar isomers judging from the location of the Fermi level. They are, however, transitional nuclei, which have smaller deformation and larger γ-softness than Hf isotopes. We show the energy levels of the low-spin members of the ground and the γ-band for some $N = 108$ isotones in fig. 3.1 , where energies are divided by those of the $2^+_{\rm gr}$ states. The nuclei ^{182}W and ^{184}Os are still deformed rotational nuclei since their ground-band spectra show the pattern of rotational motion. The energy of the γ-bandhead is, however, lowered rapidly as Z increases. It is interesting to see what is brought about to the typical K-isomers in Hf isotopes by this increase in γ-softness.

Some transitions largely violating the K-selection rule in these nuclei are compiled in table 3.1. The K^π=8^- isomers having $N \sim 106$ are thought to have a two-quasi-particle configuration ($\nu[514]7/2^-$, $\nu[624]9/2^+$) whose excitation energy is very low. In $^{178}{\rm Hf}_{106}$, $^{180}{\rm W}_{106}$, and $^{182}{\rm Os}_{106}$, the values of $f_{\rm W}$ are 74.8, 54.6, and 48.7 respectively. It is suggested that the degree of K-mixing becomes large as Z increases in this region.

The K^π=10^+ isomers in ^{182}W and ^{184}Os have much smaller $f_{\rm W}$ (~ 5) than the K^π=8^- isomers ($f_{\rm W} \sim 50$). As is already described in chapter 1, these isomers are observed to

[2] The quantum number Ω is the third component (in the intrinsic frame) of the angular momentum of a single-particle orbital.

decay very rapidly in spite of the K-selection rule. The experimental data for the decays of these isomers are summarized in fig. 3.2. In 1977 Jeltema and his collaborators observed the K^π=10^+ isomer in ^{182}W which decays directly into the ground-band states with a relatively short half-life of 1.4 μs despite the change in K as large as 10 [16]. They considered that the small values of $f_{\rm W}$ for this decay is due to the sensitiveness of the $i_{13/2}$ orbital to the Coriolis interaction. In 1988 Chowdhury and his collaborators found the K^π=10^+ isomer in ^{184}Os, which has still smaller $f_{\rm W}$ than the isomer in ^{182}W [13]. They suggested that the γ-softness of these nuclei plays the important role for these large violations of the K-selection rule, while they depreciated the role of the $\nu i_{13/2}$ orbital.

The large change in $f_{\rm W}$ between the K^π=8^- isomer and the K^π=10^+ isomer would be due to the difference in their configurations. The Z-dependence in $f_{\rm W}$ for each isomer is, however, likely to be attributed to the change in the deformation and in the γ-softness. Although the K^π=8^- isomers are found in more nuclei than the K^π=10^+ ones, the former are hard to deal with on account of the complicated structure of the normal-parity orbitals. The latter are easier to treat because of the simple configuration involving solely the $\nu i_{13/2}$ orbital [3]. Therefore we take up the K^π=10^+ isomers in this paper. We try to obtain information on the γ-degree of freedom from the decays of these K-isomers, through the estimation of the two important factors of K-mixing — the Coriolis interaction and the triaxiality — equally in a quantitative way.

[3]The two K^π=10^+ isomers in ^{182}W and ^{184}Os are the only K-isomers observed so far which involve the $\nu i_{13/2}$ orbital exclusively in prolately deformed nuclei (not oblate yrast traps [41]) [16]. This isomer has not been found in ^{180}Hf yet.

Table 3.1: Electromagnetic transitions largely violating the K-selection rule in even-even Yb - Pt nuclei. Only largely K-forbidden transitions whose partial half-lives are known are included in this table, although more isomers are found in these nuclei. Compilation of the data of other isomers are found e. g. in refs. [10] [41] [45] [46].

Nucleus	$(I,K)^\pi$ of initial state	$(I,K)^\pi$ of final state	ΔE [keV]	Half-life of the initial state	Feeding ratio of the final state, internal conversion coefficients	λ	n	f_{W}	Refs.
^{176}Yb	$(8,8)^-$	$(8,0)^+$	96.1	11.7 [s]	100 % , $\alpha = 0.38$	E1	7	94	[10] [42]
^{176}Hf	$(6,6)^+$	$(6,0)^+$	736.2	9.5 [μs]	I_γ=78	M1	5	49	[43]
		$(4,0)^+$	1043.0		I_γ=45	E2	4	43	[43]
	$(14,14)^-$	$(13,8)^-$	38.7	401. [μs]	I_γ=5.0 , $\alpha = 12$	M1	5	30	[43]
		$(12,8)^-$	302.2		I_γ=44	E2	4	23	[43]
		$(12,8')^-$	227.9		I_γ=9.8	E2	4	23	[43]
^{178}Hf	$(8,8)^-$	$(8,0)^+$	88.9	4.0 [s]	100 % , $\alpha = 0.49$	E1	7	79	[10] [42] [44]
	$(16,16)^+$	$(13,8)^-$	12.7	31 $\pm$ 1 [y]	99.8 % ,$\alpha = 1.5 \times 10^7$	E3	5	66	[10]
		$(12,8)^-$	309.5		(K) 0.13 % , $\alpha_{\mathrm{K}} = 5.2$	M4	4	64	[10]
^{180}Hf	$(8,8)^-$	$(8,0)^+$	57.5	5.5 [h]	—	E1	7	233	[10]
^{180}W	$(8,8)^-$	$(8,0)^+$	390.3	5.2 [ms]	100 %	E1	7	55	[10] [42]
^{182}W	$(10,10)^+$	$(10,0)^+$	518.5	1.4 [μs]	I_γ=63	M1	9	6.4	[16]
		$(8,0)^+$	1086.5		I_γ=73	E2	8	5.1	[10] [16]
^{182}Os	$(8,8)^-$	$(8,0)^+$	554.	0.8 [ms]	100 %	E1	7	49	[10] [13] [42]
^{184}Os	$(10,10)^+$	$(10,0)^+$	495.	20 [ns]	I_γ=6/100 (delayed)	M1	9	5.0	[13]
		$(8,0)^+$	1092.		I_γ=12/100 (delayed)	E2	8	3.6	[13]
^{184}Pt	$(8,8)^-$	$(8,0)^+$	610.1	1.0 [ms]	I_γ=64/120 (delayed)	E1	7	58	[10] [42]

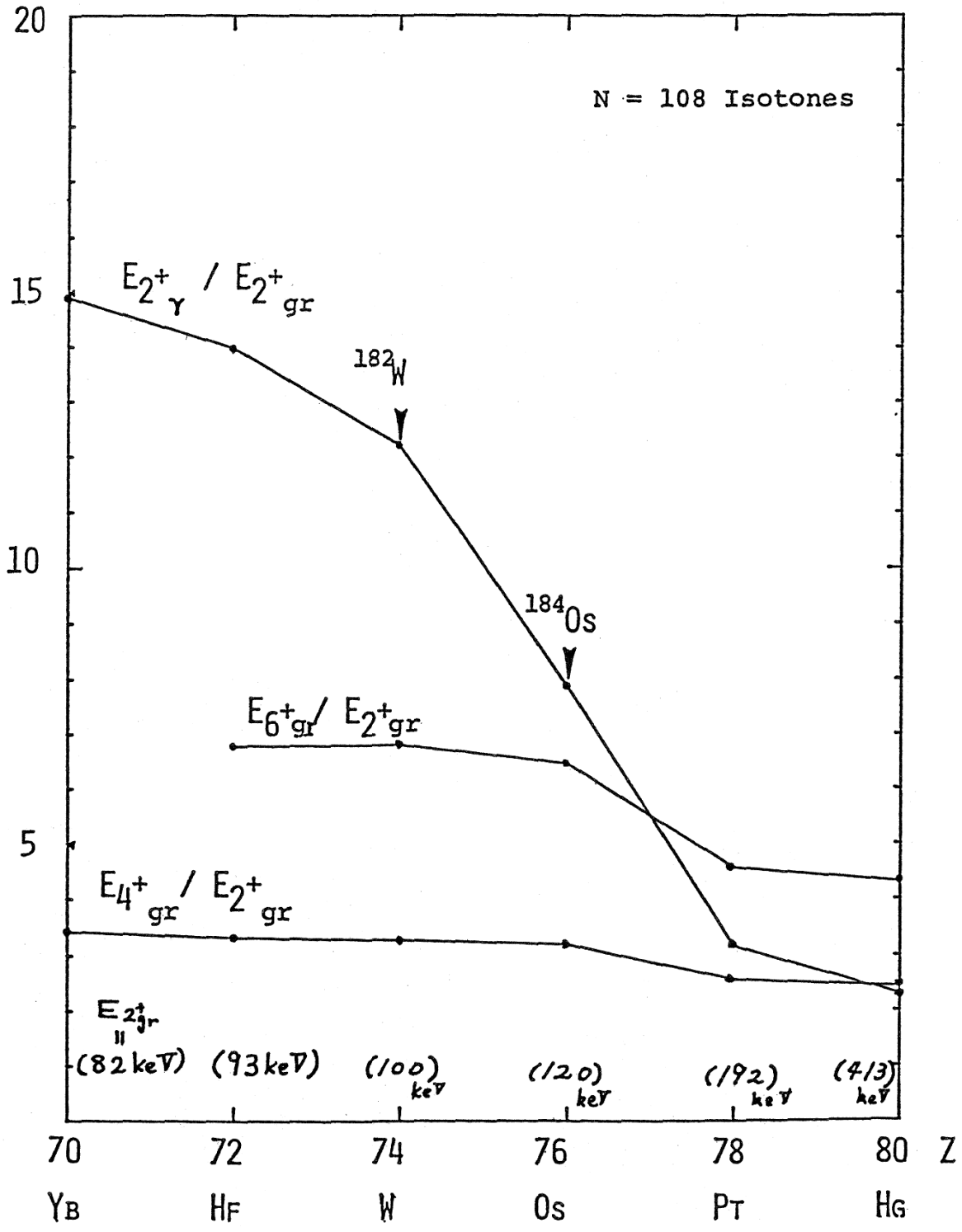

Figure 3.1: The γ-softness of N=108 isotones. The ratios of excitation energies of $4^+_{\rm gr}$, $6^+_{\rm gr}$, and 2^+_γ states to that of the $2^+_{\rm gr}$ state are shown. The energy level of the $2^+_{\rm gr}$ state is given in the parentheses.

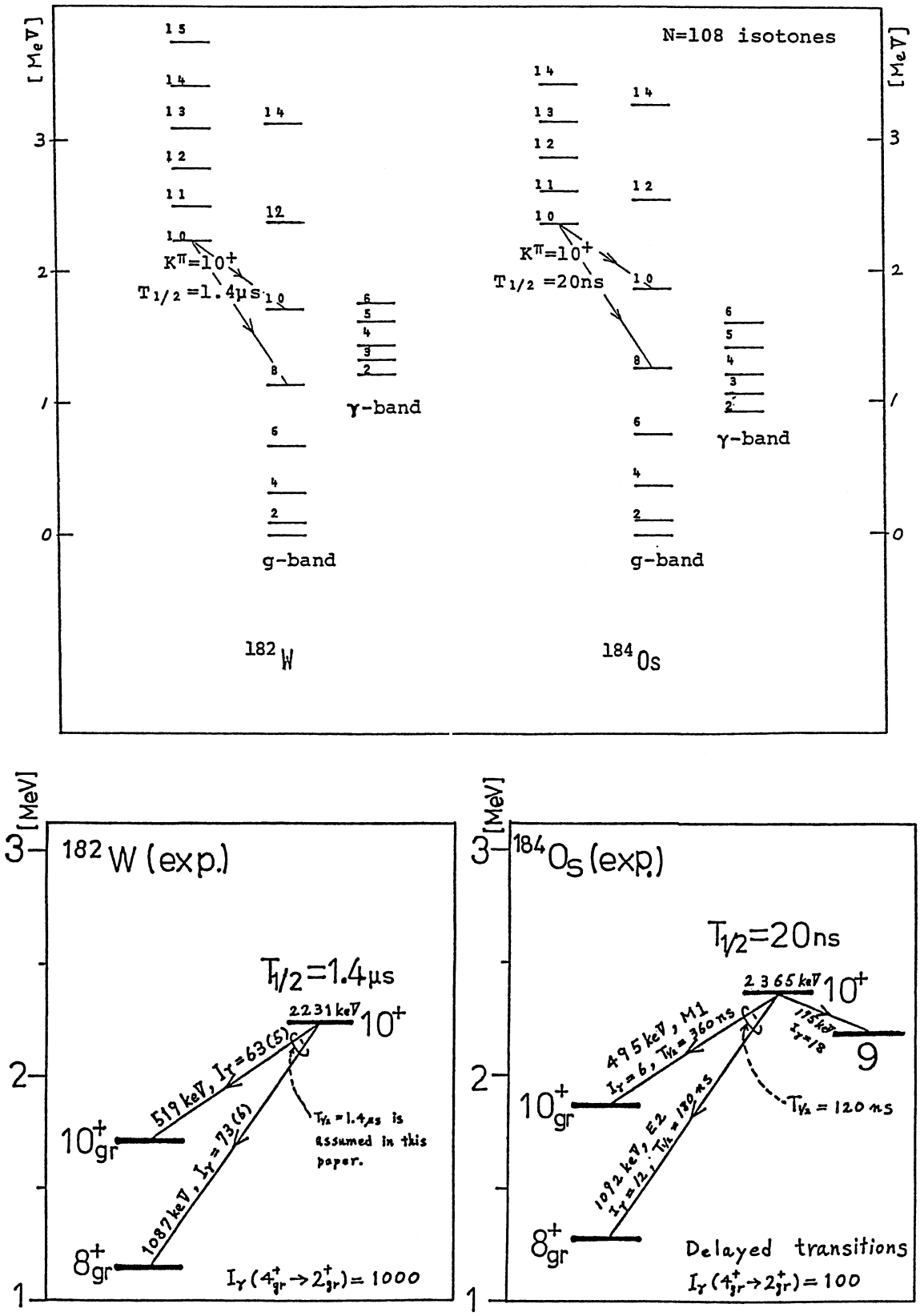

Figure 3.2: Experimental data about the $K^\pi=10^+$ isomers.

Chapter 4

The model

We use a kind of particle-rotor model to simulate the decay of these short-lived K-isomers into the states of the ground band. In our model non-collective motions, such as particle-hole excitation and rotational alignment, occur only in particles in the unique-parity orbital (intruder orbital), i. e. the $\nu i_{13/2}$ orbital in this case. Other particles in normal-parity orbitals are called *the core* and are replaced by some collective model. In this chapter the collective part of the model is described at first. Then the scheme of coupling between the collective modes and the particles in the unique-parity orbital is presented.

4.1 The Bohr model

4.1.1 The full hamiltonian

As we aim at the study of the axially asymmetric deformation of well-deformed nuclei, we employ the Bohr model of quadrupole surface vibrations and rotations [1] as the core of our model : It has explicitly a variable γ which represents the degree of freedom of axially asymmetric deformation. The Bohr model may be relevant to the giant quadrupole resonances, rather than to the low-lying quadrupole vibrations and rotations. The irrotational flow is rather a good approximation for the giant resonances but vortex flow should be introduced for the low-lying quadrupole motions [47] [48]. Nevertheless we utilize the Bohr model because of its nice feature of symmetry of a quantum liquid drop with quadrupole shape motions, e. g. the moment of inertia about the symmetry axis is zero. We do not use the value of the mass parameter B given by Bohr [1], but we reserve it for a energy-scaling parameter to simulate the low-lying quadrupole motions.

Quadrupole surface deformations are uniquely determined by the normal coordinates $\alpha_{2\mu}$ as

$$R(\theta,\varphi) = R_0\Big\{1 + \sum_{\mu=-2}^{2} (-1)^\mu \alpha_{2\mu} Y_2^{-\mu}(\theta,\varphi)\Big\} \ , \quad \alpha_{2\mu} = (-1)^\mu \alpha^*_{2-\mu} \ , \tag{4.1}$$

where $R(\theta,\varphi)$ is the distance of the surface from the center of the nucleus. In the Bohr model, the intrinsic variables (β and γ) and Euler angles ($\Omega_{\rm c}$=($\varphi_{\rm c}$,$\theta_{\rm c}$, $\psi_{\rm c}$)) are used in stead of $\alpha_{2\mu}$. These variables are defined using the deformation in the intrinsic frame (a_ν) and the rotation matrix $D^2_{\mu\nu}$ in the notation [1] of ref. [8] .

$$a_\nu = \sum_{\mu=-2}^{2} \alpha_{2\mu} D^2_{\mu\nu}(\Omega_{\rm c}) \ , \tag{4.2}$$

with

$$a_2 = a_{-2} = 2^{-1/2}\beta\sin\gamma \ , \tag{4.3}$$

$$a_1 = a_{-1} = 0 \ , \tag{4.4}$$

$$a_0 = \beta\cos\gamma \ . \tag{4.5}$$

In order to fulfill the single-valuedness of wave functions with respect to $\alpha_{2\mu}$, Bohr's symmetry is required: The wave functions must be invariant with respect to transformations relabeling the principal axes of deformation. These transformations can be generated by repeated application of the three basic transformations, i. e. R_1, R_2, and R_3 [1] .

The hamiltonian of the full Bohr model is

$$H_{\rm Bohr} = -\frac{\hbar^2}{2B}\sum_{\mu=-2}^{2}(-1)^\mu \frac{\partial^2}{\partial\alpha_{2\mu}\partial\alpha_{2-\mu}} + V(\beta,\gamma) \ , \tag{4.6}$$

$$= T_\beta + T_\gamma + T_{\rm rot} + V(\beta,\gamma) \ , \tag{4.7}$$

where

$$T_\beta = -\frac{\hbar^2}{2B}\frac{1}{\beta^4}\frac{\partial}{\partial\beta}\beta^4\frac{\partial}{\partial\beta} \ , \tag{4.8}$$

$$T_\gamma = -\frac{\hbar^2}{2B}\frac{1}{\beta^2\sin 3\gamma}\frac{\partial}{\partial\gamma}\sin 3\gamma\frac{\partial}{\partial\gamma} \ , \tag{4.9}$$

$$T_{\rm rot} = \sum_{\kappa=1}^{3}\frac{\hbar^2}{2\mathcal{J}_\kappa}R^2_\kappa \ , \quad \mathcal{J}_\kappa = 4B\beta^2\sin^2(\gamma - \frac{2}{3}\pi\kappa) \ . \tag{4.10}$$

[1] $D^I_{MK}(\Omega)$=$\langle IM|\mathcal{R}(\Omega)|IK\rangle^*$.

In the above equations T_β, T_γ, and $T_{\rm rot}$ represent the kinetic energies of β-vibration, γ-vibration, and rotation, respectively. $V(\beta,\gamma)$ is the potential energy for deformations of the intrinsic shape. In eqs. (4.10), R_κ and $\mathcal{J}_\kappa$ denote the angular momentum operator and the moment of inertia for the rotation around the κth principal axis, respectively. The sum of these kinetic energy terms is proportional to the five-dimensional laplacian with respect to $\alpha_{2\mu}$ (eq. (4.6)).

4.1.2 The γ-soft model

In this paper, we fix the variable β at a constant value β_0 and treat it as a static parameter, because we aim at studying intensively the effects of the γ-degree of freedom on K-isomerism. We call this β-fixed Bohr model as *the γ-soft model* [49] [50] from now on. This model was introduced by Wilets and Jean [51] for the γ-unstable potential ($V(\beta_0,\gamma)$ = constant). Qualitative properties of the model at high spin are discussed by Turner and Kishimoto [52]. Its hamiltonian is

$$H_{\gamma-\rm soft} = T_\gamma\Big|_{\beta=\beta_0} + T_{\rm rot}\Big|_{\beta=\beta_0} + V(\gamma)\ , \tag{4.11}$$

where

$$V(\gamma) = V(\beta_0,\gamma)\ . \tag{4.12}$$

The energy is scaled only through a quantity $(2\hbar^2/B{\beta_0}^2)$ except for $V(\gamma)$. In later sections we designate this value by $\epsilon_{\rm c}$, which is the energy of the first excited state for $V(\gamma)=0$.

Eigenstates of $H_{\gamma-\rm soft}$ are expressed as

$$|RM\alpha_{\rm c}\rangle = \sum_{K_{\rm c}=-R}^{R} |RMK_{\rm c}(\Omega_{\rm c})\rangle \ \otimes\ |\Phi^{\alpha_{\rm c}}_{RK_{\rm c}}(\gamma)\rangle\ , \tag{4.13}$$

where

$$\langle\delta(\Omega_{\rm c}-\Omega^0_{\rm c})|RMK_{\rm c}(\Omega_{\rm c})\rangle = \sqrt{\frac{2R+1}{8\pi^2}}D^R_{MK_{\rm c}}(\Omega^0_{\rm c})\ , \tag{4.14}$$

$$\langle\delta(\gamma-\gamma_0)|\Phi^{\alpha_{\rm c}}_{RK_{\rm c}}(\gamma)\rangle = \Phi^{\alpha_{\rm c}}_{RK_{\rm c}}(\gamma_0)\ . \tag{4.15}$$

In the above expression, R is the quantum number of angular momentum (R=0,2,3,4,$\cdots$). M and $K_{\rm c}$ are its components along the z-axis (of the laboratory frame) and the third principal axis, respectively. Other quantum numbers to specify a state are represented by

$\alpha_{\rm c}$. Because of Bohr's symmetry, the quantum number $K_{\rm c}$ takes on only even integers. Amplitudes for the component having $K_{\rm c}$ and that having $-K_{\rm c}$ are related to each other as

$$\Phi^{\alpha_{\rm c}}_{R,-K_{\rm c}}(\gamma) = (-1)^R \Phi^{\alpha_{\rm c}}_{RK_{\rm c}}(\gamma) \ , \tag{4.16}$$

on account of the symmetry.

We consider wave functions only in the interval $0 \leq \gamma \leq \pi/3$, utilizing Bohr's symmetry. The orthonormality of eigenstates,

$$\langle R'M'\alpha_{\rm c}{}'|RM\alpha_{\rm c}\rangle = \delta_{R'R}\delta_{M'M}\delta_{\alpha_{\rm c}'\alpha_{\rm c}} \ , \tag{4.17}$$

is satisfied by the orthonormality of D-functions,

$$\begin{aligned} & \langle R'M'K'_{\rm c}(\Omega_{\rm c})|RMK_{\rm c}(\Omega_{\rm c})\rangle \\ = & \frac{\sqrt{(2R'+1)(2R+1)}}{8\pi^2} \times \\ & \int_0^\pi d\theta_{\rm c} \sin\theta_{\rm c} \int_0^{2\pi} d\varphi_{\rm c} \int_0^{2\pi} d\psi_{\rm c} \{D^{R'}_{M'K_{\rm c}'}(\varphi_{\rm c},\theta_{\rm c},\psi_{\rm c})\}^* D^R_{MK_{\rm c}}(\varphi_{\rm c},\theta_{\rm c},\psi_{\rm c}) \\ = & \delta_{R'R}\delta_{M'M}\delta_{K_{\rm c}'K_{\rm c}} \ , \end{aligned} \tag{4.18}$$

and by a requirement for intrinsic wave functions,

$$\sum_{K_{\rm c}=-R}^{R} \langle \Phi^{\alpha'_{\rm c}}_{RK_{\rm c}}(\gamma)|\Phi^{\alpha_{\rm c}}_{RK_{\rm c}}(\gamma)\rangle = \sum_{K_{\rm c}=-R}^{R} 3\int_0^{\pi/3} \Phi^{\alpha'_{\rm c}}_{RK_{\rm c}}(\gamma)\Phi^{\alpha_{\rm c}}_{RK_{\rm c}}(\gamma)\sin 3\gamma d\gamma = \delta_{\alpha'_{\rm c}\alpha_{\rm c}} \ . \tag{4.19}$$

The potential energy for γ-deformation (γ-potential) should be a function of $\cos 3\gamma$ as a consequence of Bohr's symmetry. It can be expanded by Legendre polynomials of $\cos 3\gamma$. We take only the first two terms at most in this paper,

$$V(\gamma) = \frac{2\hbar^2}{B{\beta_0}^2} \sum_{l=1}^{2} V_l P_l(\cos 3\gamma) \ . \tag{4.20}$$

We vary V_1 to control the γ-softness and vary V_2 to shift the minimum point of the potential.

When $V(\gamma)$=0 (the γ-unstable model [51] [53] [54]), eigenstates are labeled by the quantum numbers μ and n_γ in addition to R and M. For each R, these quantum numbers take on the values of

$$\mu = \mu_{\rm min}, \mu_{\rm min}+1, \mu_{\rm min}+2, \cdots, R \quad , \tag{4.21}$$

$$n_\gamma = 0, 1, 2, 3, 4, 5, \cdots \quad , \tag{4.22}$$

where

$$\mu_{\min} = \mu_{\min}(R) = \begin{cases} R/2 & \text{for even } R \ , \\ (R+3)/2 & \text{for odd } R \ . \end{cases} \tag{4.23}$$

The seniority quantum number λ [53] is related to μ and n_γ as

$$\lambda \ = \ \mu \ + \ 3 \ n_\gamma \ . \tag{4.24}$$

The energies of states are determined only through λ,

$$E_\lambda = \frac{2\hbar^2}{B{\beta_0}^2} \frac{\lambda(\lambda+3)}{4} \ . \tag{4.25}$$

Number of states for each R and each λ is given in table 4.1.

Wave functions of eigenstates of the γ-unstable model, $G^{\lambda n_\gamma}_{RK_{\rm c}}(\gamma)$, are given in the manner of ref. [50] as follows:

$$G^{\lambda n_\gamma}_{RK_{\rm c}}(\gamma) = \sum_{\mu'=\mu_{\min(R)}}^{R} \ \sum_{{n_\gamma}'=0}^{n_\gamma} B^{R\lambda n_\gamma}_{\mu' {n_\gamma}'} (\cos 3\gamma)^{{n_\gamma}'} g^{\mu'}_{RK_{\rm c}}(\gamma) \ , \tag{4.26}$$

where

$$g^{\mu'}_{RK_{\rm c}}(\gamma) = \sum_{k=-j}^{j} f^{jk}_{RK_{\rm c}} \frac{(\sin\gamma)^{j+k}(\cos\gamma)^{j-k}}{\sqrt{(j+k)!(j-k)!}} \ , \tag{4.27}$$

with

$$j \equiv \frac{\mu'}{2} \ , \quad k = -j, -j+1, -j+2, \cdots, j \quad . \tag{4.28}$$

The coefficients $B^{R\lambda n_\gamma}_{\mu' {n_\gamma}'}$ and $f^{jk}_{RK_{\rm c}}$ can be obtained by diagonalizing $P_{\rm I}$, which is the projection operator into the invariant subspace with respect to transformations of Bohr's symmetry group. Among the eigenstates of $P_{\rm I}$, those having eigenvalue of 1 and being regular at γ=0° and γ=60° should be chosen.

When $V(\gamma) \neq$ constant, we diagonalize $H_{\gamma-\rm soft}$ using the bases of

$$|RMK_{\rm c}(\Omega_{\rm c})\rangle \ \otimes \ |G^{\lambda n_\gamma}_{RK_{\rm c}}(\gamma)\rangle \ , \tag{4.29}$$

which are truncated by

$$\lambda \ \leq \ \lambda_{\max} \ = \ 24 \ , \tag{4.30}$$

or equivalently,

$$E_\lambda \ \leq \ E_{24} \ = \ \frac{2\hbar^2}{B{\beta_0}^2} \times 162 \ \sim \ 30{\rm MeV} \ , \tag{4.31}$$

in this paper. Wave functions of γ for the eigenstates are expressed as

$$\Phi^{\alpha_c}_{RK_c}(\gamma) = \underbrace{\sum_{n_\gamma=0}^{\infty} \sum_{\mu=\mu_{\min}(R)}^{R}}_{3n_\gamma+\mu\leq\lambda_{\max}} a^{\alpha_c}_{R,3n_\gamma+\mu,n_\gamma} G^{3n_\gamma+\mu,n_\gamma}_{RK_c}(\gamma) \ . \tag{4.32}$$

The method to solve the eigenvalue equation for $H_{\gamma-\mathrm{soft}}$ is described in detail in ref. [50].

4.1.3 The triaxial rotor model

The triaxial rotor model of Davydov and Filippov in which γ is fixed at a value γ_0 is considered as a special case of the γ-soft model. It is obtained in the limit of $V_1 \to -\infty$ while keeping $V_1/3V_2 = -\cos 3\gamma_0$ in eq. (4.20). In the model, the wave-function for the variable γ is assumed to be trapped in a deep potential well which has a minimum at γ_0. The hamiltonian is

$$H_{\mathrm{triax}} = T_{\mathrm{rot}}\Big|_{\beta=\beta_0,\gamma=\gamma_0} \ . \tag{4.33}$$

Considering the requirement of Bohr's symmetry, eigenstates of H_{triax} are labeled by R and $|K_c|$, which take on the values of

$$R \ = \ 0,2,3,4,5,\cdots \quad , \tag{4.34}$$

$$|K_c| \ = \ \begin{cases} 0,2,4,\cdots,R & \text{for even } R \ , \\ 2,4,6,\cdots,R-1 & \text{for odd } R \ . \end{cases} \tag{4.35}$$

The number of states for each R is given in table 4.2.

4.1.4 The axially symmetric rotor model

For comparison, we also use the axially symmetric rotor model which does not have the γ-degree of freedom. It is obtained by setting γ=0° in the hamiltonian of eq. (4.33). The moments of inertia are changed in such a way that

$$\mathcal{J}_1 = \mathcal{J}_2 = \mathcal{J} \equiv 3B{\beta_0}^2 \ , \qquad \mathcal{J}_3 = 0 \ . \tag{4.36}$$

The hamiltonian is written as

$$H_{\mathrm{ax.sym.}} = \frac{\hbar^2}{2\mathcal{J}}(R_1^2+R_2^2) \ = \ \frac{\hbar^2}{2\mathcal{J}}R(R+1) \ , \qquad R_3 = 0 \ . \tag{4.37}$$

The eigenstates are labeled only by R which takes on non-negative even integers,

$$R \ = \ 0,2,4,6,8,\cdots \quad . \tag{4.38}$$

The number of states for each R is given in table 4.3.

4.2 The particle-rotor model

4.2.1 Derivation from the shell-model hamiltonian

4.2.1.1 The shell-model hamiltonian

We use a kind of particle-rotor model in which the particle states are described not in the intrinsic frame of the core but in the laboratory frame and are expanded with spherical bases. This model was originally used for spherical nuclei [55]. As for the earlier applications to deformed nuclei, see refs. [56]-[59]. Later works utilizing this model are found in refs. [60] - [64]. At first we demonstrate how our particle-rotor model is derived from a (spherical) shell-model hamiltonian and elucidate the bases and the scope of our model. The shell-model hamiltonian is written as [65]

$$H_{\rm SM} = \sum_j H_j^0 + \sum_{j_1 \le j_2} \sum_{j_3 \le j_4} V_{j_1 j_2; j_3 j_4} \ , \tag{4.39}$$

where

$$H_j^0 = \sum_m \epsilon_j a_{jm}^\dagger a_{jm}, \tag{4.40}$$

$$V_{j_1 j_2; j_3 j_4} = \sum_{JM} g_J(j_1 j_2; j_3 j_4) A_{JM}^\dagger(j_1 j_2) A_{JM}(j_3 j_4) \ . \tag{4.41}$$

In the above expressions, the subscript j denotes the angular momentum, and also indicates symbolically all the quantum numbers to designate a single-particle state (having an energy level ϵ_j) except for the magnetic quantum number m. The creation operator $A_{JM}^\dagger$ generates a normalized state of a nucleon-pair coupled to an angular momentum J and its z-component M:

$$A_{JM}^\dagger(j_1 j_2) = (1 + \delta_{j_1 j_2})^{-1/2} \sum_{m_1 m_2} \langle j_1 m_1 j_2 m_2 | JM \rangle a_{j_1 m_1}^\dagger a_{j_2 m_2}^\dagger \ . \tag{4.42}$$

The coefficient g_J is a matrix element of a residual two-body interaction V between normalized states of two nucleons with a coupled angular momentum J :

$$g_J(j_1 j_2; j_3 j_4) = \langle 0 | A_{JM}(j_1 j_2) V A_{JM}^\dagger(j_3 j_4) | 0 \rangle \ . \tag{4.43}$$

The $K^\pi = 10^+$ isomers in ^{182}W and ^{184}Os have a configuration of a unique-parity (intruder) orbital $\nu i_{13/2}$, which is not mixed with energetically nearby orbitals by the

single-particle potential with quadrupole deformation on account of parity conservation. Therefore we may treat only the unique-parity orbital as the particle degrees of freedom. Thus, using notations of

$$j_0 \equiv \nu\, i_{13/2} \ , \tag{4.44}$$

$$\sum_j{}' \equiv \sum_{j\,(j\neq j_0)} \ , \tag{4.45}$$

we divide $H_{\rm SM}$ into three parts

$$H_{\rm SM} = H^{\rm c}_{\rm SM} + H^{\rm p}_{\rm SM} + H^{\rm int}_{\rm SM} \ , \tag{4.46}$$

where

$$H^{\rm c}_{\rm SM} = \sum_{j_1}{}' H^0_{j_1} + \sum_{j_1\le j_2}{}' \sum_{j_3\le j_4}{}' V_{j_1j_2;j_3j_4}, \tag{4.47}$$

$$H^{\rm p}_{\rm SM} = H^0_{j_0} + V_{j_0j_0;j_0j_0}, \tag{4.48}$$

$$\begin{aligned} H^{\rm int}_{\rm SM} = & \sum_{j_1j_2}{}' V_{j_0j_1;j_0j_2} + \sum_{j_1\le j_2}{}' (V_{j_0j_0;j_1j_2} + V_{j_1j_2;j_0j_0}) \\ & + \sum_{j_1}{}'(V_{j_0j_0;j_0j_1} + V_{j_0j_1;j_0j_0}) + \sum_{j_1\le j_2}{}' \sum_{j_3}{}'(V_{j_1j_2;j_0j_3} + V_{j_0j_3;j_1j_2}) \ . \end{aligned} \tag{4.49}$$

4.2.1.2 The core part

In order to derive the particle-rotor model hamiltonian, we replace $H^{\rm c}_{\rm SM}$ by a certain collective model hamiltonian, $H_{\gamma-{\rm soft}}$ in this paper. Among the dependence of $H^{\rm c}_{\rm SM}$ on the number of particles in the core ($n_{\rm c}$), the dependence of the ground state energy is included to the linear term of $n_{\rm c}$. The dependence of other quantities, excitation energies and quadrupole matrix elements, is thought to be small and is ignored. (If required, we can change the parameters of the core model for each $n_{\rm c}$ without largely changing our formalism.) Thus we replace $H^{\rm c}_{\rm SM}$ by $H_{\rm c}$:

$$H_{\rm c} = \lambda_{\rm c}\hat{n}_{\rm c} + H_{\gamma-{\rm soft}} \ \ (,\ H_{\rm triax},\ H_{\rm ax.\ sym}\ ) \ . \tag{4.50}$$

The physical meaning of $\lambda_{\rm c}$ is the Fermi level of the core and appears only in combination with ϵ_{j_0} as $\epsilon_{j_0} - \lambda_{\rm c}$. Eigenstates of $H_{\rm c}$ are expressed as

$$|RM\alpha_{\rm c}, n_{\rm c}\rangle = |RM\alpha_{\rm c}\rangle \otimes |n_{\rm c}\rangle \ , \tag{4.51}$$

where $|RM\alpha_{\rm c}\rangle$ is given in eq. (4.13) and is operated on only by the second term in $H_{\rm c}$. The state $|n_{\rm c}\rangle$ is concerned only with the first term in $H_{\rm c}$; $\hat{n}_{\rm c}|n_{\rm c}\rangle = n_{\rm c}|n_{\rm c}\rangle$.

4.2.1.3 The particle part

We treat $H^{\rm p}_{\rm SM}$ in a fully microscopic way. As the residual interaction V in the j_0 orbital, we use the delta interaction [65] between a particle at $\vec{r_1}$ and another one at $\vec{r_2}$:

$$V(\vec{r_1},\vec{r_2}) = -4\pi V_0 \delta^{(3)}\ (\vec{r_1}-\vec{r_2})\ . \tag{4.52}$$

We define a quantity G as

$$G = V_0 \int_0^\infty \{\mathcal{R}_0(r)\}^4 r^2 dr\ , \tag{4.53}$$

where $\mathcal{R}_0(r)$ is the radial part of the wave function of the j_0 orbital. The matrix element g_J of this interaction is given by

$$g_J(j_0 j_0; j_0 j_0) = -G\ \frac{(2j_0+1)^2}{2}\frac{\langle j_0\ -\frac{1}{2}\ j_0\ \frac{1}{2}|J0\rangle^2}{2J+1}\ . \tag{4.54}$$

For J=0, it reads as

$$g_0(j_0 j_0; j_0 j_0) = -G\ \frac{2j_0+1}{2}\ . \tag{4.55}$$

The value of G is considered to be the same as that of the strength $G^{\rm BCS}$ of the ordinary pairing interaction used in the BCS model of nuclei (found e. g. in ref. [66]),

$$H^{\rm BCS}_{\rm pair} = -\frac{1}{4}G^{\rm BCS}\sum_{j_1}\sum_{m_1=-j_1}^{j_1}\sum_{j_2}\sum_{m_2=-j_2}^{j_2} a^\dagger_{j_1 m_1}(-1)^{j_1-m_1}a^\dagger_{j_1-m_1}(-1)^{j_2-m_2}a_{j_2-m_2}a_{j_2 m_2}\ . \tag{4.56}$$

Corresponding values of g_0 to this interaction is

$$g_0^{\rm BCS}(j_1 j_1; j_2 j_2) = -G^{\rm BCS}\frac{\sqrt{(2j_1+1)(2j_2+1)}}{2}\ , \tag{4.57}$$

which has the same form as eq. (4.55) for j_1=j_2=j_0. The value of $G^{\rm BCS}$ recommended by Baranger and Kumar [66] is

$$G\ =\ G^{\rm BCS}\ \simeq\ 22{\rm MeV}/A \qquad \text{for neutrons}\ , \tag{4.58}$$

where A is the mass number. The values of g_J for the $\nu i_{13/2}$ orbital of A=184 nuclei (G=22 MeV/184=0.120 MeV) are shown in table 4.4. The effective interaction of Onishi and Negele [67] for the shell-model calculations are also given for comparison.

Basis-states of n particles in the j_0 orbital are constructed using the coefficients of fractional parentage (c.f.p.)[68]. The c.f.p.'s are obtained by diagonalizing the antisymmetrization operator (the projection operator into the fully antisymmetric subspace) on

the bases composed of the direct product of the antisymmetric states of $n-1$ particles and the states of another particle. The states thus obtained are labeled by the number of particles n, the total angular momentum J, its z-component M, seniority v, and the necessary additional quantum numbers $\alpha_{\rm p}$ as

$$|{j_0}^n\ (\ v\ \alpha_{\rm p}\ )\ J\ M\ \rangle\ . \tag{4.59}$$

The following values are taken on by n and v :

$$n = 0, 2, 4, \cdots, 2j_0+1\ , \tag{4.60}$$

$$v = 0, 2, 4, \cdots, \min(n, 2j_0+1-n)\ . \tag{4.61}$$

Only even values of n have to be considered because we intend to treat positive parity states. The number of states for each set of values of n, v, and J are tabulated in tables 4.5 and 4.6 . Matrix elements of operators between these bases (eq. 4.59) are calculated using formulae given in ref. [68].

4.2.1.4 The QQ interaction

Now we approximate $H^{\rm int}_{\rm SM}$ by $H_{\rm int}$ which is suitable for interactions between a particle and the core described with the Bohr model. The first term in eq. (4.49) does not include transfer of particles and corresponds to the interaction between the surface deformation $\alpha_{2\mu}$ and the particles in the particle-rotor model. Potential energy for a particle at $\vec{r}$ exerted by the deformed core is considered to be expressed as

$$V(\vec{r}) = V_0\Big(\frac{R_0}{R(\theta,\varphi)}r\Big)\ , \tag{4.62}$$

where $R(\theta,\varphi)$ is given in eq. (4.1). Expanding $R(\theta,\varphi)$ with respect to α_2,

$$\begin{aligned} V(\vec{r}) &= V_0\Big(r - r\sum_{\mu=-2}^{2}(-1)^\mu \alpha_{2\mu}Y_2^{-\mu}(\theta,\varphi) + \mathcal{O}({\alpha_2}^2)\Big) \\ &= V_0(r) - r\frac{dV_0(r)}{dr}\sum_{\mu=-2}^{2}(-1)^\mu \alpha_{2\mu}Y_2^{-\mu}(\theta,\varphi) + \mathcal{O}({\alpha_2}^2)\ . \end{aligned} \tag{4.63}$$

The first term in the last line of above equations is the spherical mean potential and have no relation with surface deformation α_2 . The second term is a quadrupole-quadrupole

interaction between the core and the particle. Thus the first term in eq. (4.49) may be replaced by H_{QQ},

$$H_{QQ} = -\kappa \sum_{\mu} (-1)^{\mu} \frac{\alpha_{2\mu}}{\beta_0} \sum_{m'=-j_0}^{j_0} \sum_{m=-j_0}^{j_0} \langle j_0 m'(\theta,\varphi)|Y_2^{-\mu}(\theta,\varphi)|j_0 m(\theta,\varphi)\rangle a^{\dagger}_{j_0 m'} a_{j_0 m} \ , \quad (4.64)$$

where

$$\kappa = \beta_0 \left\langle \mathcal{R}_0(r) \middle| r \frac{dV_0(r)}{dr} \middle| \mathcal{R}_0(r) \right\rangle \ . \quad (4.65)$$

If we assume a harmonic oscillator single-particle potential,

$$V_0(r) = \frac{1}{2} m\omega^2 r^2 \ , \qquad \hbar\omega = 41 \text{ MeV} \times A^{-1/3} \ , \quad (4.66)$$

the matrix element of r^2 is related to N_{j_0} (the total oscillator quantum number for the j_0-orbital, N_{j_0}=6 for j_0=$i_{13/2}$) as

$$\langle \mathcal{R}_0(r)|r^2|\mathcal{R}_0(r)\rangle \ = \ \frac{\hbar}{m\omega}(N_{j_0} + \frac{3}{2}) \ . \quad (4.67)$$

Thus we obtain

$$\kappa = \hbar\omega\beta_0(N_{j_0} + \frac{3}{2}) \ . \quad (4.68)$$

4.2.1.5 The Cooper-pair exchange interaction

The second term in eq. (4.49) expresses an exchange of a pair of particles between the unique-parity orbital and the core. Because the range of the nucleon-nucleon interaction is short, the dominantly exchanged pair is the $J = 0$ one. Thus we approximate this term by a Cooper pair exchange interaction,

$$H_{\text{pair}} = -\frac{G}{4}(P_{\text{p}}^{\dagger} P_{\text{c}} + P_{\text{c}}^{\dagger} P_{\text{p}}) \ , \quad (4.69)$$

where the strength G is the same as that in eq. (4.58). $P_{\text{p}}^{\dagger}$ ($P_{\text{c}}^{\dagger}$) is a creation operator of a Cooper pair in the j_0 orbital (in the core):

$$P_{\text{p}}^{\dagger} \ = \ \sqrt{2(2j_0+1)} A^{\dagger}_{00}(j_0 j_0) \ = \ \sum_{m=-j_0}^{j_0} (-1)^{j_0-m} a^{\dagger}_{j_0 m} a^{\dagger}_{j_0 -m}, \quad (4.70)$$

$$P_{\text{c}}^{\dagger} \ = \ \sum_{j_1}{}' S_{j_1} \sqrt{2(2j_1+1)} A^{\dagger}_{00}(j_1 j_1) \ = \ \sum_{j_1}{}' \sum_{m=-j_1}^{j_1} (-1)^{j_1-m} S_{j_1} a^{\dagger}_{j_1 m} a^{\dagger}_{j_1 -m} \ , \quad (4.71)$$

where

$$S_{j_1} = \frac{2g_J(j_0, j_0; j_1, j_1)}{G\sqrt{(2j_0+1)(2j_1+1)}} \ . \tag{4.72}$$

For the matrix elements of $P_{\rm c}^\dagger$ and $P_{\rm c}$, we assume the following form [62]:

$$\langle R'M'\alpha_{\rm c}', n_{\rm c}'|(-\frac{G}{4}P_{\rm c}^\dagger)|RM\alpha_{\rm c}, n_{\rm c}\rangle = -\delta_{R'R}\delta_{M'M}\delta_{\alpha_{\rm c}'\alpha_{\rm c}}\delta_{n_{\rm c}', n_{\rm c}+2}\frac{\Delta'}{2}, \tag{4.73}$$

$$\langle R'M'\alpha_{\rm c}', n_{\rm c}'|(-\frac{G}{4}P_{\rm c})|RM\alpha_{\rm c}, n_{\rm c}\rangle = -\delta_{R'R}\delta_{M'M}\delta_{\alpha_{\rm c}'\alpha_{\rm c}}\delta_{n_{\rm c}', n_{\rm c}-2}\frac{\Delta'}{2} \ . \tag{4.74}$$

When the ordinary pairing interaction of eq. (4.56) is adopted, S_{j_1} turns out to be unity. Employing the BCS ground state as the state of the core, we find that Δ' is the pairing gap energy which does not include the contribution from the j_0 orbital,

$$\Delta' = 2\left\langle {\rm BCS}\middle|\frac{G}{4}\sum_{j_1}{}' \sum_{m=-j_1}^{j_1}(-1)^{j_1-m}a_{j_1m}^\dagger a_{j_1-m}^\dagger\middle|{\rm BCS}\right\rangle \tag{4.75}$$

$$= \frac{G}{2}\sum_{j_1}{}' \sum_{m=-j_1}^{j_1} u_{j_1m}v_{j_1m} \tag{4.76}$$

$$= \Delta - \frac{G}{2}\sum_{m=-j_0}^{j_0} u_{j_0m}v_{j_0m} \ . \tag{4.77}$$

where Δ is the (full) pairing gap energy of the nucleus.

We can rewrite $H_{\rm pair}$ as

$$H_{\rm pair} = -\frac{\Delta'}{2}\sum_m (-1)^{j_0-m}(Ta_{j_0m}^\dagger a_{j_0-m}^\dagger + T^\dagger a_{j_0-m}a_{j_0m}) \ , \tag{4.78}$$

where $T^\dagger$ and T operate only on $|n_{\rm c}\rangle$: $T^\dagger\ |n_{\rm c}\rangle = |n_{\rm c}+2\rangle$, $T\ |n_{\rm c}\rangle = |n_{\rm c}-2\rangle$. In this paper the label $n_{\rm c}$ is practically dummy. If we identify core states differing only in $n_{\rm c}$, $T^\dagger$ and T are replaced by 1 and $H_{\rm pair}$ turns out to be a pairing field in the j_0 orbital, which is used e. g. in ref. [69].

4.2.1.6 The resulting particle-rotor model hamiltonian

The third term and the fourth term in eq. (4.49) vanish due to parity conservation because we neglect contributions from much higher-lying orbitals having the same parity as the j_0 orbital. Thus $H_{\rm int}$ is finally expressed as

$$H_{\rm int} = H_{\rm QQ} + H_{\rm pair} \ . \tag{4.79}$$

The resulting hamiltonian of the particle-rotor model is given by

$$H_{\rm PR} = H_{\rm c} + H_{\rm SM}^{\rm p} + H_{\rm int} \ . \tag{4.80}$$

4.2.2 Wave functions

Eigenstates of the total system are expanded in terms of so-called weak coupling bases as

$$|IM\alpha\rangle = \sum_{R\alpha_{\rm c}nv\alpha_{\rm p}J} A^{I\alpha}_{R\alpha_{\rm c}nv\alpha_{\rm p}J}[\ |R\alpha_{\rm c}, A-n\rangle \otimes |j_0^n(v\alpha_{\rm p})J\rangle\ ]^{IM}\ . \tag{4.81}$$

On the left hand side of above equation, I is the total angular momentum and M is its z-component, while α denotes the necessary additional quantum numbers. On the right hand side, amplitudes are denoted by $A^{I\alpha}_{R\alpha_{\rm c}nv\alpha_{\rm p}J}$. The bases of the core are designated by its angular momentum R, number of particles in the core $A-n$ (A is the mass number), and the additional quantum number $\alpha_{\rm c}$. The bases of particles are labeled by the number of particles in the j_0 orbital n ($n=0,2,4,\cdots,2j_0+1$) , seniority v, angular momentum J, and the additional quantum number $\alpha_{\rm p}$. It should be noted that states of particles are described in the laboratory frame, not in the intrinsic frame of the core. Consequently spherical bases are used for the particles.

Since wave functions described in the intrinsic frame are convenient to understand the structure of states, we now express the bases on the right hand side of eq. (4.81) in terms of so-called strong coupling bases in which particles are described in the frame of the principal axis of the deformation of the core. Quantum numbers having nothing to do with rotations are included in $\alpha_{\rm c}$ and $\alpha_{\rm p}$ from now on in this paper:

$$|{j_0}^n(v\alpha_{\rm p})JM\rangle \quad\rightarrow\quad |JM\alpha_{\rm p}\rangle\ , \tag{4.82}$$

$$|RM\alpha_{\rm c}, A-n\rangle \quad\rightarrow\quad |RM\alpha_{\rm c}\rangle\ . \tag{4.83}$$

Eq. (4.81) is expressed briefly as

$$|IM\alpha\rangle = \sum_{R\alpha_{\rm c}J\alpha_{\rm p}} A^{I\alpha}_{R\alpha_{\rm c}J\alpha_{\rm p}}[\ |R\alpha_{\rm c}\rangle \otimes |J\alpha_{\rm p}\rangle\ ]^{IM}\ . \tag{4.84}$$

Due to the fact that the particle bases have definite angular momentum, we can rotate the particle bases together with the intrinsic frame of the core by a relatively simple transformation,

$$|JM\alpha_{\rm p}\rangle = \sum_{K_{\rm p}=-J}^{J} |JK_{\rm p}\alpha_{\rm p}\rangle_{\Omega_{\rm c}} D^J_{MK_{\rm p}}(\Omega_{\rm c})\ . \tag{4.85}$$

The subscript $\Omega_{\rm c}$ attached to the ket-vector indicates that the state is expressed in the intrinsic frame. Using eqs. (4.13)-(4.15) and (4.85), we obtain

$$|\,[R\alpha_{\rm c}\otimes J\alpha_{\rm p}]^{IM}\rangle = \sum_{K_{\rm c}=-R}^{R}\sum_{K_{\rm p}=-J}^{J} B^{RJI}_{K_{\rm c}K_{\rm p}}|\Phi^{\alpha_{\rm c}}_{RK_{\rm c}}(\gamma)\rangle|JK_{\rm p}\alpha_{\rm p}\rangle_{\Omega_{\rm c}}|IM,K_{\rm c}+K_{\rm p}(\Omega_{\rm c})\rangle\ , \quad (4.86)$$

where

$$B^{RJI}_{K_{\rm c}K_{\rm p}} = \sqrt{\frac{2R+1}{2I+1}}\langle RK_{\rm c}JK_{\rm p}|I,\ K_{\rm c}+K_{\rm p}\rangle\ . \quad (4.87)$$

The state of the core as for γ can be expanded by employing bases independent of R and $K_{\rm c}$,

$$|\Phi^{\alpha_{\rm c}}_{RK_{\rm c}}(\gamma)\rangle = 3\int_0^{\pi/3} d\gamma_0\ \sin 3\gamma_0\ \Phi^{\alpha_{\rm c}}_{RK_{\rm c}}(\gamma_0)\ |\delta(\gamma-\gamma_0)\rangle\ . \quad (4.88)$$

Expanding the bases on the right hand side of eq. (4.84) using eq. (4.86) and eq. (4.88), we obtain

$$|IM\alpha\rangle = 3\int_0^{\pi/3} d\gamma_0 \sin 3\gamma_0 \sum_{J\alpha_{\rm p}}\sum_{K_{\rm c}K_{\rm p}} C^{I\alpha}_{\gamma_0 J\alpha_{\rm p}K_{\rm c}K_{\rm p}}|\delta(\gamma-\gamma_0)\rangle\,|JK_{\rm p}\alpha_{\rm p}\rangle_{\Omega_{\rm c}}\,|IMK_{\rm c}+K_{\rm p}(\Omega_{\rm c})\rangle\ , \quad (4.89)$$

where

$$C^{I\alpha}_{\gamma_0 J\alpha_{\rm p}K_{\rm c}K_{\rm p}} = \sum_{R\alpha_{\rm c}} A^{I\alpha}_{R\alpha_{\rm c}J\alpha_{\rm p}} B^{RJI}_{K_{\rm c}K_{\rm p}}\Phi^{\alpha_{\rm c}}_{RK_{\rm c}}(\gamma_0)\ . \quad (4.90)$$

As an application of the new expansion (4.89), we show the expression for the probability distribution of the K-quantum number. The K-quantum number is the component of the total angular momentum I along the third principal axis of the core [2]. The third components of R and J in the intrinsic frame of the core are denoted by $K_{\rm c}$ and $K_{\rm p}$ respectively ($K = K_{\rm c}+K_{\rm p}$) . The quantum number $K_{\rm c}$ takes on only even integers due to the symmetry as for π-rotation around the 3-axis, while $K_{\rm p}$ and K take on both even and odd integers.

We can define the probability of K-quantum numbers as follows,

$$\begin{aligned}\rho_{I\alpha}(K_{\rm c},K_{\rm p}) &= 3\int_0^{\pi/3} d\gamma_0 \sin 3\gamma_0 \sum_{J\alpha_{\rm p}} |C^{I\alpha}_{\gamma_0 J\alpha_{\rm p}K_{\rm c}K_{\rm p}}|^2 \\ &= \sum_{J\alpha_{\rm p}R'\alpha'_{\rm c}R\alpha_{\rm c}} (A^{I\alpha}_{R'\alpha'_{\rm c}J\alpha_{\rm p}})^* B^{R'JI}_{K_{\rm c}K_{\rm p}}\langle\Phi^{\alpha'_{\rm c}}_{R'K_{\rm c}}(\gamma)|\Phi^{\alpha_{\rm c}}_{RK_{\rm c}}(\gamma)\rangle A^{I\alpha}_{R\alpha_{\rm c}J\alpha_{\rm p}} B^{RJI}_{K_{\rm c}K_{\rm p}} \quad (4.91)\end{aligned}$$

[2]It should be noted that the third principal axis is always the longest axis even in a γ-fluctuating model because $0\le\gamma\le\pi/3$ in our choice. This condition is explicitly taken into account in the interval of integration with respect to γ for inner product (eq. (4.19)).

Considering the R_1 symmetry of the core (eq. (4.16)) and

$$B^{RJI}_{-K_{\rm c},-K_{\rm p}} = (-1)^{R+J-I} B^{RJI}_{K_{\rm c},K_{\rm p}} \quad , \tag{4.92}$$

we can obtain

$$\begin{aligned} \rho_{I\alpha}(-K_{\rm c},-K_{\rm p}) &= \sum_{J\alpha_{\rm p}R'\alpha'_{\rm c}R\alpha_{\rm c}} (A^{I\alpha}_{R'\alpha'_{\rm c}J\alpha_{\rm p}})^* B^{R'JI}_{-K_{\rm c}-K_{\rm p}} \langle \Phi^{\alpha'_{\rm c}}_{R'-K_{\rm c}}(\gamma) | \Phi^{\alpha_{\rm c}}_{R-K_{\rm c}}(\gamma) \rangle A^{I\alpha}_{R\alpha_{\rm c}J\alpha_{\rm p}} B^{RJI}_{-K_{\rm c}-K_{\rm p}} \\ &= \rho_{I\alpha}(K_{\rm c},K_{\rm p}) \ . \end{aligned} \tag{4.93}$$

By summing up ρ for K and ρ for $-K$, we define the probability for $|K|$ as

$$\rho_{I\alpha}(|K|) = 2\ (1+\delta_{|K|\,0})^{-1} \sum_{K_{\rm c}} \rho_{I\alpha}(K_{\rm c},|K|-K_{\rm c}) \ . \tag{4.94}$$

4.2.3 The Coriolis interaction in the laboratory-frame model

In the strong-coupling particle-rotor model, the Coriolis interaction is obtained from the rotational energy term in the hamiltonian (eq. 3.9). In the weak-coupling model described in the laboratory frame, the rotational energy term $T_{\rm rot}$ (eq. 4.10) concerns only to the core coordinates and it might seem that there were no Coriolis interaction.

The two models are, however, equivalent as for the treatment of rotation. When the coordinates of the particles are transformed from those referring to the laboratory frame (say $\vec{x}$)to those based on the intrinsic frame of the core (say $\vec{\xi}$), H_{QQ} (eq. (4.64)) becomes independent of the Euler angles of the core ($\Omega_{\rm c}$):

$$\begin{aligned} H_{QQ} &= -\kappa \sum_{\mu} (-1)^{\mu} \frac{\alpha_{2\mu}}{\beta_0}\ Y_2^{-\mu}(\hat{x}) \\ &= -\kappa \sum_{\nu} (-1)^{\nu} \frac{a_{2\nu}}{\beta_0}\ Y_2^{-\nu}(\hat{\xi}) \ , \end{aligned} \tag{4.95}$$

where a_ν does not depend on $\Omega_{\rm c}$ (eq. (4.3–4.5)). Thus $\Omega_{\rm c}$ becomes a cyclic coordinate and its conjugate momentum becomes an integral of motion, i. e. the total angular momentum. Other angular-momentum operators of the partial systems are expressed through the coordinates shown below:

	Intrinsic-frame model	Laboratory-frame model
$\vec{R}$	$\Omega_{\rm c}$, $\vec{\xi}$	$\Omega_{\rm c}$
$\vec{J}$	$\vec{\xi}$	$\vec{x}$
$\vec{I}$	$\Omega_{\rm c}$	$\Omega_{\rm c}$, $\vec{x}$

Hence $T_{\rm rot}$ turns out to contain the interaction between the core coordinates and the particle coordinates, i. e. the Coriolis interaction. This situation is clearly shown by rewriting $\vec{R}$ as $\vec{I}-\vec{J}$ (since $\vec{I}$=$\vec{R}$+$\vec{J}$),

$$T_{\rm rot} \;=\; \sum_{\kappa=1}^{3} \frac{\hbar^2}{2\mathcal{J}_\kappa} R_\kappa^2 \;=\; \sum_{\kappa=1}^{3} \frac{\hbar^2}{2\mathcal{J}_\kappa} (I_\kappa - J_\kappa)^2 \;, \tag{4.96}$$

where I_κ concerns only to $\Omega_{\rm c}$ while J_κ depends solely on $\vec{\xi}$.

4.2.4 Advantages of the description in the laboratory frame

In order to treat the particle-rotor model, there are two approaches, the weak coupling one and the strong coupling one. In the former (the latter), the particle-rotor model hamiltonian is diagonalized in the weak (strong) coupling bases. Results are the same between the two approaches if they are obtained exactly. But in practical calculations, it is important to clarify merits and demerits of the two approaches.

The strong coupling approach has an advantage in the truncation of the particle states: Particle bases are usually taken as Nilsson single-particle states, which are generally thought to be good approximation. But we have to take into account more configurations than usual in treating the $K^\pi = 10^+$ isomers, because the Coriolis mixing effect is stronger in the high-j unique-parity orbital than in other orbitals. It is also stronger at high spin than at low spin. Thus it is not very clear whether we may consider only a few Nilsson orbitals.

In the weak coupling approach the number of bases is likely to become enormous. This is a shortcoming inherent in the shell model. But in treating the isomers in which only single-j configurations are involved, the number of states is small enough, so that truncation is not necessary using the computers in the present day. Hence it is not a defect of the approach.

Furthermore, the weak coupling approach has an advantage that it is relatively easy to consider various motions of the core like the γ-vibration : We can solve the core and the particle system separately and then couple them only through the quadrupole-quadrupole and the Cooper-pair exchange interactions which are strong but simple. Existing algorithms are available to solve the core models. In the strong coupling model, however,

the rotations of the total system, intrinsic collective motions like the γ-vibration, and the motions of the particles are coupled in such a complicated way that they can not be separated effectively. Thus we take the weak coupling approach.

4.2.5 Electromagnetic transitions

Operators of electromagnetic transitions are expressed as follows:

$$\mathcal{M}(\mathrm{M1},\mu) = \mu_{\mathrm{N}}\sqrt{\frac{3}{4\pi}}\left(g_{\mathrm{c}}\vec{R} + g_{\nu}\sum_{m'}\sum_{m}\langle j_0 m'|\vec{J}|j_0 m\rangle a^{\dagger}_{j_0 m'}a_{j_0 m}\right) , \tag{4.97}$$

with

$$\begin{cases} g_{\mathrm{c}} &= Z/A \ , \\ g_{\nu} &= -0.223 \quad \text{assuming} \quad g_l = -0.05 \quad \text{and} \quad g_s = 0.6 \times g_s^{\mathrm{free}} \ , \end{cases} \tag{4.98}$$

and

$$\mathcal{M}(\mathrm{E2},\mu) = \frac{3ZeR_0^2}{4\pi}\alpha_{2\mu} + \sum_{m'}\sum_{m}\langle j_0 m'|e^{\mathrm{eff}}r^2 Y_2^{\mu}(\theta,\varphi)|j_0 m\rangle a^{\dagger}_{j_0 m'}a_{j_0 m} \ , \tag{4.99}$$

with

$$\begin{cases} R_0 &= 1.2\,\mathrm{fm} \times A^{1/3} \ , \\ e^{\mathrm{eff}} &= eZ/A \ . \end{cases} \tag{4.100}$$

In the above expressions, $\mu_{\mathrm{N}}(= e\hbar/2m_{\mathrm{p}}c)$ is the nuclear magneton, and A and Z are the mass and the atomic number of the nucleus. The value of the neutron's g-factor is taken from ref. [8] (observed g_ν of the $[624]9/2^+$ orbital is -0.22 for ^{179}Hf). In order to calculate the matrix element of r^2, we assume the harmonic oscillator wave function (eq. (4.67)).

Table 4.1: Number of states of the γ-unstable core for each spin R and each seniority λ. The multiplicity of states due to the degeneracy as for M is not counted.

R	μ	$\lambda\ (=\ \mu\ +\ 3\ n_\gamma\ ;\ n_\gamma = 0, 1, 2, 3, \cdots)$															
		0	1	2	3	4	5	6	7	8	9	10	11	12	13	14	15
0	$0 \le \mu \le 0$	1			1			1			1			1			1
1	$2 \le \mu \le 1$																
2	$1 \le \mu \le 2$		1	1		1	1		1	1		1	1		1	1	
3	$3 \le \mu \le 3$				1			1			1			1			1
4	$2 \le \mu \le 4$			1	1	1	1	1	1	1	1	1	1	1	1	1	1
5	$4 \le \mu \le 5$					1	1		1	1		1	1		1	1	
6	$3 \le \mu \le 6$				1	1	1	2	1	1	2	1	1	2	1	1	2
7	$5 \le \mu \le 7$						1	1	1	1	1	1	1	1	1	1	1
8	$4 \le \mu \le 8$					1	1	1	2	2	1	2	2	1	2	2	1
9	$6 \le \mu \le 9$							1	1	1	2	1	1	2	1	1	2
10	$5 \le \mu \le 10$						1	1	1	2	2	2	2	2	2	2	2
11	$7 \le \mu \le 11$								1	1	1	2	2	1	2	2	1
12	$6 \le \mu \le 12$							1	1	1	2	2	2	3	2	2	3
13	$8 \le \mu \le 13$									1	1	1	2	2	2	2	2
14	$7 \le \mu \le 14$								1	1	1	2	2	2	3	3	2
15	$9 \le \mu \le 15$										1	1	1	2	2	2	3
16	$8 \le \mu \le 16$									1	1	1	2	2	3	3	3
17	$10 \le \mu \le 17$											1	1	1	2	2	2
18	$9 \le \mu \le 18$										1	1	1	2	2	2	3
19	$11 \le \mu \le 19$												1	1	1	2	2
20	$10 \le \mu \le 20$											1	1	1	2	2	2
21	$12 \le \mu \le 21$													1	1	1	2
22	$11 \le \mu \le 22$												1	1	1	2	2
23	$13 \le \mu \le 23$														1	1	1
24	$12 \le \mu \le 24$													1	1	1	2

Table 4.2: Number of states of the triaxial rotor model for each R. The multiplicity of states due to the degeneracy as for M is not counted.

R	0	1	2	3	4	5	6	7	8	9	10	11	12	13	14	15	16	17	18	19	20
min K_c	0	2	0	2	0	2	0	2	0	2	0	2	0	2	0	2	0	2	0	2	0
max K_c	0	0	2	2	4	4	6	6	8	8	10	10	12	12	14	14	16	16	18	18	20
# states	1	0	2	1	3	2	4	3	5	4	6	5	7	6	8	7	9	8	10	9	11

Table 4.3: Number of states of the axially symmetric rotor model for each R. The multiplicity of states due to the degeneracy as for M is not counted.

R	0	1	2	3	4	5	6	7	8	9	10	11	12	13	14	15	16	17	18	19	20
# states	1	0	1	0	1	0	1	0	1	0	1	0	1	0	1	0	1	0	1	0	1

Table 4.4: The two-body interaction for the neutrons in the $i_{13/2}$ orbital.

	delta int.	delta int. G=0.120 MeV	Onishi-Negele A=176,Z=76
J	g_J/G	g_J [MeV]	g_J [MeV]
0	−7.0000	−0.840	−0.907
2	−1.7231	−0.207	−0.400
4	−0.9329	−0.112	−0.142
6	−0.6062	−0.073	−0.078
8	−0.4168	−0.050	−0.046
10	−0.2818	−0.034	−0.027
12	−0.1642	−0.020	+0.010

Table 4.5: Number of states of n fermions in a single j orbital ($1/2 \leq j \leq 7/2$). The multiplicity of states due to the degeneracy as for M is not counted.

j=1/2		
$2 \times J$	0	Total
v=0	1	1
$2 \times J$	1	Total
v=1	1	1

j=3/2				
$2 \times J$	0	2	4	Total
v=0	1			1
v=2			1	1
$2 \times J$	1	3	5	Total
v=1		1		1

j=5/2						
$2 \times J$	0	2	4	6	8	Total
v=0	1					1
v=2			1		1	2
$2 \times J$	1	3	5	7	9	Total
v=1			1			1
v=3		1			1	2

j=7/2										
$2 \times J$	0	2	4	6	8	10	12	14	16	Total
v=0	1									1
v=2			1		1		1			3
v=4			1		1	1			1	4
$2 \times J$	1	3	5	7	9	11	13	15	17	Total
v=1				1						1
v=3		1	1		1	1		1		5

Table 4.6: Number of states of n fermions in a single j orbital ($9/2 \leq j \leq 13/2$). The multiplicity of states due to the degeneracy as for M is not counted.

j=9/2														
$2 \times J$	0	2	4	6	8	10	12	14	16	18	20	22	24	Total
v=0	1													1
v=2			1		1		1		1					4
v=4	1		1	1	2	1	2	1	1	1	1		1	13
$2 \times J$	1	3	5	7	9	11	13	15	17	19	21	23	25	Total
v=1					1									1
v=3		1	1	1	1	1	1	1	1		1			9
v=5	1		1	1	1	1	1	1	1	1			1	10

j=11/2																				
$2 \times J$	0	2	4	6	8	10	12	14	16	18	20	22	24	26	28	30	32	34	36	Total
v=0	1																			1
v=2			1		1		1		1		1									5
v=4	1		2	1	3	2	3	2	3	2	2	1	2	1	1		1			27
v=6	1		1	2	2	1	3	2	2	2	2	1	2	1	1	1			1	25
$2 \times J$	1	3	5	7	9	11	13	15	17	19	21	23	25	27	29	31	33	35	37	Total
v=1						1														1
v=3		1	1	1	2	1	1	2	1	1	1	1		1						14
v=5	1	1	2	3	2	3	3	3	3	3	2	2	2	1	1	1		1		34

j=13/2																				
$2 \times J$	0	2	4	6	8	10	12	14	16	18	20	22	24	26	28	30	32	34	36	
v=0	1																			
v=2			1		1		1		1		1		1							
v=4	1		3	1	4	3	4	3	5	3	4	3	3	2	3	1	2	1	1	
v=6	2	1	3	4	6	4	8	6	7	7	7	5	7	5	5	4	4	2	3	
$2 \times J$	38	40	42	44	46	48														Total
v=0																				1
v=2																				6
v=4		1																		48
v=6	2	1	1	1		1														96
$2 \times J$	1	3	5	7	9	11	13	15	17	19	21	23	25	27	29	31	33	35	37	
v=1							1													
v=3		1	1	1	2	2	1	2	2	1	2	1	1	1	1		1			
v=5	1	2	4	4	5	5	6	6	6	6	6	5	5	4	4	3	2	2	2	
v=7	2	1	2	4	3	4	5	4	5	5	4	4	5	3	3	3	2	2	2	
$2 \times J$	39	41	43	45	47	49														Total
v=1																				1
v=3																				20
v=5	1	1		1																81
v=7	1	1	1			1														67

Chapter 5

Details of the numerical calculation

5.1 Parameters of the model

The following values are used for the parameters of the model:

parameter	^{182}W	(^{182}W)	^{184}Os
$\epsilon_{\rm c}$	given in table 5.1		
β_0	0.24	(0.22)	0.20
κ	$=\hbar\omega\beta_0(N_{j_0}+3/2)$		
G	0.120 MeV		
Δ'	0.527 MeV	(0.564 MeV)	0.639 MeV
$\epsilon_{j_0}-\lambda_{\rm c}$	-0.629 MeV	(-0.552 MeV)	-0.480 MeV

As for ^{182}W, besides the best fitted parameter set ($\beta_0 = 0.24, \cdots$), we used another set ($\beta_0 = 0.22, \cdots$) for the sake of comparison. These values are determined in the manners described below:

1. $\epsilon_{\rm c}$: The energy-scaling parameter of the core ($=2\hbar^2/B{\beta_0}^2$).
   It is adjusted so as to fit the excitation energy of the $2^+_{\rm gr}$ state to the experimental value (0.100 MeV for ^{182}W and 0.120 MeV for ^{184}Os) including the effects of coupling with the particles.

2. β_0 : The deformation parameter.
   The value of β_0 is determined in order to reproduce the experimental transition amplitudes between the $0^+_{\rm gr}$ state and the $2^+_{\rm gr}$ state [70] including the effects of coupling with the particles. Calculated reduced matrix elements for this transition

are given in table 5.2. It can be seen from the table that the experimental values are reproduced within ±2% by using β_0=0.24 for ^{182}W and within the interval from −3% to +1% by setting β_0=0.20 for ^{184}Os. Thus we determine not to change the value of β_0 from core to core and to fix it at the single value for each nucleus. As for ^{182}W, we also use β_0=0.22 for comparison.

3. κ : The strength of the quadrupole-quadrupole interaction.
   Its value is obtained using eq. (4.68), where a harmonic oscillator single-particle potential is assumed. We calculated the value of κ for a Woods-Saxon potential with parameters given in ref. [8] (for A=182 and Z=76) and obtained $\kappa = 1.07 \times \hbar\omega\beta_0\ (N_{j_0} + 3/2)$ for the $\nu i_{13/2}$ orbital. But we do not employ this value because the parameters for the spherical potentials do not seem very reliable especially in deformed nuclei.

4. G : The strength of the two body interaction in the $\nu i_{13/2}$ orbital.
   We used eq. (4.58) to determine its value.

5. Δ' : The strength of the Cooper-pair exchange interaction.
   Its value is determined so that the experimental excitation energy of the $K^\pi = 10^+$ isomer (2.231 MeV for ^{182}W and 2.365 MeV for ^{184}Os) is reproduced when the axially symmetric rotor is employed as the core. The obtained values of Δ' are used for all the cores because the difference of core models does not affect significantly the energy level of the isomer.
   By using eq. (4.76), we can estimate the value of Δ' microscopically. By employing the single-particle space of two oscillator shells (N=5,6), where the parameters of the Nilsson potential are taken from ref. [8], we solved the BCS gap equation with G=0.120 MeV under a constraint $\langle\#\text{neutron}\rangle = 108$ and obtained

$$\Delta'_{\text{micro}} = 0.633 \text{ MeV} \quad (\Delta_{\text{micro}} = 0.821 \text{ MeV}) \text{ for } ^{182}\text{W},\ \beta_0 = 0.24\ ,$$
$$\Delta'_{\text{micro}} = 0.714 \text{ MeV} \quad (\Delta_{\text{micro}} = 0.943 \text{ MeV}) \text{ for } ^{184}\text{Os},\ \beta_0 = 0.20\ .$$

   These values are only a little larger (by 11-20%) than the adopted values.

6. $(\epsilon_{j_0} - \lambda_{\rm c})$: The energy necessary to transfer a neutron from the Fermi level to the $i_{13/2}$ orbital.

   It is determined so that the expectation value of n (the number of neutrons in the $i_{13/2}$ orbital) becomes 10 in the ground state when the axially symmetric rotor is used as the core. The value of n is expected to be 10 from the Nilsson diagram of energy levels for N=108 isotones. These values are used for all the cores because the expectation value of n is found not sensitive to the shape of the γ-potential.

5.2 Truncation of states and its convergence

5.2.1 Full inclusion of the particle states

We solve the eigenvalue equation for $H_{\rm PR}$ by numerical diagonalization. The number of particle states $|j_0^n\rangle$ $(n = 0, 2, 4, \cdots, 14)$ is 428 (see table 4.6, the multiplicity due to the degeneracy with respect to m is not counted) and all of them are taken into account. Therefore we do not have to assume the weakness of the coupling between the core and the particles, although we use so-called weak coupling bases.

In the early works using the laboratory-frame particle-rotor model, only low-seniority ($v \leq 2$) states are included in order to keep the matrix dimensions in manageable size [56]-[58]. The seniority truncation was, however, shown to be a poor approximation at least when the j_0-orbital is half occupied [59]. This result is plausible considering the deformation of the nucleus. Therefore we should not truncate states according to the value of seniority, which is a suitable quantum number for labeling states in spherical nuclei.

We take into account all the allowed values also for n. The probability distribution of n are shown in table 5.3 for states of the particles $\otimes$ core system. It seems that states with $n \leq 2$ may be excluded on account of their small probabilities. But reduction of matrix size due to such truncation is only very small. Thus such truncation is useless.

5.2.2 Truncation of the core states

The angular momentum of the core is restricted by $R \leq 20$. This truncation is confirmed to have no effects on the decay amplitudes of the $K^\pi = 10^+$ isomers. The number of

states of the γ-soft core is, however, infinite at each spin R and we must truncate them in numerical diagonalization. We use two schemes of truncation.

1. **The λ'-truncation scheme**

   In this scheme, core states with $\lambda \leq \lambda'_{\max}$ are included in the case of the γ-unstable model, where $\lambda'_{\max}$ is an arbitrarily chosen number. When $V(\gamma)$ is not constant, the same number of states from the yrast level for each R are taken into account as are included in the γ-unstable case using the same $\lambda'_{\max}$. An illustration of this truncation scheme is given in figure 5.1 for a rather γ-soft core. The energy spectrum of this core is hardly disturbed compared to the unperturbed ($V(\gamma) = 0$) spectrum (eq. (4.25)) except for in the neighborhood of the yrast levels.

   It should be noted that the core states are obtained by diagonalizing $H_{\gamma-\text{soft}}$ in the space of $\lambda \leq 24$ when $V(\gamma) \neq 0$. Thus for more γ-stiff potentials, less number of core eigenstates are necessary since the coupling with the particles has smaller effects compared to $V(\gamma)$. The energy spectrum for a rather γ-stiff core is shown in figure 5.2. By using the same $\lambda'_{\max}$, higher-lying states can be included in comparison with the case of the γ-soft core (figure 5.1).

2. **The N_γ-truncation scheme**

   In the harmonic γ-vibrational model (neglecting the rotation-vibration coupling), states are labeled by R, N_γ, and $|K_{\rm c}|$, where N_γ is the number of γ-vibrational phonons. The following values are taken on by $|K_{\rm c}|$ for each N_γ :

   $$|K_{\rm c}| = 2N_\gamma, 2N_\gamma - 4, 2N_\gamma - 8, \cdots, \begin{cases} 0 & \text{for even } N_\gamma \ , \\ 2 & \text{for odd } N_\gamma \ . \end{cases} \tag{5.1}$$

   In the N_γ-truncation scheme, we include core states having N_γ not greater than $N_\gamma^{\max}$, where $N_\gamma^{\max}$ is an arbitrarily chosen number. For anhamonic cores (like cores of the γ-soft model and the triaxial rotor model), the same number of states from the yrast level for each R are taken into account. The number of states for each $N_\gamma^{\max}$ and each R is given in table 5.4. Figure 5.3 illustrates this truncation scheme.

We show the effects of truncation of core states on isomeric decay probabilities and some energy levels for ^{182}W in table 5.5 and for ^{184}Os in table 5.6. The employed cores are

those of the γ-soft model whose γ-softness V_1 is determined to reproduce the experimental energy of the γ-bandhead while V_2 is assumed to be zero.

In the N_γ-truncation scheme, some isomeric decay probabilities do not converge with respect to $N_\gamma^{\max}$ even if 4-phonon states are included. In order to calculate small quantities like transition matrix elements of isomeric decays, small components of wave functions must be treated very carefully. This truncation scheme is not suitable for treating isomeric decays in γ-soft nuclei.

On the other hand, in the λ'-truncation scheme, it seems sufficient to take into account the core states with $\lambda_{\max}$=11 in order to obtain enough accuracy in the calculation of the decay probabilities. Hence in the calculations where the γ-soft model is employed, we include core states with $R \leq 20$ and $\lambda_{\max} = 11$. In other words, in terms of energy levels, we include the core states with energies about less than 8 MeV. ($\epsilon_c \simeq 0.2$ MeV.)

As for the triaxial rotor model, number of states at each spin R are finite and relatively small, and we can include all the states (satisfying Bohr's symmetry) with $R \leq 20$. The energy spectrum for γ_0=15° rotor is shown in figure 5.4.

5.3 Convergence in the Lanczos algorithm for the Diagonalization

The dimension of the matrix to be diagonalized at $I = 10$ is 3158 if only the ground band states of the core are taken into account. It is 40362 when core states with $\lambda_{\max} = 11$ and $R \leq 20$ are employed. (See table 5.6.) Thus some efficient methods are necessary in numerical diagonalization.

We use the Lanczos algorithm [71]. In this method an initial vector is multiplied by the hamiltonian to generate the second vector with intervening orthogonalization. And the descendent vectors are generated by iterating this procedure. The sequence of vectors thus obtained makes new bases which almost exhaust the eigenstates whose eigenvalues are near the both ends of the spectrum, even when the procedure is stopped in the half-way.

The convergence of isomeric decay amplitudes are confirmed as for the number of iterations, i. e. the number of new bases thus obtained. It is found sufficient to iterate about 110 times. Energy levels converge more quickly. We obtained the results presented

in this paper by iterating $120 \sim 150$ times.

Table 5.1: The energy-scaling parameter of the core ϵ_c ($=2\hbar^2/B{\beta_0}^2$) used in the calculation. They are determined so as to fit the experimental values of $E(2^+_{gr})$ (and also $E(2^+_\gamma)$ in parts (C)$\sim$(E)) including the effects of coupling with the particles.

Core model	ϵ_c [MeV]		
(V_1, V_2) or γ	^{182}W β_0=0.24	^{182}W β_0=0.22	^{184}Os β_0=0.20
(A) γ-vibrational model			
$(0, 0)$	—	0.1630	0.1780
$(-2, 0)$	0.1831	0.1754	0.1973
$(-4, 0)$	0.1914	0.1844	0.2115
$(-6, 0)$	0.1974	0.1909	0.2215
$(-8, 0)$	0.2019	0.1957	0.2286
$(-10, 0)$	0.2054	0.1994	0.2337
$(-12, 0)$	0.2081	0.2023	0.2377
(B) Triaxial rotor model			
γ_0=30°	—	—	0.1758
γ_0=25°	0.1655	0.1617	0.1916
γ_0=20°	0.1881	0.1835	0.2173
γ_0=15°	0.2100	0.2048	0.2426
γ_0=12°	0.2213	0.2158	0.2556
γ_0=10°	0.2277	0.2220	0.2630
γ_0=0°	0.2429	0.2367	0.2805
(C) Those reproducing $E(2^+_\gamma)$ of ^{184}Os, β_0=0.20			
$(-2.99, 0)$	—	—	0.2050
$(-5.71, 3)$	—	—	0.2071
$(-10.05, 7)$	—	—	0.2097
$(-20.12, 15)$	—	—	0.2129
$(-41.59, 30)$	—	—	0.2165
$(-72.96, 50)$	—	—	0.2194
γ_0=14.89°	—	—	0.2431
(D) Those reproducing $E(2^+_\gamma)$ of ^{182}W, β_0=0.22			
$(-6.96, 0)$	—	0.1935	—
γ_0=12.18°	—	0.2152	—
(E) Those reproducing $E(2^+_\gamma)$ of ^{182}W, β_0=0.24			
$(-6.05, 0)$	0.1975	—	—
γ_0=12.32°	0.2202	—	—

Table 5.2: Calculated and experimental reduced E2 matrix elements between the 0^+_{gr} state and the 2^+_{gr} state.

Core model	$\langle 0^+_{gr}\|\|\mathcal{M}(E2)\|\|2^+_{gr}\rangle$ [e fm^2]		
(V_1, V_2) or γ	^{182}W β_0=0.24	^{182}W β_0=0.22	^{184}Os β_0=0.20
(A) γ-vibrational model			
$(0, 0)$	—	—	173
$(-2, 0)$	200	184	173
$(-4, 0)$	200	184	174
$(-6, 0)$	201	185	174
$(-8, 0)$	202	185	175
$(-10, 0)$	202	186	175
$(-12, 0)$	202	186	175
(B) Triaxial rotor model			
γ_0=30°	—	—	179
γ_0=25°	201	186	175
γ_0=20°	200	184	174
γ_0=15°	202	186	176
γ_0=12°	204	188	177
γ_0=10°	205	189	178
γ_0=0°	208	191	181
(C) Those reproducing $E(2^+_\gamma)$ of ^{184}Os, β_0=0.20			
$(-2.99, 0)$	—	—	173
$(-5.71, 3)$	—	—	173
$(-10.05, 7)$	—	—	173
$(-20.12, 15)$	—	—	173
$(-41.59, 30)$	—	—	173
$(-72.96, 50)$	—	—	173
γ_0=14.89°	—	—	176
(D) Those reproducing $E(2^+_\gamma)$ of ^{182}W, β_0=0.22			
$(-6.96, 0)$	—	185	—
γ_0=12.18°	—	188	—
(E) Those reproducing $E(2^+_\gamma)$ of ^{182}W, β_0=0.24			
$(-6.05, 0)$	201	—	—
γ_0=12.32°	204	—	—
Experiment	204	204	179

Table 5.3: Probability distribution of the number of particles in the $\nu i_{13/2}$ orbital.

^{184}Os, $(V_1, V_2) = (-2.99, 0)$, β_0=0.20				
n	Probability at $10^+_{\rm gr}$	Probability at $10^+_{K=10}$	The number of particle states	The Number of states of the total system at I=10
0	9.05×10^{-8}	$1.\times10^{-12}$	1	11
2	1.49×10^{-5}	6.98×10^{-7}	7	591
4	8.40×10^{-4}	1.14×10^{-4}	55	5247
6	1.99×10^{-2}	6.09×10^{-3}	151	14332
8	1.94×10^{-1}	1.25×10^{-1}	151	14332
10	6.05×10^{-1}	8.30×10^{-1}	55	5247
12	1.73×10^{-1}	3.89×10^{-2}	7	591
14	6.83×10^{-3}	1.38×10^{-7}	1	11
Total	1	1	428	40362

Table 5.4: The number of states of the γ-vibrational model.

Truncation scheme	R																	
	0	1	2	3	4	5	6	7	8	9	10	11	12	13	14	15	16	$\cdots$
$N_\gamma^{\max}$=0	1		1		1		1		1		1		1		1		1	
$N_\gamma^{\max}$=1	1		2	1	2	1	2	1	2	1	2	1	2	1	2	1	2	
$N_\gamma^{\max}$=2	2		3	1	4	2	4	2	4	2	4	2	4	2	4	2	4	
$N_\gamma^{\max}$=3	2		4	2	5	3	6	4	6	4	6	4	6	4	6	4	6	
$N_\gamma^{\max}$=4	3		5	2	7	4	8	5	9	6	9	6	9	6	9	6	9	
$N_\gamma^{\max}$=5	3		6	3	8	5	10	7	11	8	12	9	12	9	12	9	12	

Table 5.5: Effects of the truncation of the core states on the isomeric decays and some energy levels for ^{182}W. B(M1) and B(E2)$^{\rm a}$ belong to the transition from the 10^+_2 to $10^+_{\rm gr}$. B(E2)$^{\rm b}$ belongs to the transition to $8^+_{\rm gr}$. The last column gives the number of states of the core without counting the degeneracy with respect to the magnetic quantum number.

^{182}W, $(V_1, V_2) = (-6.05, 0)$, β_0=0.24, $R \leq 20$							
Truncation scheme	B(M1) [$\mu_{\rm N}^2$]	B(E2)$^{\rm a}$ [e^{2}fm^4]	B(E2)$^{\rm b}$ [e^{2}fm^4]	E(2^+_γ) [MeV]	E($10^+_{\rm gr}$) [MeV]	E(10^+_2) [MeV]	Number of core states
$\lambda'_{\rm max} = 11$	5.87×10^{-8}	1.77×10^{-4}	6.10×10^{-5}	1.222	1.626	2.199	123
$\lambda'_{\rm max} = 10$	5.87×10^{-8}	1.77×10^{-4}	6.10×10^{-5}	1.222	1.626	2.199	98
$\lambda'_{\rm max} = 9$	5.97×10^{-8}	1.80×10^{-4}	6.21×10^{-5}	1.222	1.627	2.199	76
$\lambda'_{\rm max} = 8$	6.08×10^{-8}	1.82×10^{-4}	6.70×10^{-5}	1.224	1.636	2.199	57
$\lambda'_{\rm max} = 7$	5.87×10^{-8}	2.14×10^{-4}	7.66×10^{-5}	1.230	1.679	2.200	42
$N_\gamma^{\rm max} = 4$	5.76×10^{-8}	1.67×10^{-4}	6.10×10^{-5}	1.224	1.625	2.199	133
$N_\gamma^{\rm max} = 3$	7.68×10^{-8}	2.86×10^{-4}	6.63×10^{-5}	1.237	1.625	2.198	92
$N_\gamma^{\rm max} = 2$	1.90×10^{-9}	7.17×10^{-5}	2.84×10^{-5}	1.304	1.623	2.197	58
$N_\gamma^{\rm max} = 1$	5.90×10^{-7}	3.53×10^{-3}	2.26×10^{-4}	1.452	1.613	2.191	30
$N_\gamma^{\rm max} = 0$	6.63×10^{-6}	1.43×10^{-2}	7.81×10^{-3}	—	1.723	2.222	11

Table 5.6: Effects of the truncation of the core states on the isomeric decays and some energy levels for ^{184}Os. B(M1) and B(E2)$^{\rm a}$ belong to the transition from the 10^+_2 to $10^+_{\rm gr}$. B(E2)$^{\rm b}$ belongs to the transition to $8^+_{\rm gr}$. The last column gives the number of states of the coupled system consisting of the core and the $i_{13/2}$ neutrons at I=10 and at a certain value of M.

^{184}Os, $(V_1, V_2) = (-2.99, 0)$, β_0=0.20, $R \leq 20$							
Truncation scheme	B(M1) [$\mu_{\rm N}^2$]	B(E2)$^{\rm a}$ [e^{2}fm^4]	B(E2)$^{\rm b}$ [e^{2}fm^4]	E(2^+_γ) [MeV]	E($10^+_{\rm gr}$) [MeV]	E(10^+_2) [MeV]	Dimension at I=10
$\lambda'_{\rm max} = 11$	2.64×10^{-5}	4.51×10^{-2}	1.45×10^{-2}	0.943	1.791	2.354	40362
$\lambda'_{\rm max} = 10$	2.64×10^{-5}	4.50×10^{-2}	1.45×10^{-2}	0.943	1.791	2.354	31848
$\lambda'_{\rm max} = 9$	2.64×10^{-5}	4.50×10^{-2}	1.46×10^{-2}	0.943	1.792	2.354	24256
$\lambda'_{\rm max} = 8$	2.68×10^{-5}	4.51×10^{-2}	1.56×10^{-2}	0.944	1.799	2.354	17786
$\lambda'_{\rm max} = 7$	3.04×10^{-5}	5.15×10^{-2}	2.16×10^{-2}	0.946	1.836	2.354	12456
$N_\gamma^{\rm max} = 4$	2.63×10^{-5}	4.50×10^{-2}	1.45×10^{-2}	0.944	1.791	2.354	42274
$N_\gamma^{\rm max} = 3$	2.77×10^{-5}	4.70×10^{-2}	1.51×10^{-2}	0.949	1.791	2.354	29068
$N_\gamma^{\rm max} = 2$	2.21×10^{-5}	2.97×10^{-2}	1.25×10^{-2}	0.991	1.788	2.354	17966
$N_\gamma^{\rm max} = 1$	1.25×10^{-4}	2.10×10^{-1}	5.25×10^{-2}	1.189	1.780	2.357	9160
$N_\gamma^{\rm max} = 0$	9.45×10^{-4}	3.95×10^{-1}	7.02×10^{-1}	—	1.916	2.423	3158

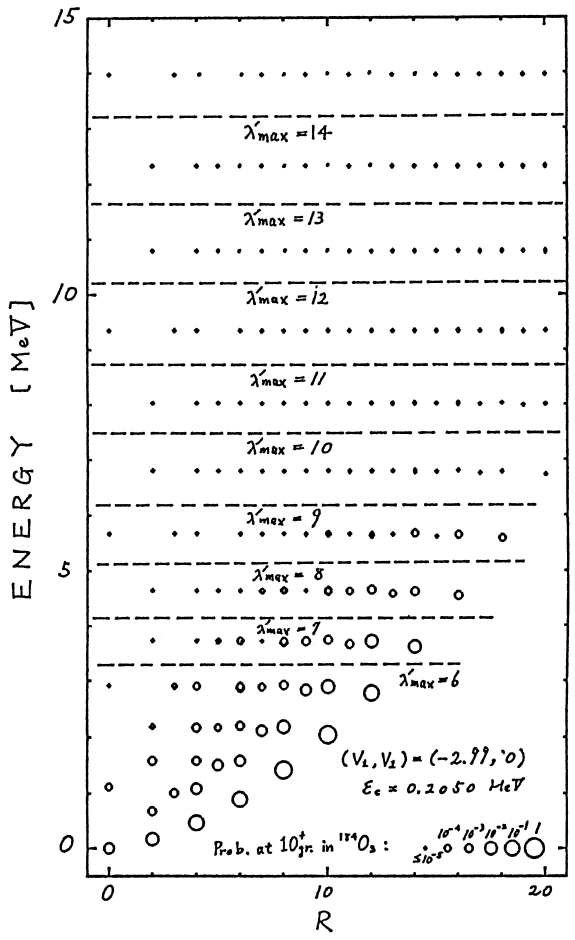

Figure 5.1: The scheme of the λ'-truncation for the states of the core. A rather γ-soft core is used.

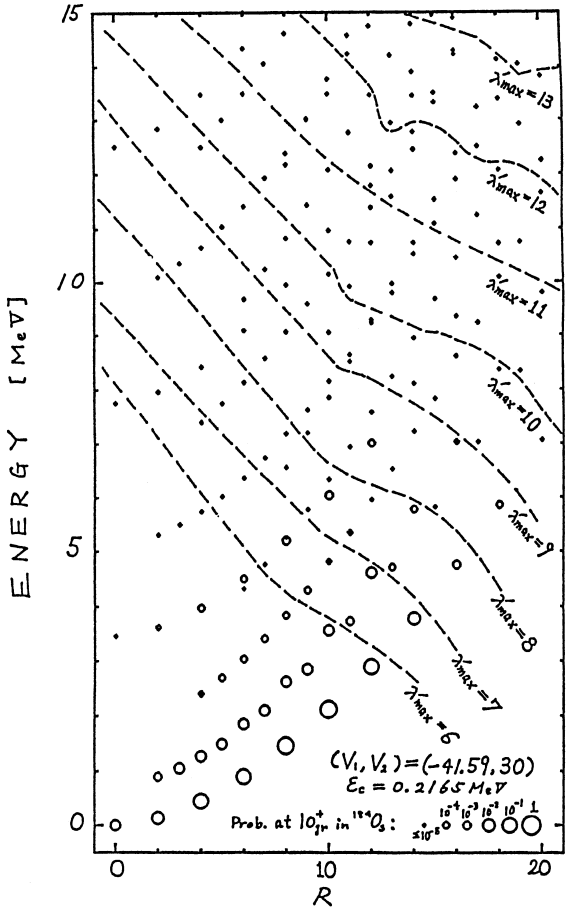

Figure 5.2: The scheme of the λ'-truncation for the states of the core. A rather γ-stiff core is used.

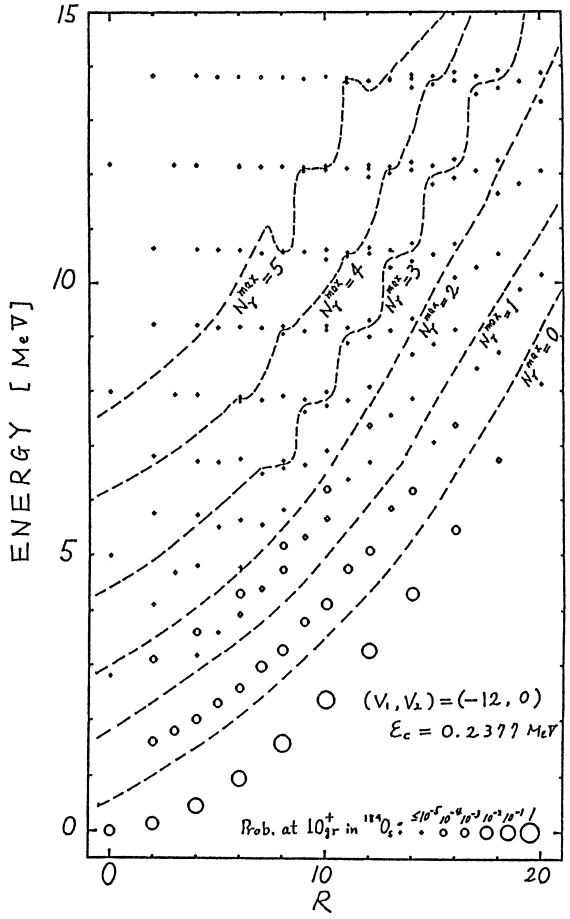

Figure 5.3: The scheme of the N_γ-truncation for the states of the core.

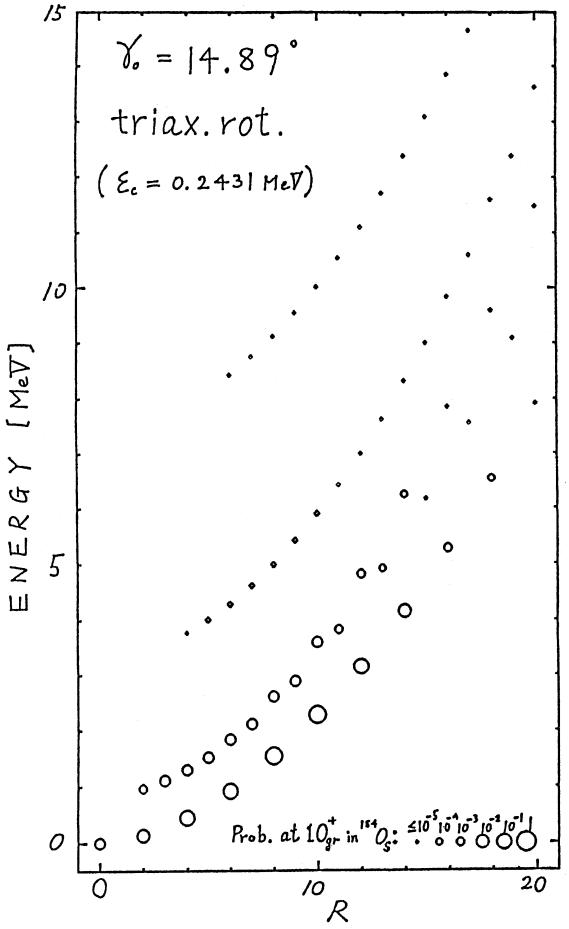

Figure 5.4: Energy spectrum of the triaxial rotor model with γ_0=14.89°.

Chapter 6

Results of numerical calculations

6.1 Features of axially symmetric rotor $\otimes$ ν $i_{13/2}$ system

At first let us learn the decay of high-K isomers in a model in which the axially symmetric rotor is coupled with the $i_{13/2}$ neutrons in order to see the effects of Coriolis mixing separately from those concerning the γ-degree of freedom.

We calculate the partial half-lives of the $K^\pi = 10^+$ isomers, considering only the M1 and the E2 transitions into the members of the ground band (the $8^+_{\rm gr}$ and the $10^+_{\rm gr}$ states). Transition energies used in calculating transition probabilities are taken from experiments to concentrate our attention on the changes in wave functions. The contribution of internal electron conversion process is negligible ($\alpha_{\rm K} < 6 \times 10^{-2}$) for the enegies and the multipolarities of these transitions [13] [72].

Using parameters described in chapter 5, we obtain the follwoing partial half-lives.

	^{182}W		^{184}Os
	β_0=0.24		β_0=0.20
Experiment	1.4μs	$\overset{\times 12}{\leftarrow}$	120 ns
	$\downarrow \times$ 2300		$\downarrow \times$ 17
Calculation	3.20 ms	$\overset{\times 1600}{\leftarrow}$	2.05μs

The calculated half-lives are much longer than the experimental ones.

Now we show the effects of changing parameters. Among the parameters of the model, $\epsilon_{\rm c}$ and κ (or β_0) have large effects on the decay amplitudes of the isomer, while G, Δ',

and $\epsilon_{j_0} - \lambda_c$ do not affect them much (see figure 6.1).

Effects of changing the energy scaling parameter of the core (ϵ_c) are shown in table 6.1. Other parameters are those adjusted for ^{184}Os described in chapter 5. The energy level of the 2^+_{gr} state (including the effects of coupling with the particles) is shown in the second column (E(2^+_{gr})). The half-life of the isomer decrease rapidly with the increase in ϵ_c: The B(M1) and the B(E2) values of the decay from the isomer increase by a factor of about 10 when E(2^+_{gr}) increases by 10 keV from 120 keV. But the large ϵ_c reproducing the experimental half-life can not consistently reproduce the experimental energy spectrum of the ground band.

This strong dependence of isomeric decay probabilities on ϵ_c is due to the fact that ϵ_c is the factor of the Coriolis mixing perturbation (see eqs. (3.9) and (**??**)). The probability distribution of the K-quantum number is shown in figure 6.2 for the 10^+_{gr} state and the $K^\pi = 10^+$ isomer. We can see that the degree of K-mixing becomes large when ϵ_c increases. The anomalous enhancement of the probability around K=10 (K=0) for the 10^+_{gr} state (the $K^\pi = 10^+$ isomer) means the mixing of the two states caused by the crossing of their energy levels.

In table 6.2, we show the effects of changing the strength κ of the quadrupole-quadrupole interaction for ^{184}Os. The quantity $\kappa/\hbar\omega(N_{j_0} + 3/2)$ given in the first column is equal to the deformation parameter β_0 when a harmonic oscillator single-particle potential is assumed, although we did not change the value of β_0 in the definition (4.99) of the E2 transition operator $\mathcal{M}$(E2) ($\alpha_{2\mu} \propto \beta = \beta_0$). Since the change in κ largely affects the number of neutrons (n) in the $i_{13/2}$ orbital, we adjust the value of $\epsilon_{j_0} - \lambda_c$ for each value of κ in order to maintain $\langle n \rangle = 10$ in the ground state. From the table, it can be said that κ has also large effects on the decay amplitudes. In order to reproduce the experimental half-life of the isomer, $\kappa/\hbar\omega(N_{j_0} + 3/2)$ must be 0.17, which means, however, too small deformation for ^{184}Os.

These large effects of the change in κ on the half-lives of the isomer can be explained as follows: The quadrupole-quadrupole interaction H_{QQ} separates the energy levels of orbitals having different Ω. When its strength κ becomes large, the energy denominator of the Coriolis perturbation increases and the mixing of K is depressed. The changes in

the K-mixing are shown in figure 6.3.

Considering this strong dependence of the Coriolis mixing on parameters, we can say that the *difference* in the half-lives of the isomer between the two nuclei are not simply ascribed to the diffecrence in the γ-softness. In fact, from table 6.1, when the energy level of the $2^+_{\rm gr}$ state is decreased from 120 keV (like in ^{184}Os) to 100 keV (like in ^{182}W), the half-life becomes longer by a factor of 40. From table 6.2, when the deformation parameter β_0 ($=\kappa/\hbar\omega(N_{j_0}+3/2)$) is increased from 0.20 (like in ^{184}Os) to 0.24 (like in ^{182}W), the half-life becomes longer by a factor of 30. Totally, the calculated half-life for ^{182}W is 1600 times as large as that for ^{184}Os, which exceeds the experimental difference (12 times) without the γ-degree of freedom.

In conclusion, using the axially symmetric rotor, the *absolute values* of the experimental half-lives are overestimated with reasonable values of κ (or deformation β_0) and $\epsilon_{\rm c}$ (or moment of inertia). The analyses in this section invoke the introduction of the γ-degree of freedom.

6.2 Effects of the γ-degree of freedom

Next, we take into account the γ-degree of freedom and calculate the half-lives of the isomers. In this section we employ the two extreme models treating the γ-degree of freedom. One is the γ-vibrational model, i. e. the γ-soft model of eq. (4.11) which has a γ-potential of eq. (4.20) with V_2=0:

$$V(\gamma) \;=\; \epsilon_{\rm c} V_1 \cos 3\gamma \;. \tag{6.1}$$

In the model, the variable γ fluctuates around γ=0°. The other is the triaxial rotor model of eq. (4.33), in which γ is fixed at some constant value γ_0.

The parameters of the model are fixed at the values described in chapter 5. In the calculation of half-lives, we take into account only the M1 and the E2 transitions into the ground band states ($8^+_{\rm gr}$ and $10^+_{\rm gr}$). Although the isomer can decay into the 8^+_γ state in our model, its contribution to the total half-life is very small according to our calculation: The transition from the isomer to the 8^+_γ state and the transition to the $8^+_{\rm gr}$ state have amplitudes of the same order, but the energy of the γ-ray in the former transition is about

one-tenth as large as that in the latter transition. The I=9 state to which the isomer decays with a large fraction in experiment for ^{184}Os does not exist in our model space. The transition energies are taken from the experiments as in the last section.

In figures 6.4-6.6 we show the relationship between the half-life of the $K^\pi = 10^+$ isomer and the energy level of the γ-bandhead for ^{184}Os using β_0=0.20, ^{182}W using β_0=0.22, and ^{182}W using β_0=0.24, respectively. Figure 6.5 (β_0=0.22) is given for reference, although the experimental value of B(E2;$2^+_{\rm gr} \rightarrow 0^+_{\rm gr}$) is reproduced well when β_0=0.24 (as in figure 6.6). The two models with some values of V_1 (for the γ-vibrational model) and γ (for the triaxial rotor model) are used in each fugure. We can see a general tendency, as we expected, that the half-lives of the isomers become shorter as the core becomes more γ-soft or more γ-deformed. When the triaxial rotor model is used in figures 6.5–6.6, however, the partial half-life behaves irregularly with respect to γ_0. This anomaly would be due to the interference between the Coriolis interaction and the triaxial potential exerted by the core.

The most remarkable point in figures 6.4–6.6 is that the half-lives calculated with the γ-vibrational model are shorter than those calculated with the triaxial rotor model by more than two orders of magnitude. This characteristic feature is discussed in detail in the following sections in comparison with quantities of collective character which are not changed much between the two models.

When the γ-softness (V_1) or the size of the γ-deformation (γ_0) is determined by fitting the energy of the γ-bandhead to the experimental value (including the effects of coupling with the particles) for each core model, the experimental half-lives are located between (or in the neighborhoods of) those calculated with the two extreme models. Assuming the present set of parameters are reliable, we can say that the nucleus ^{182}W is much like the γ-vibrational model while the nucleus ^{184}Os is rather like the triaxial rotor model from the viewpoint of K-isomeric decays. It should be noted that this result does not necessarily mean the rigid triaxial nature of some transitional nuclei (^{184}Os), as the success of Meyer-ter-Vehn's model did not (see chapter 2). In later sections, we show that the crucial point in these K-isomeric decays is how large the quantum fluctuation in the size of triaxial deformation is, not whether the equilibrium shape is triaxial or not. It can be

said that we can extend our knowledge about the shape of the γ-potential from the degree of violation of the K-selection rule.

We show the probability distribution of the K-quantum number, defined by eq. (4.94), for the $10^+_{\rm gr}$ state and the isomer in ^{184}Os in figs. 6.7 and 6.8. The γ-vibrational model is employed in figure 6.7, while the triaxial rotor model is utilized in figure 6.8. If we utilize the axially symmetric rotor model (γ=0°), the probability distribution is linear in the logarithmic scale: The Coriolis interaction is just perturbative. If we introduce the γ-degree of freedom, the probabilities of large-K (small-K) components increase largely in the ground band state (in the isomer) for the both models. Since the probabilities of the mixing of the K-quantum number have strong correlations with the calculated half-lives shown in figure 6.4, we can say, as we expected, that the reduction in the half-lives follows the mixing of K-quantum number.

6.3 Effects of the coupling with the particles on the core

Before discussing the K-isomeric decays more intensively, we just mention how the properties of the core are changed through the coupling with the ∼10 neutrons in the $i_{13/2}$ orbital.

1. The moment of inertia increase by ∼20% (judging from the energy of the $2^+_{\rm gr}$ state when the axially symmetric rotor model is used).

2. The E2 transition amplitudes increase by ∼7% (in the transition from the $2^+_{\rm gr}$ state to the $0^+_{\rm gr}$ state).

3. The M1 transitions occur through the coupling with the particles, while they do not exist between the states of bare cores (since $\mathcal{M}(\mathrm{M1})_{\rm core} \propto \vec{R}$, where $\vec{R}$ is a conserved quantity).

4. The γ-softness is decreased when the γ-soft model is used. The probability distribution function of γ for the state $|IM\alpha\rangle$ (eq. (**??**)) of the system consisting of the

core and the particles are defined as

$$\rho_{I\alpha}(\gamma_0) = \frac{1}{3\sin 3\gamma_0}\langle IM\alpha|\delta(\gamma-\gamma_0)|IM\alpha\rangle = \sum_{J\alpha_{\rm p}RK_{\rm c}}\Big|\sum_{\alpha_{\rm c}} A^{I\alpha}_{R\alpha_{\rm c}J\alpha_{\rm p}}\Phi^{\alpha_{\rm c}}_{RK_{\rm c}}(\gamma_0)\Big|^2 , \quad (6.2)$$

which satisfies the normalization condition of

$$3\int_0^{\pi/3}\rho_{I\alpha}(\gamma_0)\sin 3\gamma_0 d\gamma_0 \;=\; 1 \; . \quad (6.3)$$

In figure 6.10, these probability distributions are shown for the γ-potentials given in the upper right hand portion of figure 6.9. Comparing the distributions with those for the bare cores (also given in the figure), we can see the γ-stiffening effects of the particles.

The γ-driving effects of the particles are likely to be simulated by an effective γ-potential, which can be estimated using the single-j Nilsson model: We put 10 neutrons into the $i_{13/2}$ orbital with a quadratically deformed single-particle potential specified by β_0 and γ_0. The energy of the ground state configuration is regarded as the potential energy for deformation $V^{\rm p}(\beta_0,\gamma_0)$, where the superscript p attached to V indicates that the potential is of the particles. We determine the value of $V_1^{\rm p}$ so that $2\epsilon_{\rm c}V_1^{\rm p} = V^{\rm p}(\beta_0,0^\circ) - V^{\rm p}(\beta_0,60^\circ)$. We obtain $\epsilon_{\rm c}V_1^{\rm p} = -1.27$ MeV (i. e. $V_1^{\rm p} \simeq -6$) for ^{182}W (β_0=0.24) and $\epsilon_{\rm c}V_1^{\rm p} = -1.05$ MeV (i. e. $V_1^{\rm p} \simeq -5$) for ^{184}Os. These effective γ-potentials of the particles and the γ-potentials of the bare core are of the same order of magnitude. We must include this contribution from the particles together with the γ-potential of the bare core in order to obtain the effective γ-potential for the entire nucleus.

5. The effective size of γ-deformation of the coupled system ($\gamma^{\rm eff}$) is hardly changed from the value of γ_0 of the bare core when the triaxial rotor model is used. We can define $\gamma^{\rm eff}$ for each state in such a way that the quadrupole moment [1] of a bare triaxial rotor having $\gamma_0 = \gamma^{\rm eff}$ agrees with that of the coupled system. In the case of $\gamma_0 = 15^\circ$ for ^{184}Os, $\gamma^{\rm eff}$ turns out nearly equal to γ_0 at low spin and slightly less (by $\sim 1^\circ$) than γ_0 at $I \sim 10$ in the states of the ground band.

[1] Quadrupole moments ($\propto \langle I||\mathcal{M}(\mathrm{E2})||I\rangle$) are sensitive to the γ-deformation, while E2 transitions ($\langle I-2||\mathcal{M}(\mathrm{E2})||I\rangle$) are not.

6.4 Effects of the potential shape

We investigate the effects of the shape of the γ-potential to explain the difference in the half-life of the K-isomer between the two extreme models. The γ-soft model having positive values of V_2 mediates between the two models studied in the last section. We consider the isomer only in ^{184}Os in this section.

We use the γ-potentials of the form of eq. (4.20). We vary V_2 to change the shape of the γ-potential, while V_1 is determined for each V_2 so that the experimental energy level of the γ-bandhead is reproduced including the effects of coupling with the particles. Other parameters are fixed at the values adjusted for ^{184}Os as described in chapter 5. The shapes of the γ-potentials used in the calculation are illustrated in the upper right hand portion of figure 6.9. The γ-potential changes in the shape from a potential having a relatively shallow minimum at γ=0° (the γ-vibrational model) to a deep potential well having a minimum at a finite value of γ (close to the limit of the triaxial rotor model). In the upper left hand portion of figure 6.9, the shapes of γ-potentials for the γ-vibrational model (V_2=0) are also shown for comparison.

On the left hand side of figure 6.11, we show the effects of changing the shape of the γ-potential on the decay probabilities of the $K^\pi = 10^+$ isomer. The probabilities of the decay of the isomer decrease rapidly as the shape of the γ-potential approaches the limit of the triaxial rotor model.

Collective transitions are, however, not affected much. Some of them are shown on the right hand side of figure 6.11. Among the transitions and moments in the ground band, the γ-band, and the $K^\pi = 10^+$ band ($I \leq 12$), the most largely changing ones of collective character are the quadrupole moments of the high spin states of the γ-band. They are presented as B(E2) values in the figure, which change by a factor of order one with the replacement of the γ-vibrational core by the triaxial rotor one. But their changes are much less than the changes in the isomeric transitions which vary by a factor of order two. Calculated transition probabilities from the isomer are summarized in table 6.3. Other reduced E2 transition probabilities at low spin are shown in table 6.4 for reference.

The lower right hand portion of figure 6.9 shows the probability distribution of the

variable γ in the ground state. (The particles are not coupled with [2].) It is defined as

$$\rho'_{R\alpha_c}(\gamma_0) = \langle RM\alpha_c|\delta(\gamma-\gamma_0)|RM\alpha_c\rangle = 3\sin 3\gamma_0 \sum_{K_c=-R}^{R} |\Phi^{\alpha_c}_{RK_c}(\gamma_0)|^2 \ . \tag{6.4}$$

The prime ($'$) is attached to $\rho_{R\alpha_c}$ in order to designate that the volume element $(3\sin 3\gamma)$ is inlcuded. The follwoing normalization condition is fulfilled by $\rho'_{R\alpha_c}$,

$$\int_0^{\pi/3} \rho'_{R\alpha_c}(\gamma_0)d\gamma_0 \ = \ 1 \ . \tag{6.5}$$

We can see that the peak of the distribution of γ stays at almost the same location, but the tail of the distribution decreases drastically with the change in the shape of the γ-potential. Therefore the origin of the difference between collective transitions and the isomeric ones seems that the former are determined by the average value of γ, while the latter are determined by the fluctuation in γ, i. e. the tail of the wave function at large γ: The components of large γ-deformation are necessary to mix the K-quantum number and to violate the K-selection rule. Further investigations are given in the next section.

As for this enhancement of the K-isomeric transitions due to the γ-softness, other explanations are conceivable, which turn out unsuccessful in this case.

1. The γ-soft core can change its shape at high spin (so as to increase the moment of inertia), while the triaxial rotor can not. But in our calculation such a change in shape is found very small up to I=10, which is seen from figure 6.10. More specifically, the value of $\gamma^{\rm eff}$ (defined in section 6.3) varies from $\gamma^{\rm eff} \simeq 17^\circ$ (at I=2) to $\gamma^{\rm eff} \simeq 15.5^\circ$ (at I=10) in the ground band states of the system consisting of the particles and the γ-soft core with $(V_1, V_2) = (-2.99, 0)$. This change in $\gamma^{\rm eff}$ is opposite [50] [52] to explain the difference in the half-life between the two models.

2. The isomeric state is expected to be more γ-soft than no-quais-particle states on account of the change in the configuration, when γ-soft cores are used. The γ-driving forces of the particles in the isomer are estimated to be weaker than those in the ground band states by a factor of 0.7 judging from the effective γ-potential calculated for the lowest one-particle one-hole state in the framework of the single-j

[2]Probability distribution of γ for the coupled system are found in figure 6.10, where the volume element of $(3\sin 3\gamma)$ is not included.

Nilsson model described in section 6.2 . But such effects are also small, as is shown in figure 6.10.

Now let us check the details of the isomeric decay for ^{184}Os. The multipolarity of the transition from the isomer to the $10^+_{\rm gr}$ state is dominantly M1 in experiment. In our calculation, the contribution of M1 is ≥ 0.97 for the cases given in the part (C) of table 6.3, in good agreement with the experiment.

The experimental branching ratio of the $8^+_{\rm gr}$ state to the $10^+_{\rm gr}$ state is 2.0 in the decay of the isomer. The calculated ratios are 0.47 to 0.67 for the cases given in the part (C) of table 6.3, which are not in quantitative agreements with the experiment.

Before ending this section, we discuss the shape of the γ-potential preferred by the K-isomeric decay rates for ^{184}Os. In order to reproduce the experimental half-life of the isomer in addition to $E(2^+_\gamma)$, we have to employ a γ-potential having $(V_1, V_2) \simeq (-62, 43)$, which is obtained by interpolating the calculated half-lives given in table 6.3. The shape of this γ-potential is shown in figure 6.12. It is worth while noting that the form of the γ-potential is restricted to linear combinations of $P_1(\cos 3\gamma)$ and $P_2(\cos 3\gamma)$ (eq. 4.20) in our calculations. Inclusion of higher order terms ($P_3(\cos 3\gamma)$, $P_4(\cos 3\gamma)$,$\cdots$) will bring about different γ-potentials which also reproduce the half-life and $E(2^+_\gamma)$. In particular, the shape of $V(\gamma)$ near $\gamma = 0^\circ$ may be easily changed through such inclusion of the higher order terms, since neither the K-isomeric decay rates nor collective quantities like $E(2^+_\gamma)$ have much information on the wave function at small γ. The potential energy at $\gamma = 60^\circ$ also has large ambiguities: it is very high (29 MeV from the ground state energy) and is unlikely to have significant meaning. The determination of the coefficints of the higher order terms $(V_3, V_4, \cdots)$ is a problem for future works.

6.5 Further investigation of the fast K-isomeric decays due to the γ-softness

In this section, we investigate the mechanism through which the K-isomer decays quickly. At first we calculate the probability distribution of the K-quantum number for each value of γ. It is defined for the state $|IM\alpha\rangle$ (eq. (**??**)) as

$$\begin{aligned}\rho_{I\alpha}(\gamma_0, K_{\rm c}, K_{\rm p}) &= \sum_{J\alpha_{\rm p}} |C^{I\alpha}_{\gamma_0 J\alpha_{\rm p} K_{\rm c} K_{\rm p}}|^2 \qquad (6.6)\\ &= \sum_{J\alpha_{\rm p} R'\alpha'_{\rm c} R\alpha_{\rm c}} \{A^{I\alpha}_{R'\alpha'_{\rm c} J\alpha_{\rm p}} B^{R'JI}_{K_{\rm c}K_{\rm p}} \Phi^{\alpha'_{\rm c}}_{R'K_{\rm c}}(\gamma_0)\}^* A^{I\alpha}_{R\alpha_{\rm c} J\alpha_{\rm p}} B^{RJI}_{K_{\rm c}K_{\rm p}} \Phi^{\alpha_{\rm c}}_{RK_{\rm c}}(\gamma_0) \ .\end{aligned}$$

It fulfills the normalization condition of

$$\sum_{K_{\rm c}K_{\rm p}} 3\int_0^{\pi/3} \rho_{I\alpha}(\gamma_0, K_{\rm c}, K_{\rm p}) d\gamma_0 \sin 3\gamma_0 \ = \ 1 \ . \qquad (6.7)$$

The expression for the total K-quantum number, $\rho_{I\alpha}(\gamma_0, |K|)$, is given in the same manner as eq. (4.94).

In figures 6.13 and 6.14, $\rho_{I\alpha}(\gamma, |K|)$ is shown for the $10^+_{\rm gr}$ state and the K^π=10^+ isomer, respectively, for ^{184}Os. The γ-potentials are those reproducing the experimental $E(2^+_\gamma)$ including the effects of coupling with the particles. The distribution of the K-quantum number,

$$\rho_{I\alpha}(|K|) = 3\int_0^{\pi/3} \rho_{I\alpha}(\gamma_0, |K|) \sin 3\gamma_0 d\gamma_0, \qquad (6.8)$$

is also shown. (The definition (6.8) is equivalent to eq. (4.94).) From figure 6.14, we can see that the large deviation from the Coriolis-like K-mixing (i. e. probability distributions linear in logarithmic scale) is mainly due to the components of the wave function with large γ-deformations. When we alter the core from the γ-vibrational one (part **A** of the figure) to the γ-stiff one (part **C**), the components with large γ-deformations are depressed on account of the decrease in the amplitude of the quantum fluctuation in γ. Consequently, the anomalous K-mixing diminishes.

Another point to be seen in figure 6.14 is the existence of the second peak around K=0 when $\gamma \sim 0°$: The two states mix with each other in spite of the large difference in the structure and in the energy level ($\sim$ 0.5MeV). The height of the second peak is lowered when the core becomes γ-stiff (**A** $\rightarrow$ **C**). Therefore this mixing is likely to be caused by

the γ-softness. It may be regarded as the result of the barrier penetration process through the γ=60° shape presented by Chowdhury and his coworkers [13] described in chapter 1 [3].

Next, we study the distribution of the isomeric transition amplitudes with respect to γ. The E2 transition amplitude can be expressed as an integral with respect to the size of γ-deformation,

$$\langle \text{final state}||\mathcal{M}(\text{E2})||\text{initial state}\rangle \;=\; 3\int_0^{\pi/3} t(\gamma_0)\sin 3\gamma_0 d\gamma_0 \;, \tag{6.9}$$

where

$$t(\gamma_0) \;=\; \frac{1}{3\sin 3\gamma_0}\langle \text{final state}||\mathcal{M}(\text{E2})\delta(\gamma-\gamma_0)||\text{initial state}\rangle \;. \tag{6.10}$$

The values of $t(\gamma_0)$ are shown in figure 6.15 for the transitions from the isomer, where the effective charge of the $i_{13/2}$ neutrons (e^{eff}) is set to 0 (i. e. only the core part of $\mathcal{M}$(E2) is considered): The transition amplitudes due to the particles are smaller than those by the core by an order of magnitude. It is seen from the figure that the main contribution to the isomeric transitions comes from small γ-deformation components, in spite of the fact that the large-K mixing is principally due to large γ-deformation componets.

In conclusion, the anomalously large K-mixing in the γ-vibrational model is attributed to the quantum fluctuation in shape into large γ-deformations, as is speculated in section 4. The K-isomeric transitions occur, however, mainly at small γ-deformations. Therefore the isomeric transitions are likely to occur principally from the small-amplitude ground-band-like components (with small γ) to the main component of the ground-band state (and from the main component of the isomer to the small-amplitude K=10 component in the ground-band state), not directly between the components having large γ. The fluctuation in γ plays the crucial role in mixing the ground-band state and the isomer. A probable picture for such mixing is the the barrier penetration mechanism via the largely γ-deformed shape. But treatments based on such picture can not be quantitative, since the transition amplitudes are rather widely spread as for γ.

[3]It should be noted, however, that we can not see the second peak in the probability distribution of K, on the contrary to the conjecture in the figure 10 of ref. [13], if we integrate the probability with respect to γ: The peak is covered by the larger-amplitude components having large γ-deformations, i. e. the components at the potential barrier, at least for the K^π=10^+ isomer. This situation is attributed to the mismatching in energy. It is also worth while noting that the γ-potential of ^{184}Os is like that in (**C**), not like that in (**A**).

6.6 Effects of the shape of the γ-potential on energy levels

In this section we compare the calculated energy levels (including the effects of coupling with the particles) with the experimental ones for the nucleus ^{184}Os. When we limit the shape of the γ-potential to those with $V_2 = 0$, we have to use $V_1 \simeq -3$ so as to reproduce the experimental energy level of the γ-bandhead. But if we fit the spectrum of the ground band to the experimental one, the best value for V_1 is about -5. Thus γ-potentials including higher multipolarity terms (eq. (4.20)) are required.

In figure 6.16 we show the energy spectrum of the ground, the γ-, and the $K^\pi = 10^+$ bands for the γ-potentials shown in the upper right hand portion of figure 6.9, in which the energy level of the γ-bandhead is fitted to the experimental value. The agreement of the spectrum of the ground band with the experimental one is improved by using $V_2 > 0$. The odd-even staggering of the spectrum of the γ-band is also reproduced rather well by using a core which lies between the γ-vibrational model and the triaxial rotor model. The γ-potentials required by these energy levels are consistent with those preferred by the half-life of the K-isomer in a qualitative way. They are also consistent with microscopically calculated potentials for nearby nuclei [19] in a qualitative way. The energy spectra of the same bands for the γ-vibrational potentials (V_2=0) are also shown in figure 6.17 for reference.

The energy spectrum of the yrast band at the first backbending region is shown in figure 6.18. Experimental and calculated spectra are expressed in terms of the angular velocity $\omega_{\rm rot}$ and the kinematical moment of inertia $\mathcal{J}^{(1)}$. Assuming that the energy levels of a rotational band are expressed by a function of L^2 where $L = \hbar\sqrt{I(I+1)}$, these new quantities are defined as follows.

$$\omega_{\rm rot} = \frac{dE}{dL} \simeq \frac{E_{I+1} - E_{I-1}}{2\hbar} \quad \text{at } I\,, \tag{6.11}$$

$$\mathcal{J}^{(1)} = \frac{L}{\omega_{\rm rot}} \simeq \frac{\hbar^2(2I+1)}{E_{I+1} - E_{I-1}} \quad \text{at } I\,. \tag{6.12}$$

We used three kinds of cores, i. e. , the axially symmetric rotor model, the triaxial rotor model with $\gamma_0 = 14.89°$, and the γ-soft model with (V_1, V_2)=$(-2.99, 0)$. The latter two

models reproduce the experimental $E(2^+_\gamma)$ including the effects of coupling with the particles. In the γ-soft model, we truncate the core states according to the N_γ-truncation scheme with $N_\gamma^{\max}$=4 so as to include enough number of states at high spin. Among the three models, the triaxial rotor model reproduces the experimental backbending behavior most excellently. This result is consistent with the prediction of the K-isomeric decay rate. But other factors like the β-vibration would also affect the yrast spectrum as strong as the γ-degree of freedom. Therefore more elaborate studies seem necessary to draw any conclusion about the γ-degree of freedom from the backbending behavior.

Now we point out the defects of our model in the energy levels. The moment of inertia of the calculated γ-band is smaller than that of the experimental γ-band. It is also smaller than the moment of inertia of the calculated ground band: This is a characteristic of the γ-soft model, at least when the γ-potential of the form of eq. (4.20) is assumed. On the contrary, the calculated moment of inertia of the $K^\pi = 10^+$ band is larger than the experimental one.

To summarize, the γ-potential which fits the partial half-life of the K-isomer also improves the agreement of the some calculated energy levels with the experimental ones. But for some of other levels, we do not obtain very good agreements between the calculated energy levels and the experimental ones. This is not a very surprising result because we concentrated on the γ-degree of freedom and suppressed many others, e. g. the β-vibrational degree of freedom.

Table 6.1: Effects of changing the energy scaling parameter of the core ($\epsilon_{\rm c}$) on the partial half-life of the $K^\pi = 10^+$ isomer in ^{184}Os. When $\epsilon_{\rm c}$=$\epsilon_{\rm c}^0$ (=0.2805 MeV), the experimental $E(2^+_{\rm gr})$ is reproduced including the effects of coupling with the particles. The last column gives the branching ratio of the $8^+_{\rm gr}$ state to the $10^+_{\rm gr}$ state in the depopulation of the K^π=10^+ isomer.

$\epsilon_{\rm c}/\epsilon_{\rm c}^0$	E($2^+_{\rm gr}$) [MeV]	$\tau_{1/2}$ [sec]	Br($8^+_{\rm gr}/10^+_{\rm gr}$)
0.4	0.052	1.43×10^{0}	2×10^{-5}
0.5	0.064	4.75×10^{-2}	0.030
0.6	0.076	4.10×10^{-3}	0.095
0.7	0.087	5.26×10^{-4}	0.201
0.8	0.098	8.12×10^{-5}	0.353
0.9	0.109	1.34×10^{-5}	0.572
1.0	0.120	2.05×10^{-6}	0.882
1.1	0.130	2.28×10^{-7}	1.28
1.2	0.141	5.11×10^{-9}	1.75
exp.	0.120	1.20×10^{-7}	2.0

Table 6.2: Effects of changing the strength of the quadrupole-quadrupole interaction (κ) on the partial half-life of the $K^\pi = 10^+$ isomer in ^{184}Os. As for the last column, see the comments of table 6.1.

$\kappa/\hbar\omega(N_{j_0}+3/2)$	$\tau_{1/2}$ [sec]	Br($8^+_{\rm gr}/10^+_{\rm gr}$)
0.14	4.18×10^{-9}	1.22
0.16	4.64×10^{-8}	1.12
0.18	3.38×10^{-7}	0.995
0.20	2.05×10^{-6}	0.882
0.22	1.08×10^{-5}	0.780
0.24	5.82×10^{-5}	0.685
0.26	3.32×10^{-4}	0.620
exp.	1.20×10^{-7}	2.0

Table 6.3: Summary of decay properties of the $K^\pi = 10^+$ isomer.

Summary of the transitions from the K^π=10^+ isomers						
Core model (V_1, V_2) or γ_0	$E(2^+_\gamma)$ [MeV]	B(M1) to 10^+_{gr} [μ_N^2]	B(E2) to 10^+_{gr} [e^2fm^4]	B(E2) to 8^+_{gr} [e^2fm^4]	$\tau_{1/2}$ to 8^+_{gr} and 10^+gr (Using experimental energies)	Br($8^+_{gr}/10^+$gr)
(A) ^{184}Os, γ-vibrational model						
$(0, 0)$	0.631	4.06×10^{-4}	$1.99\times10^{+2}$	6.41×10^{-2}	84.6 ps	0.015
$(-2, 0)$	0.838	4.42×10^{-5}	8.30×10^{-2}	2.14×10^{-2}	5.04 ns	0.413
$(-4, 0)$	1.048	1.57×10^{-5}	2.68×10^{-2}	9.56×10^{-3}	13.2 ns	0.521
$(-6, 0)$	1.247	6.15×10^{-6}	1.13×10^{-2}	4.34×10^{-3}	32.0 ns	0.603
$(-8, 0)$	1.429	2.85×10^{-6}	5.51×10^{-3}	2.18×10^{-3}	66.9 ns	0.653
$(-10, 0)$	1.596	1.55×10^{-6}	3.12×10^{-3}	1.25×10^{-3}	120. ns	0.685
$(-12, 0)$	1.751	9.77×10^{-7}	2.00×10^{-3}	8.17×10^{-4}	188. ns	0.711
(B) ^{184}Os, triaxial rotor model						
$\gamma_0 = 30°$	0.243	8.40×10^{-6}	1.34×10^{-1}	2.08×10^{-3}	25.9 ns	0.171
$\gamma_0 = 25°$	0.311	3.59×10^{-6}	4.15×10^{-6}	1.31×10^{-3}	68.5 ns	0.321
$\gamma_0 = 20°$	0.497	1.84×10^{-6}	1.09×10^{-3}	9.47×10^{-4}	121. ns	0.447
$\gamma_0 = 15°$	0.929	5.85×10^{-7}	8.81×10^{-4}	4.56×10^{-4}	324. ns	0.667
$\gamma_0 = 12°$	1.492	2.64×10^{-7}	5.45×10^{-4}	2.41×10^{-4}	670. ns	0.774
$\gamma_0 = 10°$	—	1.65×10^{-7}	3.70×10^{-4}	1.59×10^{-4}	1.05 μs	0.815
$\gamma_0 = 0°$	—	8.08×10^{-8}	1.96×10^{-4}	8.44×10^{-5}	2.05 μs	0.882
(C) ^{184}Os, Those reproducing $E(2^+_\gamma)$						
$(-2.99, 0)$	0.943	2.64×10^{-5}	4.51×10^{-2}	1.45×10^{-2}	8.13 ns	0.470
$(-5.71, 3)$	0.943	1.32×10^{-5}	1.83×10^{-2}	7.43×10^{-3}	16.2 ns	0.485
$(-10.05, 7)$	0.944	6.65×10^{-6}	8.08×10^{-3}	3.87×10^{-3}	31.9 ns	0.501
$(-20.12, 15)$	0.943	3.34×10^{-6}	3.71×10^{-3}	2.00×10^{-3}	62.9 ns	0.517
$(-41.59, 30)$	0.943	2.11×10^{-6}	2.26×10^{-3}	1.30×10^{-3}	98.9 ns	0.532
$(-72.96, 50)$	0.943	1.62×10^{-6}	1.76×10^{-3}	1.03×10^{-3}	127. ns	0.548
$\gamma_0 = 14.89°$	0.944	5.70×10^{-7}	8.68×10^{-4}	4.46×10^{-4}	332. ns	0.671
Experiment	0.943	9.0×10^{-7}	—	2.0×10^{-3}	120 ns	2.0
(D) ^{182}W, β_0=0.22						
$(-6.96, 0)$	1.222	1.96×10^{-7}	4.65×10^{-4}	1.21×10^{-4}	957 ns	0.442
$\gamma_0 = 12.18°$	1.222	2.70×10^{-9}	1.83×10^{-6}	6.41×10^{-6}	67.3 μs	0.485
γ_0=0°	—	6.27×10^{-10}	1.04×10^{-6}	4.17×10^{-7}	294 μs	0.483
(E) ^{182}W, β_0=0.24						
$(-6.05, 0)$	1.222	5.87×10^{-8}	1.77×10^{-4}	6.10×10^{-5}	2.62 μs	0.738
$\gamma_0 = 12.32°$	1.222	8.93×10^{-15}	2.85×10^{-8}	2.35×10^{-7}	11.0 ms	4.85
γ_0=0°	—	4.85×10^{-11}	2.28×10^{-7}	4.72×10^{-8}	3.20 ms	0.671
Experiment	1.222	9.3×10^{-8}	—	1.4×10^{-4}	1.4 μs	1.2

Table 6.4: Reduced E2 transition probabilities at low spin. Parameters are those adjusted for ^{184}Os which reproduce the experimental $E(2^+_\gamma)$. Experimental values are taken from the figures in ref. [73].

B(E2) values in units of [e^2 fm^4] at low spin for ^{184}Os

	Core models, (V_1, V_2) or γ_0						
	$(-2.99, 0)$	$(-5.71, 3)$	$(-10.05, 7)$	$(-20.12, 15)$	$(-41.59, 30)$	$(-71.96, 50)$	14.89 deg.
$2_1 \to 0_1$	$5.98E+3$	$5.98E+3$	$5.98E+3$	$5.98E+3$	$5.98E+3$	$5.98E+3$	$6.19E+3$
$2_2 \to 0_1$	$4.57E+2$	$4.84E+2$	$4.96E+2$	$4.98E+2$	$4.88E+2$	$4.76E+2$	$3.24E+2$
$2_1 \to 2_1$	$7.84E+3$	$7.84E+3$	$7.92E+3$	$7.92E+3$	$8.00E+3$	$8.00E+3$	$8.48E+3$
$2_2 \to 2_1$	$1.40E+3$	$1.39E+3$	$1.36E+3$	$1.32E+3$	$1.26E+3$	$1.22E+3$	$8.03E+2$
$2_2 \to 2_2$	$7.52E+3$	$7.45E+3$	$7.52E+3$	$7.60E+3$	$7.76E+3$	$7.84E+3$	$8.48E+3$
$3_1 \to 2_1$	$8.10E+2$	$8.53E+2$	$8.78E+2$	$8.84E+2$	$8.71E+2$	$8.47E+2$	$5.79E+2$
$3_1 \to 2_2$	$8.78E+3$	$9.43E+3$	$9.80E+3$	$1.00E+4$	$1.02E+4$	$1.04E+4$	$1.10E+4$
$3_1 \to 3_1$	$2.36E-4$	$2.25E-4$	$2.24E-4$	$2.26E-4$	$2.34E-4$	$2.42E-4$	$4.41E-4$
$4_1 \to 2_1$	$8.77E+3$	$8.77E+3$	$8.77E+3$	$8.77E+3$	$8.77E+3$	$8.77E+3$	$8.96E+3$
$4_1 \to 2_2$	$5.42E+1$	$6.66E+1$	$7.39E+1$	$7.80E+1$	$7.86E+1$	$7.68E+1$	$5.23E+1$
$4_2 \to 2_1$	$8.28E+1$	$8.52E+1$	$8.71E+1$	$8.89E+1$	$9.02E+1$	$8.96E+1$	$6.61E+1$
$4_2 \to 2_2$	$4.09E+3$	$3.68E+3$	$3.48E+3$	$3.40E+3$	$3.40E+3$	$3.40E+3$	$3.56E+3$
$4_1 \to 3_1$	$7.59E+2$	$8.10E+2$	$8.35E+2$	$8.39E+2$	$8.21E+2$	$7.97E+2$	$5.33E+2$
$4_2 \to 3_1$	$5.67E+3$	$6.24E+3$	$6.50E+3$	$6.72E+3$	$6.88E+3$	$7.05E+3$	$7.80E+3$
$4_1 \to 4_1$	$6.24E+3$	$6.13E+3$	$6.08E+3$	$6.13E+3$	$6.18E+3$	$6.24E+3$	$7.00E+3$
$4_2 \to 4_1$	$1.49E+3$	$1.52E+3$	$1.52E+3$	$1.49E+3$	$1.46E+3$	$1.41E+3$	$9.52E+2$
$4_2 \to 4_2$	$3.64E+2$	$8.82E+2$	$1.22E+3$	$1.46E+3$	$1.62E+3$	$1.68E+3$	$1.65E+3$
$5_1 \to 3_1$	$5.81E+3$	$5.77E+3$	$5.72E+3$	$5.72E+3$	$5.72E+3$	$5.72E+3$	$5.91E+3$
$5_1 \to 4_1$	$4.46E+2$	$4.62E+2$	$4.71E+2$	$4.76E+2$	$4.72E+2$	$4.63E+2$	$3.24E+2$
$5_1 \to 4_2$	$3.89E+3$	$4.44E+3$	$4.85E+3$	$5.23E+3$	$5.50E+3$	$5.68E+3$	$6.05E+3$
$5_1 \to 5_1$	$1.37E+3$	$1.60E+3$	$1.83E+3$	$2.07E+3$	$2.24E+3$	$2.35E+3$	$2.72E+3$
$6_1 \to 4_1$	$1.00E+4$	$1.00E+4$	$1.00E+4$	$1.00E+4$	$1.00E+4$	$1.00E+4$	$1.00E+4$
$6_1 \to 4_2$	$1.34E+2$	$1.64E+2$	$1.87E+2$	$2.08E+2$	$2.20E+2$	$2.23E+2$	$1.72E+2$
$6_2 \to 4_1$	$2.04E+1$	$1.92E+1$	$1.77E+1$	$1.59E+1$	$1.44E+1$	$1.36E+1$	$8.80E+0$
$6_2 \to 4_2$	$7.58E+3$	$7.10E+3$	$6.83E+3$	$6.64E+3$	$6.51E+3$	$6.51E+3$	$6.83E+3$
$6_1 \to 5_1$	$1.03E+3$	$1.12E+3$	$1.18E+3$	$1.22E+3$	$1.24E+3$	$1.22E+3$	$8.64E+2$
$6_2 \to 5_1$	$2.69E+3$	$2.80E+3$	$2.86E+3$	$2.92E+3$	$2.98E+3$	$3.07E+3$	$3.65E+3$
$6_1 \to 6_1$	$5.20E+3$	$5.04E+3$	$4.92E+3$	$4.84E+3$	$4.88E+3$	$4.96E+3$	$5.98E+3$
$6_2 \to 6_1$	$1.44E+3$	$1.46E+3$	$1.44E+3$	$1.38E+3$	$1.32E+3$	$1.28E+3$	$8.80E+2$
$6_2 \to 6_2$	$1.16E+3$	$2.30E+3$	$3.20E+3$	$4.06E+3$	$4.69E+3$	$5.00E+3$	$5.24E+3$

Ratios of B(E2) values at low spin for ^{184}Os

	Core models, (V_1, V_2) or γ_0					
	$(-2.99, 0)$	$(-10.05, 7)$	$(-41.59, 30)$	$(-71.96, 50)$	14.89 deg.	Exp.
$B(E2;3_1 \to 2_1)/B(E2;3_1 \to 4_1)$	1.89	1.87	1.88	1.89	1.93	1.4
$B(E2;2_2 \to 0_1)/B(E2;2_2 \to 2_1)$	0.325	0.363	0.385	0.390	0.404	0.5
$B(E2;4_2 \to 3_1)/B(E2;4_2 \to 2_2)$	1.385	1.87	2.02	2.07	2.19	—
$B(E2;2_2 \to 2_1)/B(E2;2_1 \to 0_1)$	0.234	0.228	0.212	0.204	0.130	—
$B(E2;4_2 \to 4_1)/B(E2;4_2 \to 2_2)$	0.365	0.437	0.432	0.417	0.267	0.2
$B(E2;3_1 \to 2_1)/B(E2;3_1 \to 2_2)$	0.092	0.090	0.085	0.081	0.053	—

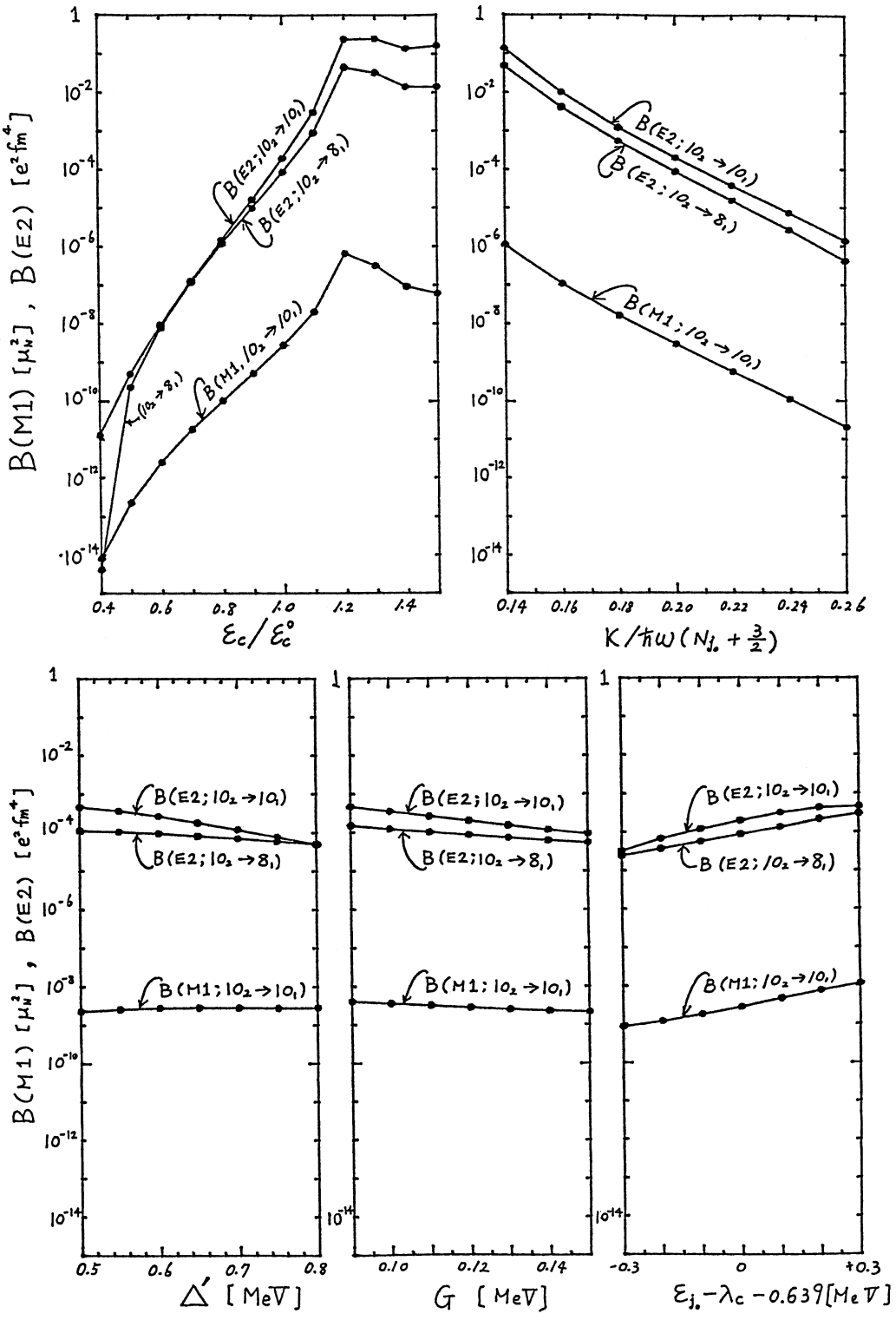

Figure 6.1: The effects of changing parameters of the model on the reduced transition probabilities of the decay of the $K^\pi = 10^+$ isomer. The axially symmetric rotor is employed as the core. Other parameters as those adjusted for ^{184}Os. See the comments in tables 6.1 and 6.2.

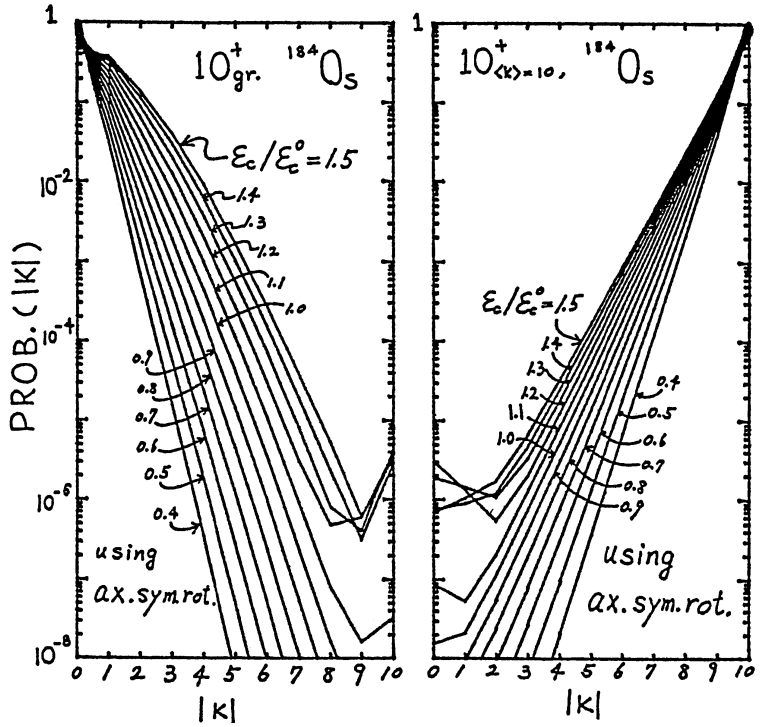

Figure 6.2: Effects of changing ϵ_c on the probability distribution of the K-quantum number. The axially symmetric rotor is employed as the core. Other parameters as those adjusted for ^{184}Os. When ϵ_c=ϵ_c^0 (=0.2805 MeV), the experimental $E(2^+_{gr})$ is reproduced including the effects of coupling with the particles.

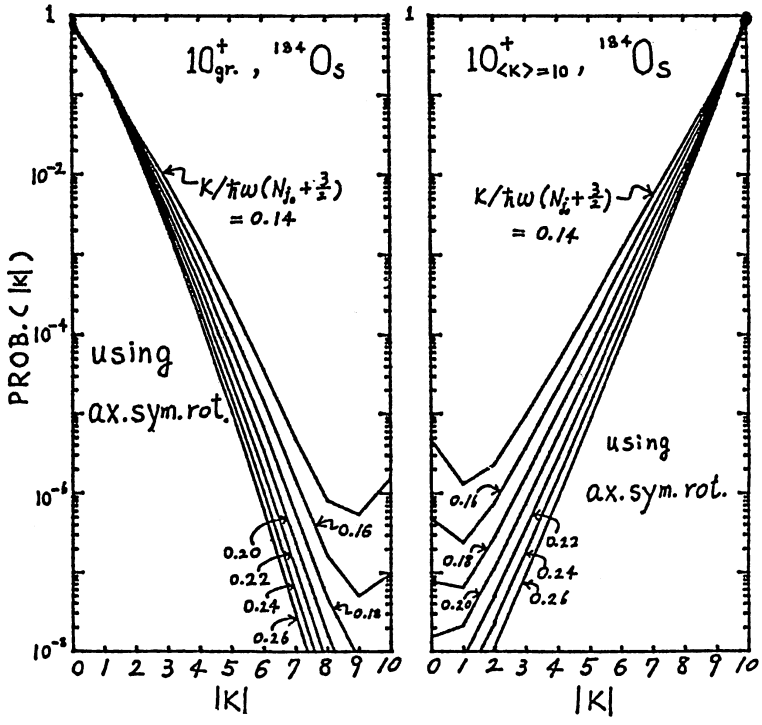

Figure 6.3: Effects of changing κ on the probability distribution of the K-quantum number. The axially symmetric rotor is employed as the core. Other parameters as those adjusted for ^{184}Os.

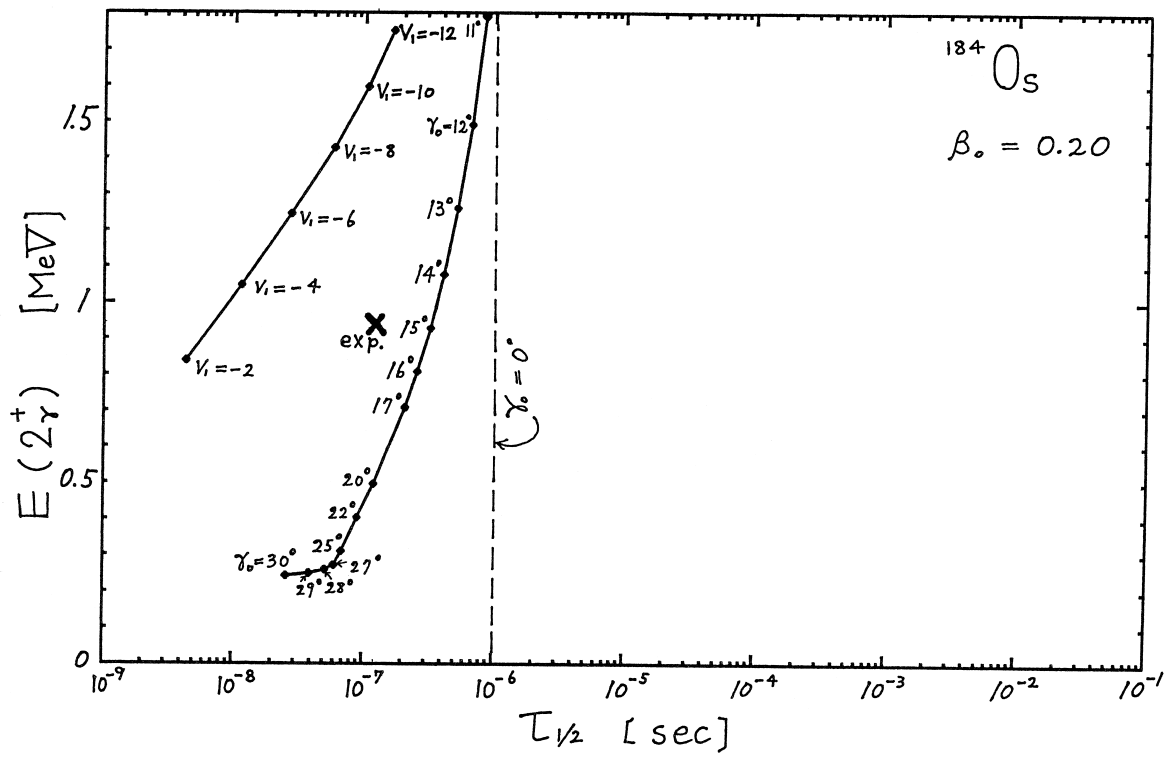

Figure 6.4: The excitation energy of the γ-bandhead versus the partial half-life of the $K^\pi = 10^+$ isomer with M1 and E2 transitions into the ground band states in ^{184}Os. Transition energies are taken from experiments in calculating the partial half-life.

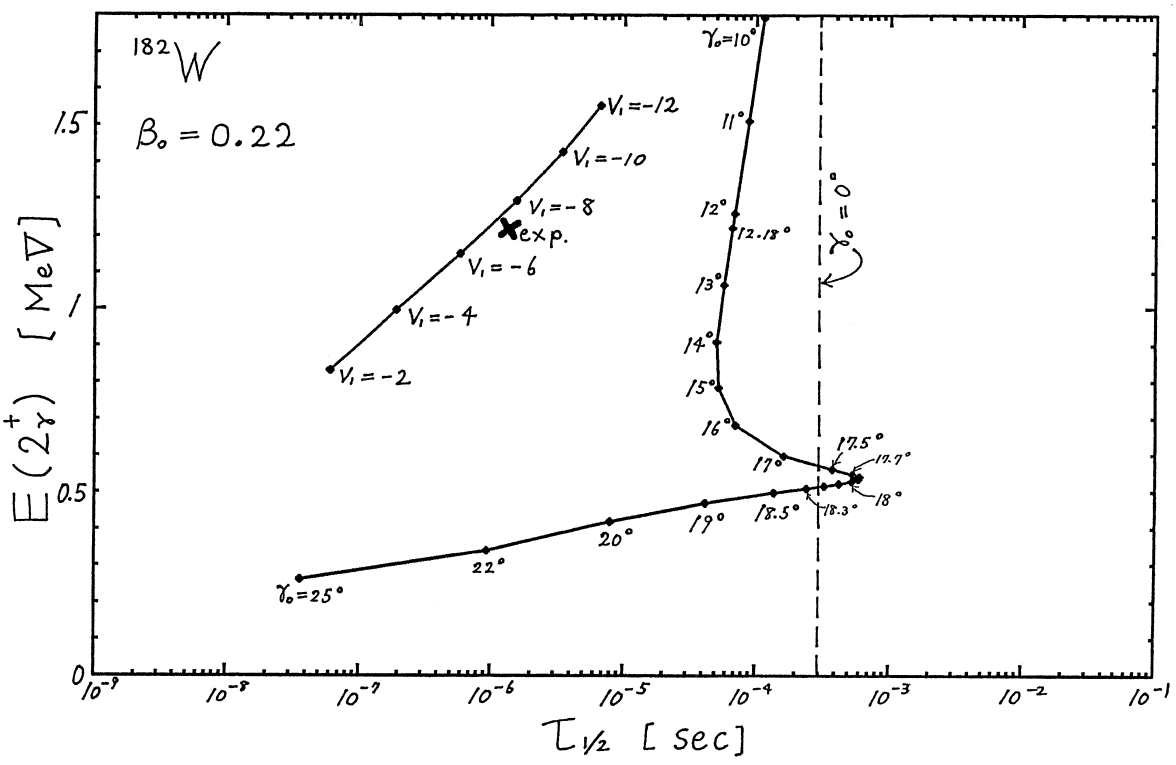

Figure 6.5: The same as figure 6.4, but for ^{182}W using β_0=0.22.

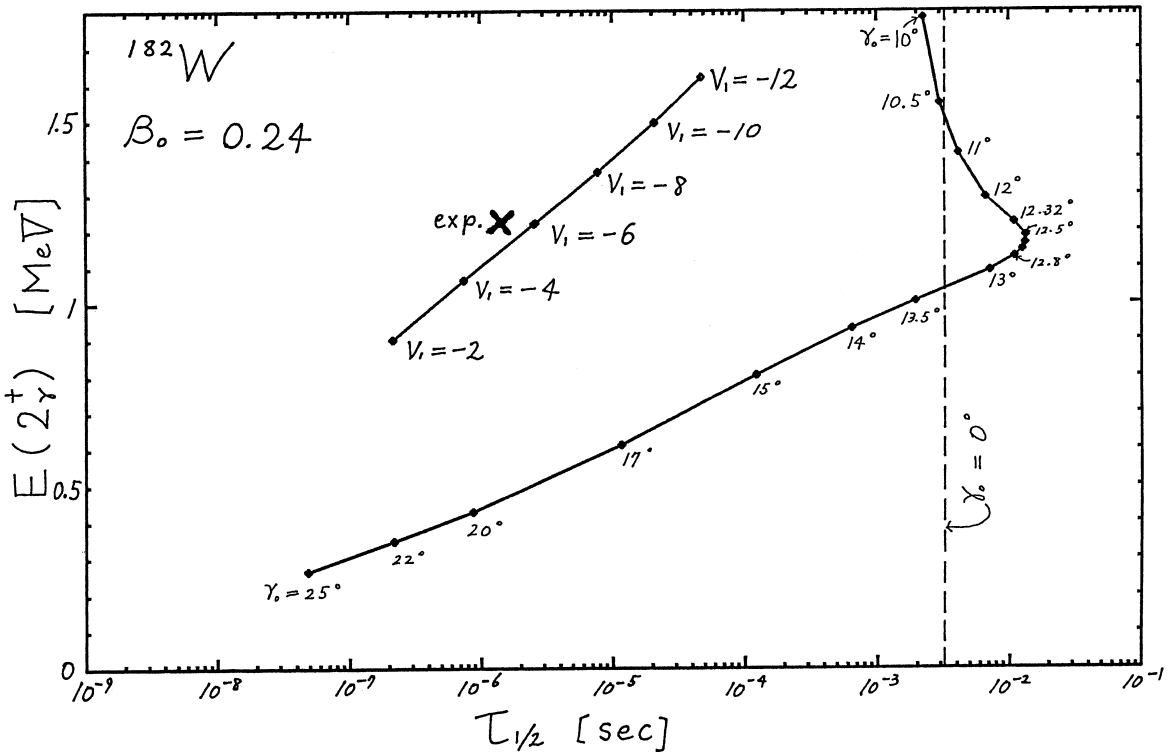

Figure 6.6: The same as figure 6.4, but for ^{182}W using β_0=0.24.

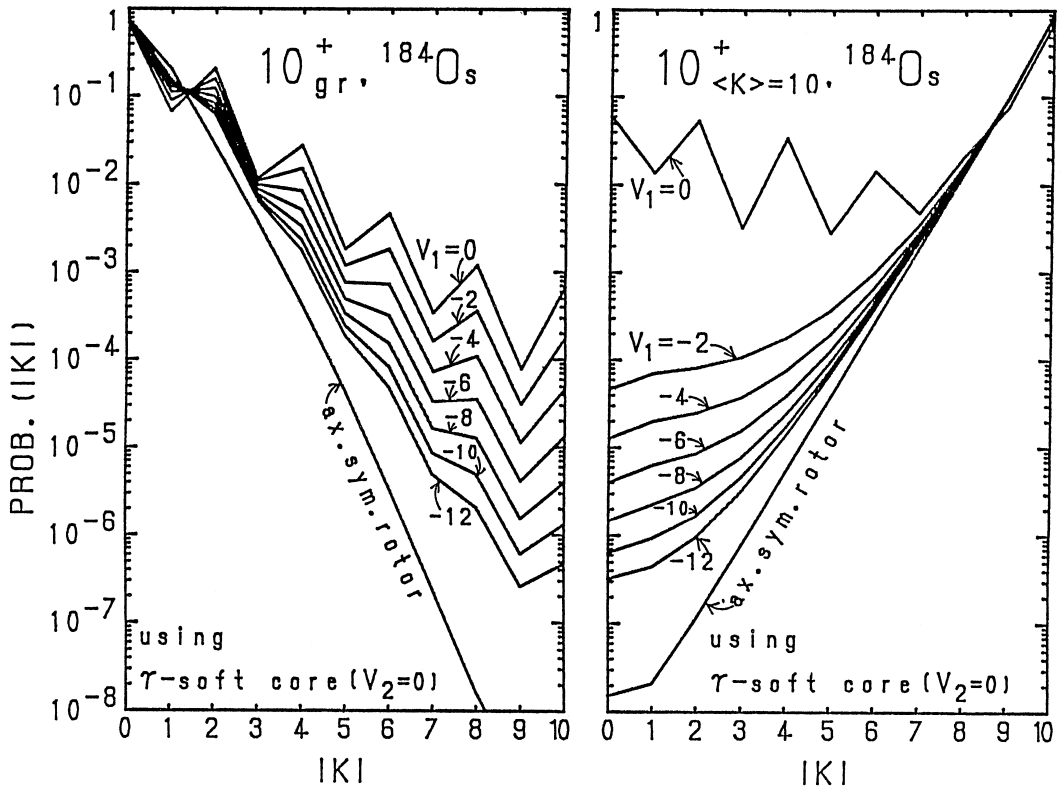

Figure 6.7: The probability distribution of the K-quantum number for the $10^+_{\rm gr}$ state and the $K^\pi = 10^+$ isomer in ^{184}Os using the γ-vibrational model (V_2=0).

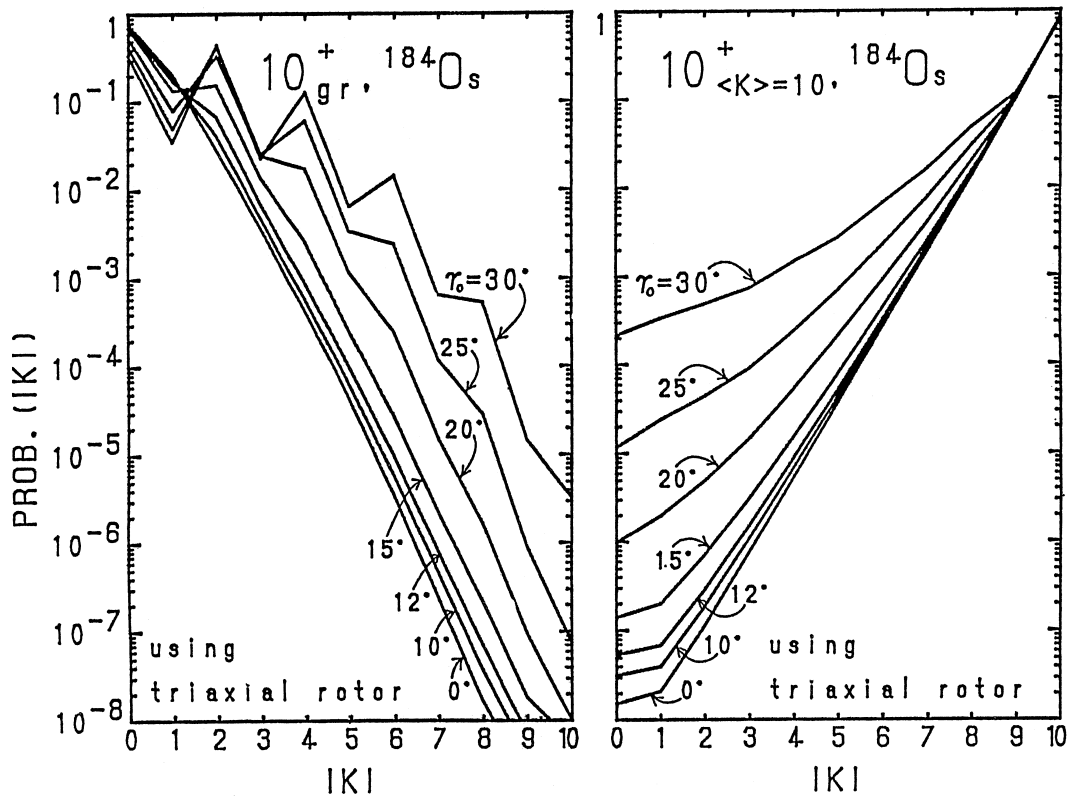

Figure 6.8: The same as figure 6.7, but using the triaxial rotor model.

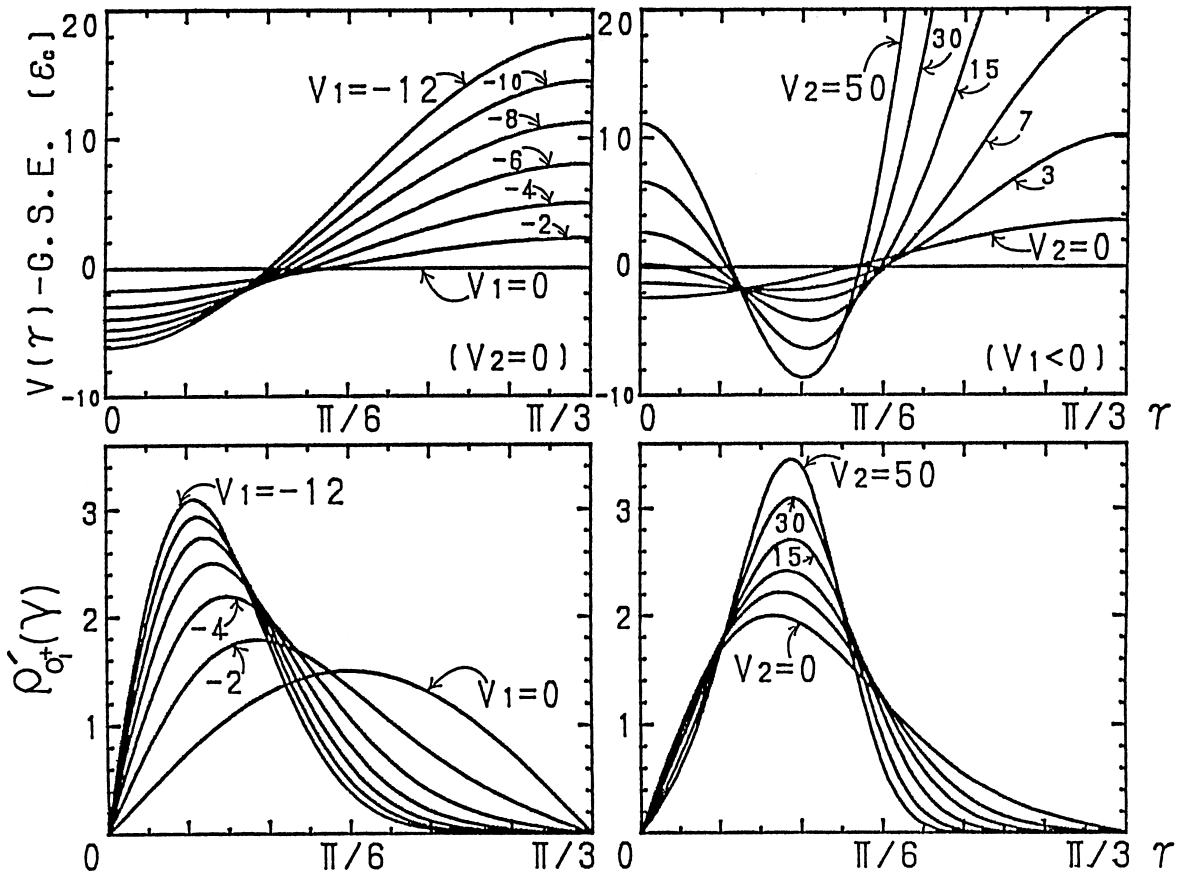

Figure 6.9: The γ-potential $V(\gamma)$ in units of ϵ_c (~ 0.2 MeV) and the probability distribution of γ of the bare (i. e. the particles are not coupled with) core in the ground state. The γ-potential is measured from the ground state energy. The values of V_1 of the potentials given in the upper right-hand portion are given in the part (C) of table 5.1.

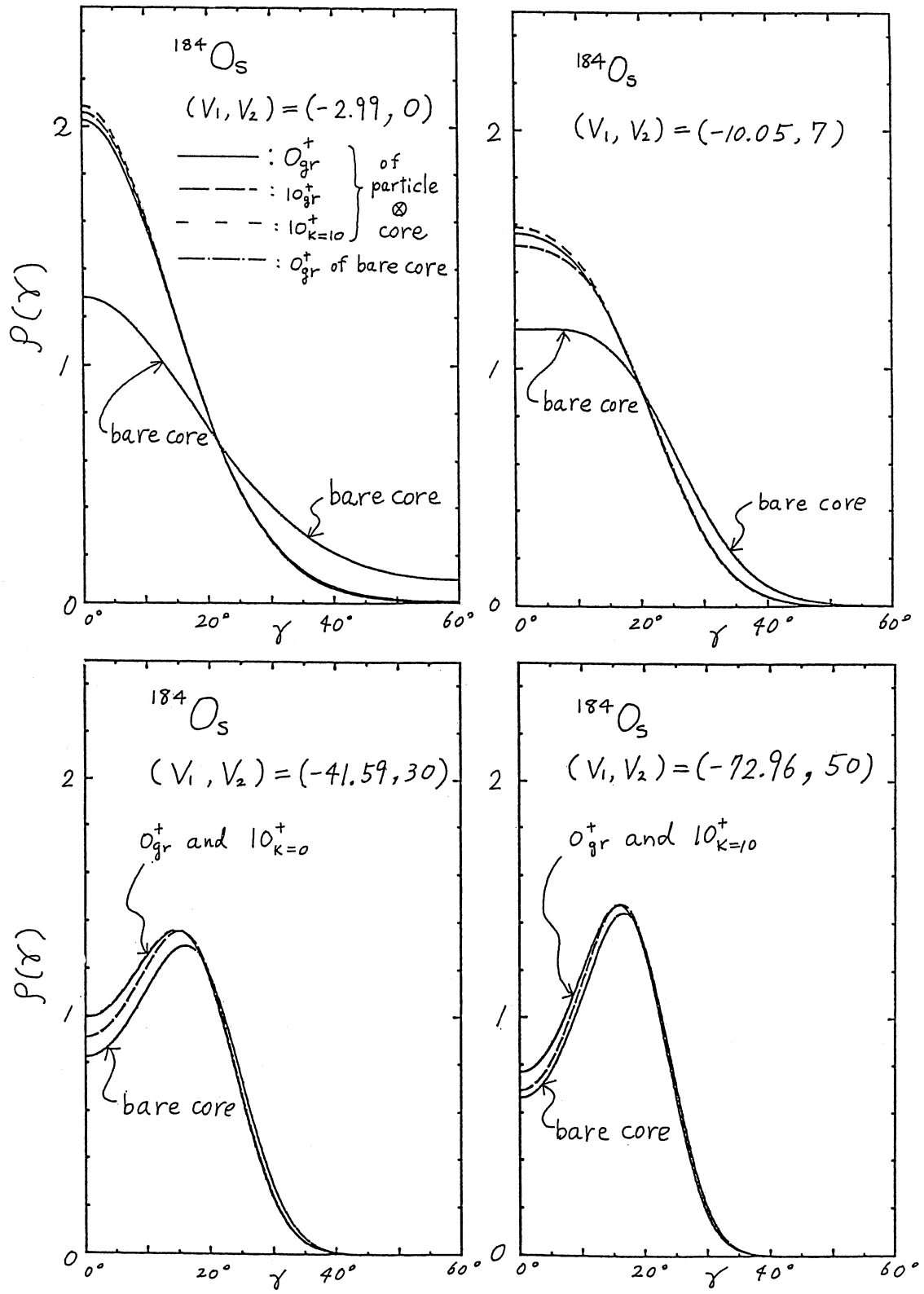

Figure 6.10: The probability distribution of γ in the coupled system of the core and the particles. Parameters are those adjusted for ^{184}Os which reproduce the experimental $E(2^+_\gamma)$.

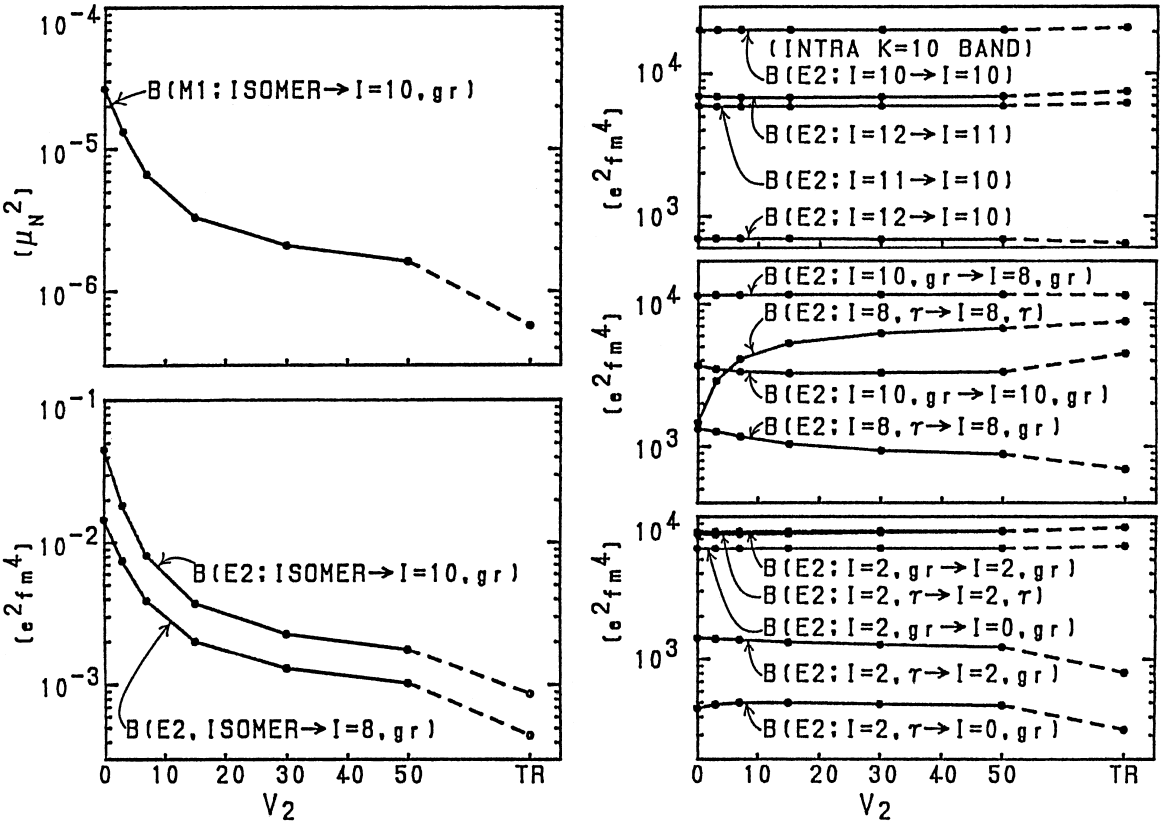

Figure 6.11: Reduced probabilities of isomeric and collective transitions using various shapes of the γ-potential. In the right-hand side, we give collective E2 transitions in the K^π=10^+ band (in the top) and in the ground and the γ-band (for high spin in the middle and for low spin in the bottom).

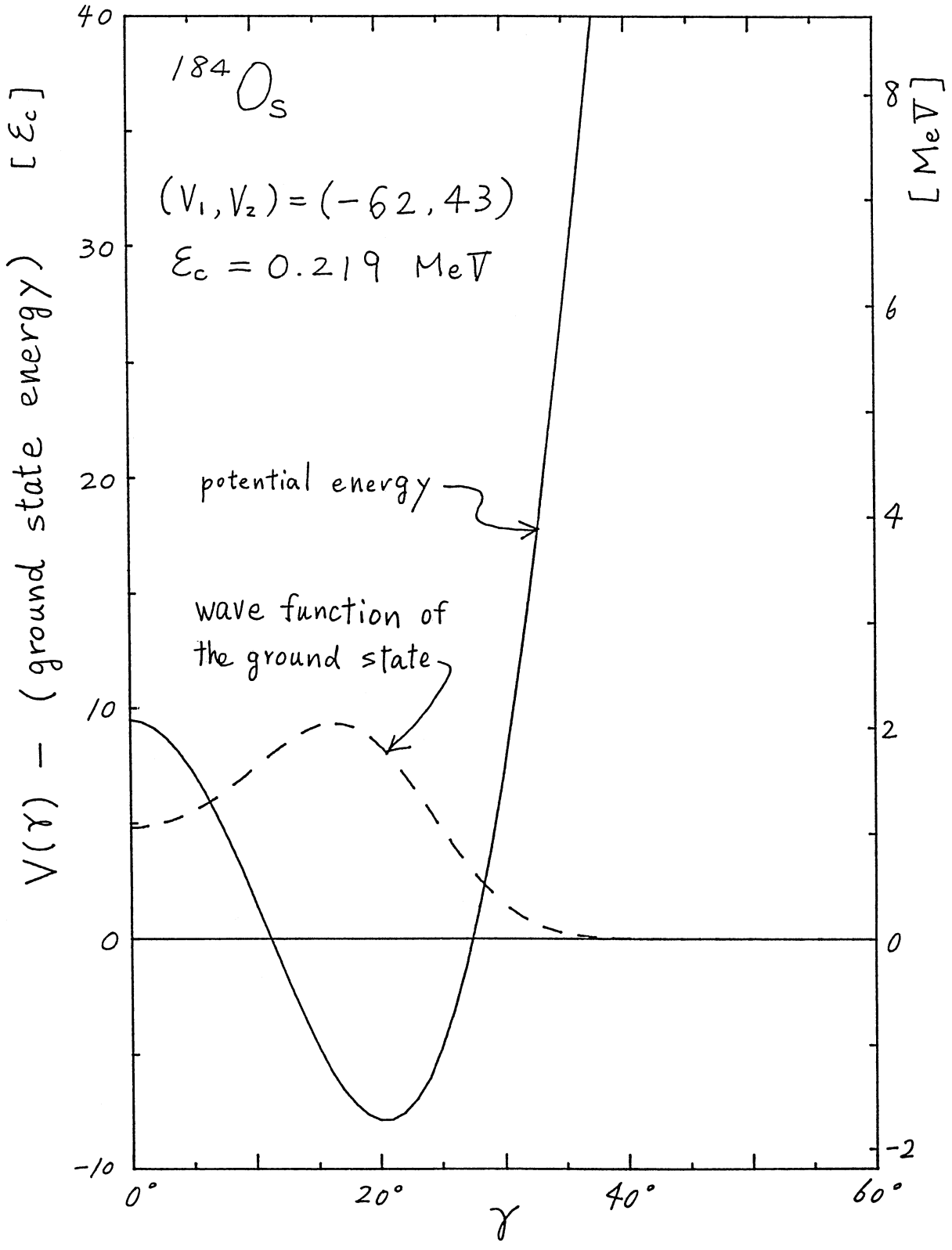

Figure 6.12: The γ-potential reproducing the half-life of the K-isomer and $E(2^+_\gamma)$ for ^{184}Os.

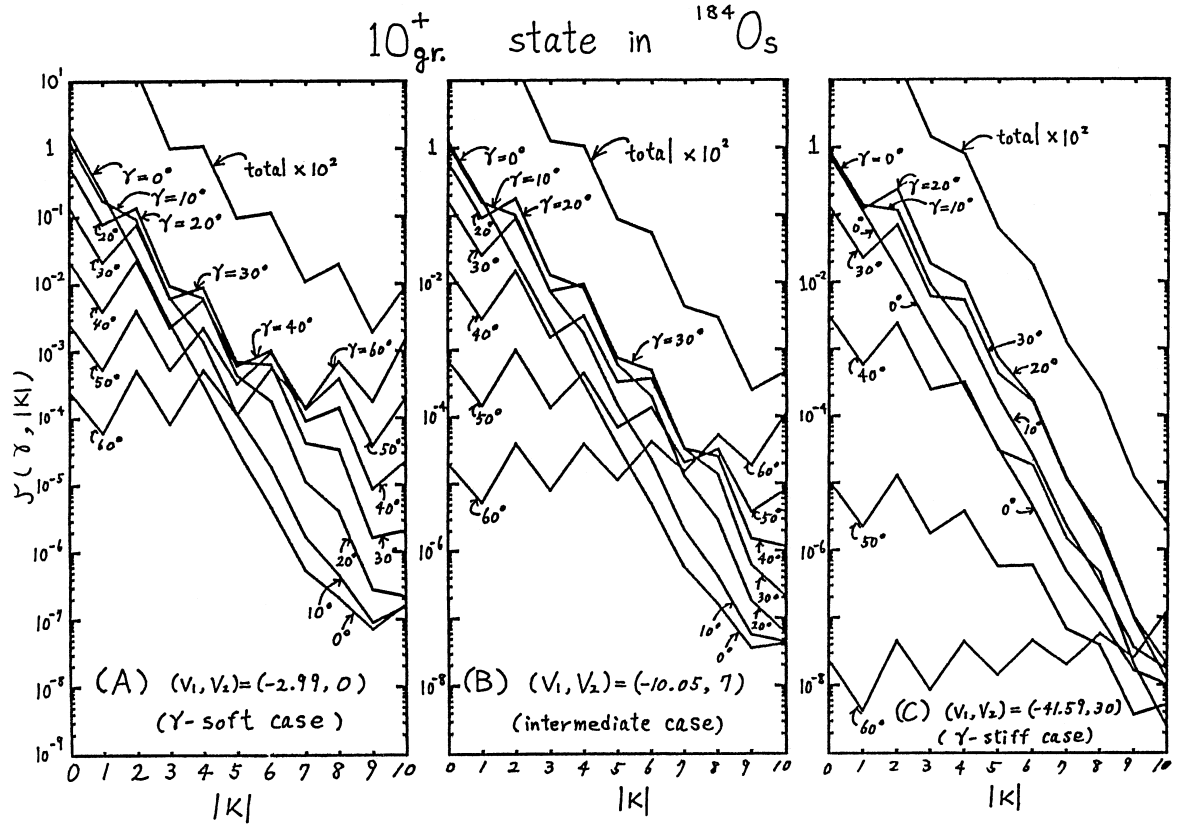

Figure 6.13: Probabilty distribution of γ and $|K|$ in the $10^+_{\rm gr}$ state. Parameters are those adjusted for ^{184}Os which reproduce the experimental $E(2^+_\gamma)$.

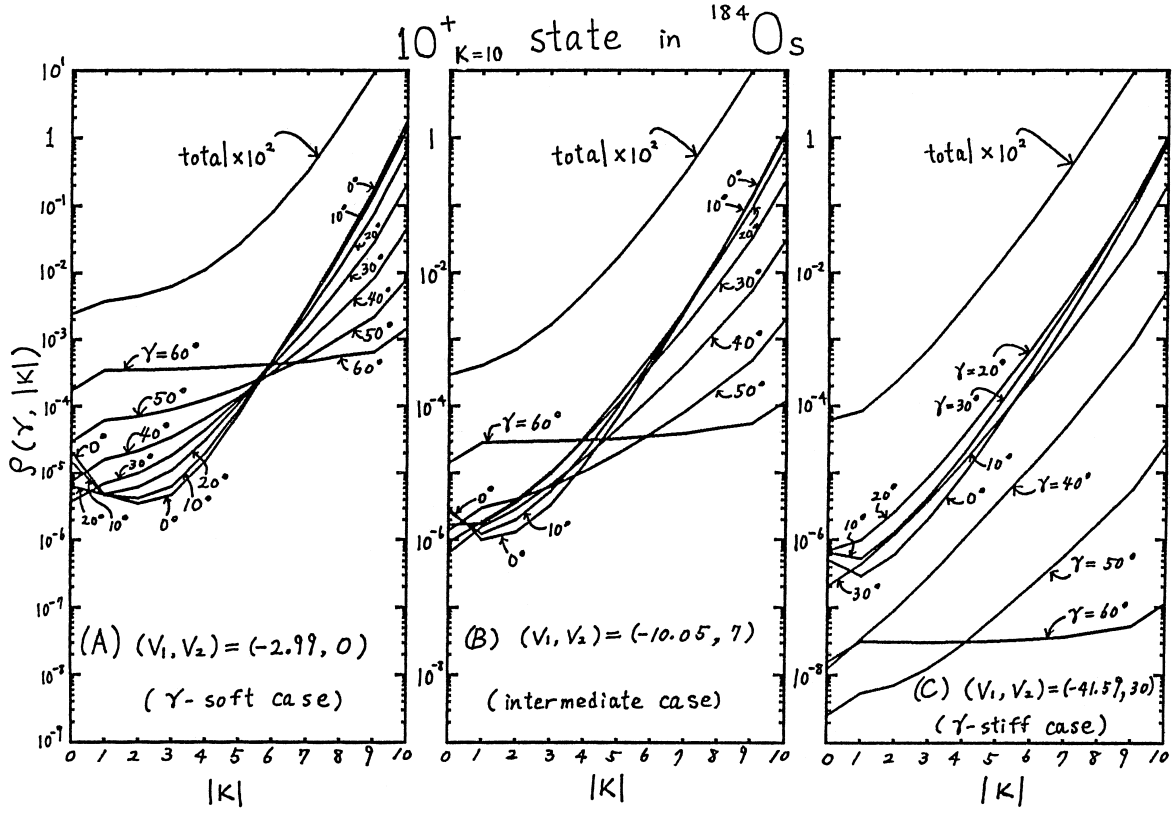

Figure 6.14: Probabilty distribution of γ and $|K|$ in the $K^\pi = 10^+$ isomer. Parameters are those adjusted for ^{184}Os which reproduce the experimental $E(2^+_\gamma)$.

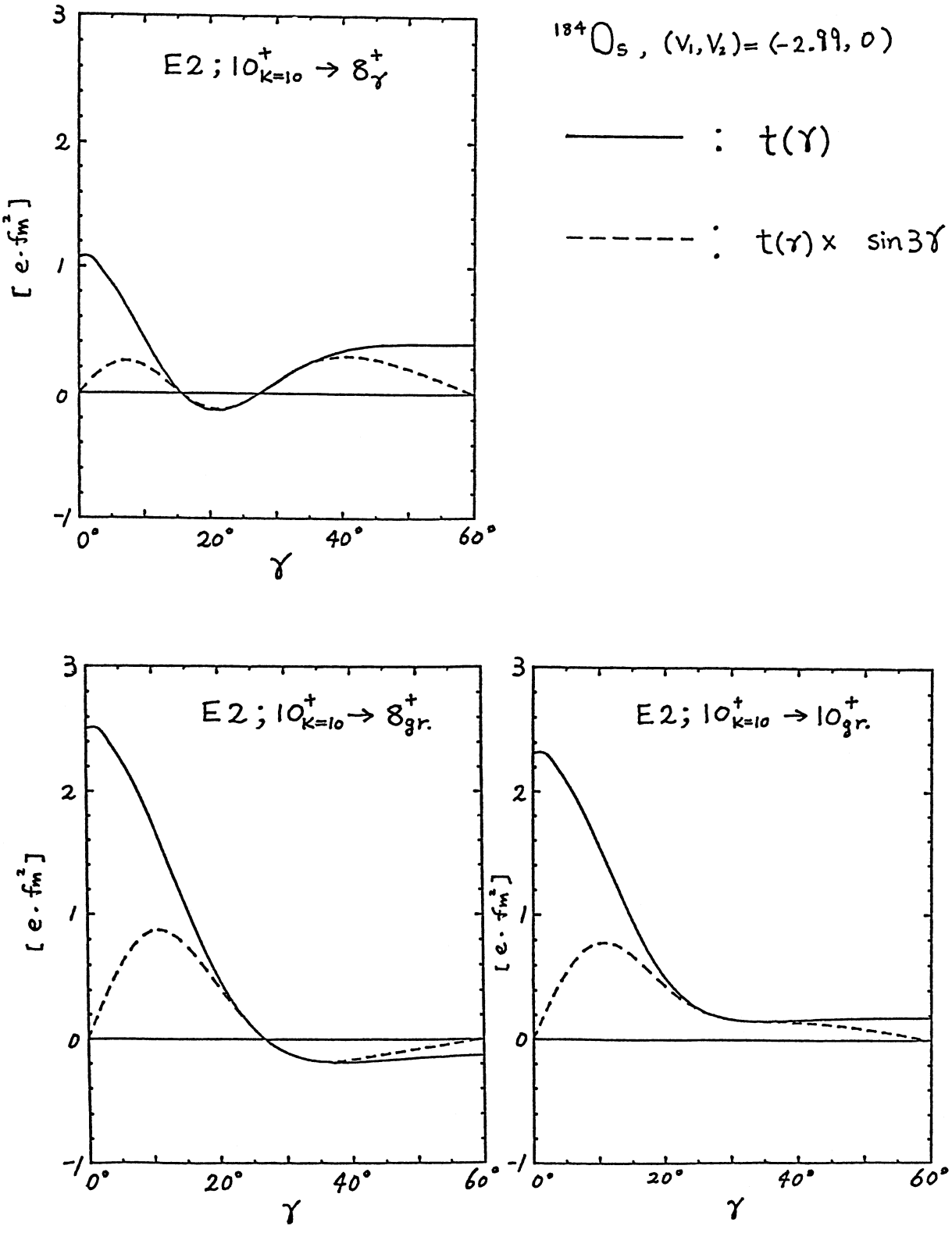

Figure 6.15: Distribution of the isomeric E2 transition amplitudes with respect to the size of γ-deformation.

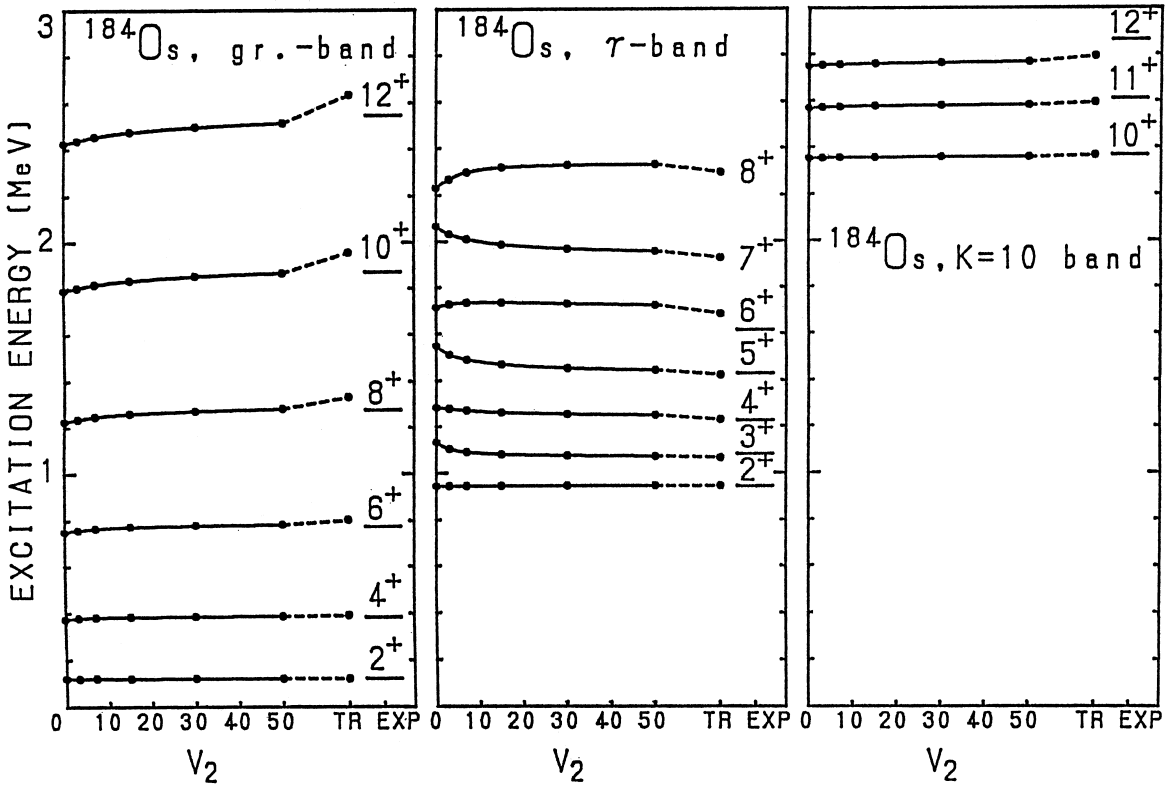

Figure 6.16: Energy levels of the ground band, the γ-band, and the $K^\pi = 10^+$ band for ^{184}Os. V_2 is varied from 0 to 50, while V_1 is adjusted so that the experimental E(2^+_γ) is reproduced. (See γ-potentials given in the upper right hand portion of figure 6.9.) The limiting case of the triaxial rotor model ($\gamma = 14.89°$) is included (denoted by TR). Experimental spectra are also shown (denoted by EXP).

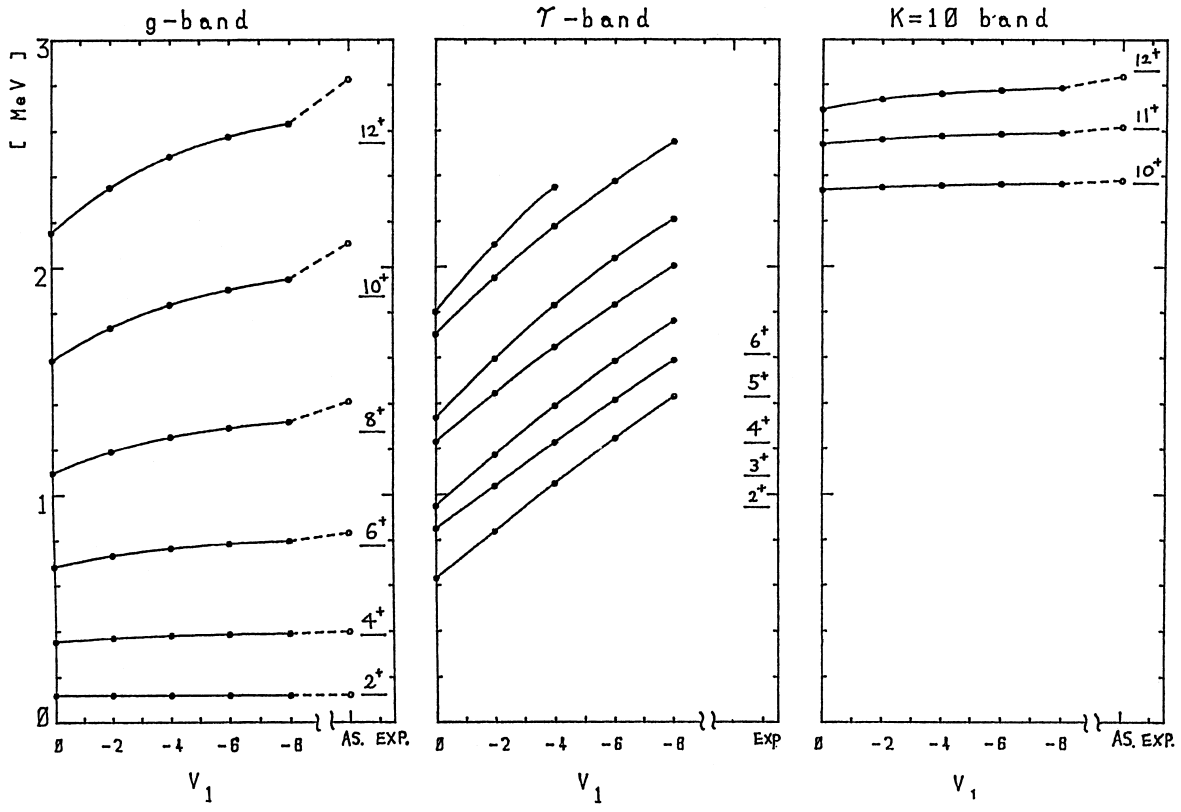

Figure 6.17: Energy levels of the ground band, the γ-band, and the $K^\pi = 10^+$ band for ^{184}Os using the γ-vibrational model (V_2=0). Parameters are those adjusted for ^{184}Os. The limiting case of the axially symmetric rotor model is denoted by AS.

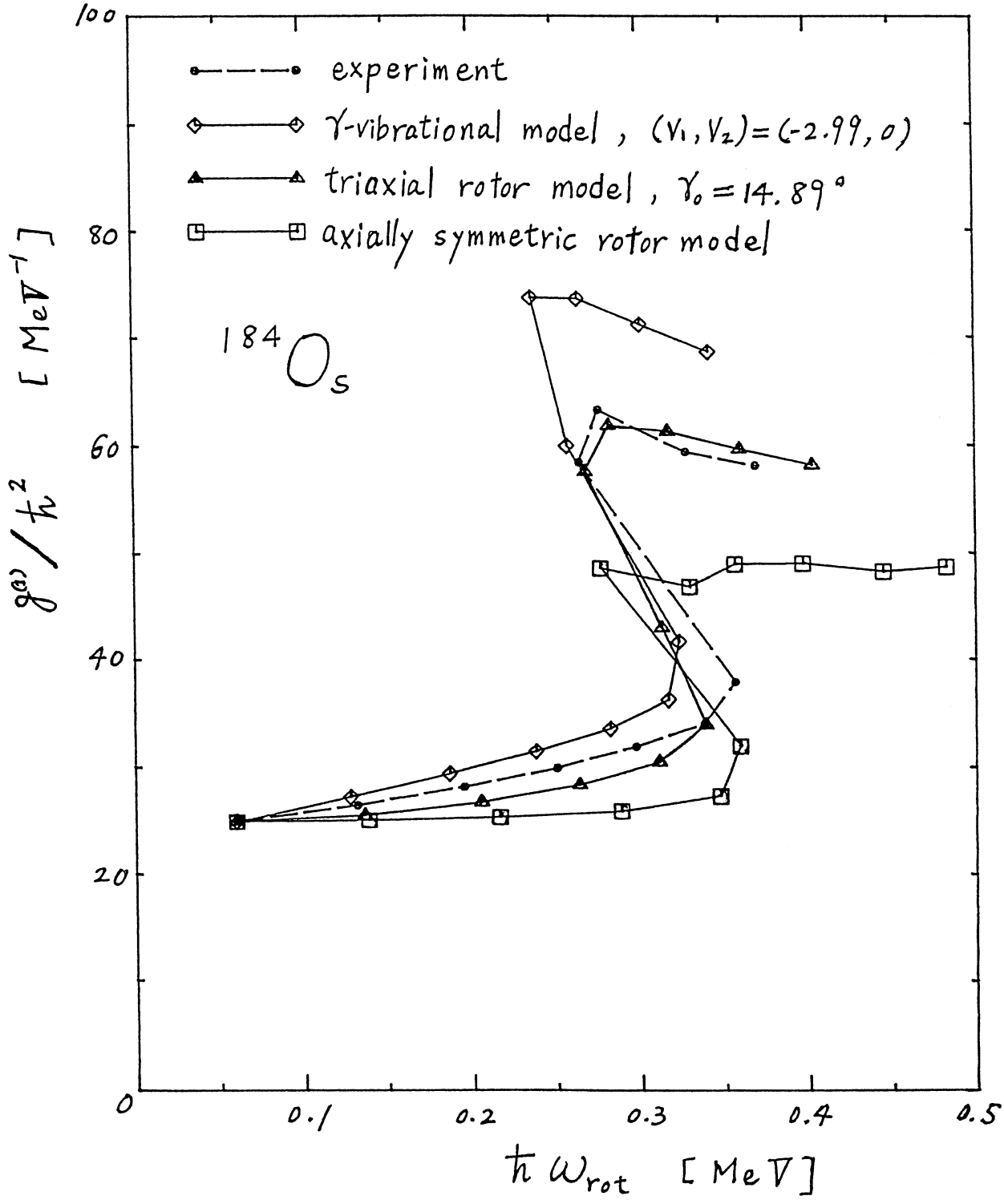

Figure 6.18: Kinematical moment of inertia versus the angular velocity for the yrast band of ^{184}Os.

Chapter 7

Summary

We examined the effects of the γ-degree of freedom on the decay properties of K-isomers. Aiming at the dynamical treatment of γ, we employed a γ-soft version of Bohr's quantum liquid drop model as the rotor of the particle-rotor model and treated the coupling between the large-amplitude surface motions and the motions of particles in an intruder orbital in a fully quantum mechanical way. The feature of our model is the description in the laboratory frame using the so-called weak coupling bases. Special efforts are made so that the results of calculations converge with respect to the truncation of bases of highly excitated γ-vibrational character.

We studied the strong violation of the K-selection rule observed in the decays of the $K^\pi=10^+$ isomers in ^{182}W and ^{184}Os. Before introducing the γ-degree of freedom, we investigated the effects of the Coriolis interaction on the mixing of the K-quantum number. It was found that the short half-lives of the isomers can not be reproduced assuming axially symmetric nuclear shape, although the Coriolis interaction is rather strong in these less-deformed transitional nuclei.

Next, we took into account the γ-degree of freedom. We changed the shape of the potential for γ-deformation and mediated two extreme models: One is the γ-vibrational model of Bohr and Mottelson, in which γ fluctuates around $\gamma=0^\circ$ in a relatively shallow potential. The other is the triaxial rotor model of Davydov and Filippov, which treats γ as a static parameter and fix it at some constant value γ_0.

The result is that the relatively short half-lives of the isomers can be reproduced when we introduce the γ-degree of freedom. The half-lives calculated with the γ-vibrational

model are shorter than those calculated with the triaxial rotor model by a factor of more than order two. The experimental half-lives are located between (or in the vicinities of) the values calculated with the two models. It is rather surprising that the two models can be distinguished so clearly: They have no distinct difference in the quantities of collective character like intraband E2 transitions.

This difference originates in the quantum fluctuation in γ. The γ-vibrational model has a very shallow potential for γ-deformation and the wave function has a long tail. The amplitudes of isomeric decays are affected remarkably by this large-γ tail of the wave function, as is illustrated by the fact that the components at large γ-deformations play the crucial role to mix the K-quantum number.

It is worth while noting, however, that the transitions occur mainly from the small-γ components, not from these large-γ ones. Hence we had better suppose indirect processes through which the quantum fluctuation in shape hastens the isomeric decays. The most likely process is the barrier penetration mechanism given by Chowdhury and his coworkers, where the ground-band state and the isomer mix with each other — in spite of the large difference in their structures — via largely γ-deformed states. But any quantitative approximations do not seem possible on the basis of such semiclassical picture at leat for the $K^{\pi}=10^{+}$ isomers because of the rather wide spread of the strength distribution of the isomeric transition.

On the contrary, quantities of collective character are determined by the bulk properties of the wave function. When we use the triaxial rotor model, we can simulate the bulk properties by adjusting the size of the static γ-deformation γ_0. But there is no tail, because γ is fixed at a constant value, and the mixing of the K-quantum number is much smaller than in the γ-vibrational model. Hence we can estimate the size of the fluctuation in γ from the degree of violation of the K-selection rule by utilizing the average value of γ, which has already been obtained from e. g. the excitaion energy of the γ-bandhead.

From the present calculations, it seems that the nucleus ^{182}W is much like the γ-vibrational model while the nucleus ^{184}Os is rather like the triaxial rotor model, in agreements with other microscopic calculations. But it is worth while noting that there are many degrees of freedom excluded in our model. At first, our γ-potential has only two

degrees of freedom. More detailed study of the potential shape is a future problem. Another important thing to be considered is the β-vibration, which enables us to take into account the change in the size of deformation due to high spin in a dynamical way.

.

Acknowledgements

I wish to express my sincere gratitude to Professor Naoki Onishi for all the guidance and discussions concerning this thesis. I am also grateful to the members of of the nuclear theory group of the Institute of Physics, College of General Education, University of Tokyo for their stimulating comments.

I also express my gratitude to Drs. J. Pedersen, J. Borggreen, and G. Sletten for sending us experimental data before publication. I thank also to Dr. Tord Bengtsson for suggesting our studying the $K^{\pi}=10^{+}$ isomers.

The computer calculation for this work was financially supported in part by the Grant-in-Aid for Scientific Research of the Japan Ministry of Education, Science and Culture, and in part by Research Center for Nuclear Physics, Osaka University.

Bibliography

[1] A. Bohr, Mat. Fys. Medd. Dan. Vid. Selsk. **26** (1952) no. 14; A. Bohr and B.R. Mottelson, Mat. Fys. Medd. Dan. Vid. Selsk. **27** (1953) no. 16.

[2] A.S. Davydov and G.F. Filippov, Nucl. Phys. **8** (1958) 237.

[3] J.M. Eisenberg and W. Greiner, *Nuclear models* (North-Holland, Amsterdam, 1970).

[4] D. Cline, Ann. Rev. Nucl. Part. Sci. **36** (1986) 683.

[5] D. Cline, Proc. of the Int. Conf. on Nucl. Shapes, ed. J.D. Garret, C.A. Kalfas, G. Anagnostatos, E. Kossionides, and R. Vlastou, World Scientific, pp. 1-20 (1988).

[6] L.I. Rusinov, Usp. Fiz. Nauk. **73** (1961) 615 ; Soviet Phys. Usp. **4** (1961) 282.

[7] K.E.G. Löbner, Phys. Lett. **B26** (1968) 369.

[8] A. Bohr and B.R. Mottelson, *Nuclear Structure*, vol. 1 (Benjamin, New York, 1969); vol. 2 (Benjamin, New York, 1975).

[9] R.G. Helmer and C.W. Reich, Nucl. Phys. **A211** (1973) 1.

[10] J. van Klinken, W.Z. Venema, R.V.F. Janssens, and G.T. Emery, Nucl. Phys. **A339** (1980) 189, and references therein.

[11] J. Pedersen, B.B. Back, S. Bjørnholm, J. Borggreen, M. Diebel, G. Sletten, F. Azgui, H. Emling, H. Grein, G. Seiler-Clark, W. Spreng, H.J. Wollersheim, P. Walker and S. Åberg, Phys. Rev. Lett. **54** (1985) 306.

[12] J. Pedersen, B.B. Back, S. Bjørnholm, J. Borggreen, G. Sletten, F. Azgui, H. Emling, H. Grein, G. Seiler-Clark, W. Spreng, H.J. Wollersheim, and P. Walker, Z. Phys. **A321** (1985) 567.

[13] P. Chowdhury, B. Fabricius, C. Christensen, F. Azgui, S. Bjørnholm, J. Borggreen, A. Holm, J. Pedersen, G. Sletten, M.A. Bentley, D. Howe, A.R. Mokhtar, J.D. Morrison, J.F. Sharpey-Schafer, P.M. Walker, and R.M. Lieder, Nucl. Phys. **A485** (1988) 136.

[14] N. Tajima and N. Onishi, Phys. Lett. **B179** (1986) 187.

[15] T. Bengtsson, private communication.

[16] B.D. Jeltema, F.M. Bernthal, T.L. Khoo, and C.L. Dors, Nucl. Phys. **A280** (1977) 21.

[17] J. Pedersen, private communication.

[18] Y.R. Shimizu, Soryushiron Kenkyu (Kyoto) **72** (1986) no. 6, p. F61.

[19] K. Kumar and M. Baranger, Nucl. Phys. **A110** (1968) 529; **A122** (1968) 273.

[20] A. Arima and F. Iachello, Phys. Rev. Lett. **35** (1975) 1069; Ann. Phys. (N. Y.) **99** (1976) 253, **111** (1978) 201, **123** (1979) 123.

[21] A.S. Davydov and A.A. Chaban, Nucl. Phys. **20** (1960) 499.

[22] A. Bohr et al. , discussion after Davydov's talk in *Proc. Int. Conf. on Nuclear Structure* (Kingston, Toronto, 1960, Univ. of Toronto Press) 807.

[23] T. Tamura and T. Udagawa, Nucl. Phys. **16** (1960) 460.

[24] V.I. Belyak and D.A. Zaikin, Nucl. Phys. **30** (1962) 442.

[25] A. Faessler, W. Greiner, and R.K. Sheline, Phys. Rev. **135** (1964) B591; Nucl. Phys. **70** (1965) 33.

[26] T. Yamazaki, Nucl. Phys. **49** (1964) 1.

[27] J. Meyer-ter-Vehn, F.S. Stephens, and R.M. Diamond, Phys. Rev. Lett. **32** (1974) 1383; J. Meyer-ter-Vehn, Nucl. Phys. **A249** (1975) 111,141.

[28] H. Toki and A. Faessler, Nucl. Phys. **A253** (1975) 213.

[29] T. Yamazaki, H. Nakayama, T. Numao, and T. Shibata, J. of Phys. Soc. Japan **44** (1978) 1421.

[30] F. Dönau and S. Frauendorf, Phys. Lett. **B71** (1977) 263.

[31] P. Kemnitz, F. Dönau, L. Funke, H. Strusny, D. Venos, and J. Meyer-ter-Vehn, Nucl. Phys. **A293** (1977) 314.

[32] A.Hayashi, K. Hara, and P. Ring, Phys. Rev. Lett. **53** (1984) 337.

[33] T. Otsuka and M. Sugita, Phys. Rev. Lett. **59** (1987) 1541.

[34] I. Hamamoto, Suppl. Prog. Theor. Phys. **74** & **75** (1983) 157.

[35] M. Matsuo and K. Matsuyanagi, Prog. Theor. Phys. **78** (1987) 591.

[36] C. Baktash, J.X. Saladin, J.J. O'Brien, and J.G. Alessi, Phys. Rev. **C22** (1980) 2383.

[37] D. Bonatsos, Phys. Lett. **B200** (1988) 1.

[38] B. Elbeck and P.O. Tjøm, Single nucleon transfer in deformed nuclei *in Adv. in Nucl. Phys.* , vol. **3** (Plenum, New York, 1969); A. Ikeda, private communication.

[39] J.M. Blatt and V.F. Weisskopf, *Theoretical nuclear physics* (Wiley, New York, 1952), ch. 12 and app. B.

[40] S. Åberg, Nucl. Phys. **A306**, 89 (1978)

[41] M.J.A. de Voigt, J. Dudek and Z. Szymanski, Rev. Mod. Phys. **55** (1983) 949.

[42] J. Burde, R.M. Diamond, and F.S. Stephens, Nucl. Phys. **85** (1966) 481.

[43] T.L. Khoo, F.M. Bernthal, R.A. Warner, G.F. Bertsch, and G. Hamilton, Phys. Rev. Lett. **35** (1975) 1256.

[44] T.L. Khoo and G. Løvhøiden, Phys. Lett. **B67** (1977) 271.

[45] P.M. Walker, Phys. Scripta **T5** (1983) 29.

[46] K.E.G. Löbner and S.G. Malmskog, Nucl. Phys. **80** (1966) 505.

[47] T. Suzuki and D.J. Rowe, Nucl. Phys. **A286** (1977) 307.

[48] A. Schuh, J. Kunz, and U. Mosel, Nucl. Phys. **A412** (1984) 34.

[49] I. Hamamoto and N. Onishi, Phys. Lett. **B150** (1985) 6.

[50] N. Onishi, I. Hamamoto, S. Åberg, and A. Ikeda, Nucl. Phys. **A452** (1986) 71.

[51] L. Wilets and M. Jean, Phys. Rev. **102** (1956) 788.

[52] R.J. Turner and T. Kishimoto, Nucl. Phys. **A217** (1973) 317.

[53] G. Rakavy, Nucl. Phys. **4** (1957) 289.

[54] D. R. Bes, Nucl. Phys. **10** (1959) 373.

[55] G. Alaga, Proc. Int. School Phys. "Enrico Fermi" Course XL, Varenna on Lake Como, 1967, ed. M. Jean and R.A. Ricci (Academic Press, London, 1969) p. 28, and references therein.

[56] P.J. Evans and S.M. Harris, Nucl. Phys. **A277** (1977) 109.

[57] A. Ikeda, M. Kitajima, M. Miyawaki, and N. Onishi, Phys. Lett. **B85** (1979) 172.

[58] F. Grümmer, K.W. Schmid, and A. Faessler, Nucl. Phys. **A317** (1979) 287.

[59] F. Grümmer, K.W. Schmid, and A. Faessler, Nucl. Phys. **A326** (1979) 1.

[60] M. Reinecke, H. Herold, H. Ruder, G. Wunner, Nucl. Phys. **A361** (1981) 435.

[61] R.R. Hilton, H.J. Mang, P. Ring, J.L. Egido, H. Herold, M. Reinecke, H. Ruder, and G. Wunner, Nucl. Phys. **A366** (1981) 365.

[62] A. Ikeda and N. Onishi, Progr. Theor. Phys. **70** (1983) 128.

[63] A. Ikeda, Nucl. Phys. **A452** (1986) 423.

[64] A. Ikeda, Nucl. Phys. **A453** (1986) 241.

[65] R.D. Lawson, *Theory of the Nuclear Shell Model* (Clarendon, Oxford, 1980)

[66] M. Baranger and K. Kumar, Nucl. Phys. **A110** (1968) 490.

[67] N. Onishi and J.W. Negele, Nucl. Phys. **A301** (1978) 336.

[68] A. De-Shalit and I. Talmi, *Nuclear shell theory* (Academic press, New York 1963).

[69] J. Almberger, I. Hamamoto, and G. Leander, Nucl. Phys. **A333** (1980) 184; Phys. Scripta **22** (1980) 331.

[70] S. Raman, C.H. Malarkey, W.T. Milner, C.W. Nestor, JR., and P.H. Stelson, Atomic data and Nuclear data tables **36** (1987) 1.

[71] R.R. Whitehead, A. Watt, B.J. Cole, and I. Morrison,Computational Methods for Shell Model Calculations *in Adv. in Nucl. Phys.* , vol. **9** (Plenum, New York, 1977)

[72] R.S. Hager and E.C. Seltzer, Nucl. Data **A4** (1968) 1.

[73] R. Bijker, A.E.L. Dieperint, O. Scholten, and R. Spanhoff, Nucl. Phys. **A344** (1980) 207.